multi-Risk sciEnce for resilienT commUnities undeR a changiNgclimate
Codice progetto MUR: **PE00000005** – CUP LEAD PARTNER H93C22000610002

Deliverable title: "Multiscale modeling framework for contaminants transport and reaction with uncertainty quantification in marine coastal systems"

Deliverable ID: DV 4.3.4

Due date: month 36

Submission date:

AUTHORS

Angela Rizzo, Donata Canu, Alessandra Cincinelli, Ilaria Colzi, Laura Cutroneo, Daniela Piazzese, Silvia Serranti

1. Technical references

Project Acronym	RETURN
Project Title	multi-Risk sciEnce for resilienT commUnities undeR a changiNg climate
Project Coordinator	Domenico Calcaterra UNIVERSITA DEGLI STUDI DI NAPOLI FEDERICO II domcalca@unina.it
Project Duration	December 2022 – November 2025 (36 months)

Deliverable No.	DV 4.3.4
Dissemination level*	PU
Work Package	WP 4.3 - Enhancing capability to observe, model, and assess environmental hazards
Task	T 4.3.2 - Contaminants and microplastic fate and transport in coastal and marine areas and their bioaccumulation and magnification: novel observation methodologies; modelling space-time distribution of emerging contaminants; bottom sea distribution and vertical fluxes of plastic; plastic food web; reducing uncertainty
Lead beneficiary	UNIBA
Contributing beneficiary/ies	OGS, UNIFI, UNIGE, UNIPA, UNIROMA1

* PU = Public

PP = Restricted to other programme participants (including the Commission Services)

RE = Restricted to a group specified by the consortium (including the Commission Services)

CO = Confidential, only for members of the consortium (including the Commission Services)

Document history

Version	Date	Lead contributor	Description
0.1	31/07/2025	OGS: Ginevra Rosati UNIBA: Angela Rizzo UNIFI: Alessandra Cincinelli, Laura Sforzi UNIGE: Laura Cutroneo UNIPA: Daniela Piazzese UNIROMA1: Silvia Serranti	First submission of the preliminary contributions
0.2	20/11/2025	OGS: Shawn Booth, Gaia Buccino, Donata Canu, Marco Fianchini, Celia Laurent, Simone Libralato, Andrea Petronio, Ginevra Rosati, Amira Saidi, Cosimo Solidoro, Serena Zunino UNIBA: Vincenzo De Santis, Antonella Marsico, Giuseppe Mastronuzzi, Isabella Lapietra, Stefania Lisco, Isabella Serena Liso, Mario Parise, Angela Rizzo, Giovanni Scardino UNIFI: Alessandra Cincinelli, Ilaria Colzi, Sara Falsini, Cristina Gonnelli, Alessio Papini, Laura Sforzi UNIGE: Marco Capello, Laura Cutroneo, Irene Geneselli UNIPA: Giuseppe Ciraolo, Laura Corbari, Daniela Piazzese UNIROMA1: Giuseppe Bonifazi, Giuseppe Capobianco, Pietro Cocozza, Eleonora Gorga, Silvia Serranti.	First submission of the thematic chapters
0.3	2/12/2025	Angela Rizzo, Manuela Antonelli, Claudio Lubello	First revision of the thematic chapters
0.4	23/01/2025	Donata Canu, Alessandra Cincinelli, Laura Cutroneo, Daniela Piazzese, Ginevra Rosati, Silvia Serranti, Laura Sforzi	Submission of the required revisions
0.5	28/01/2025	Angela Rizzo, Manuela Antonelli, Claudio Lubello	Final revision of the document

2. ABSTRACT

Deliverable (DV) 4.3.4 "**Multiscale modeling framework for contaminants transport and reaction with uncertainty quantification in marine coastal systems**" represents the second document to be delivered in the frame of Task 4.3.2 "Contaminants and microplastic fate and transport in coastal and marine areas and their bioaccumulation and magnification: novel observation methodologies; modelling space-time distribution of emerging contaminants; bottom sea distribution and vertical fluxes of plastic; plastic food web; reducing uncertainty" of Work Package (WP) 4.3 in the vertical Spoke VS4 "Environmental degradation". DV4.3.4 describes the research activities, methodologies, and results achieved up to the month 36 of the Return Project.

The Deliverable presents a comprehensive overview of multidisciplinary research activities addressing the distribution, transport, and impact of contaminants in coastal and marine environments, with special focus on microplastics (MPs), macro litter, mercury, and pharmaceuticals. The activities integrate field sampling and surveys, advanced modeling tools, and innovative analytical techniques to understand contaminant dynamics and their implications on human health and biota in different spatial and temporal scales.

The modeling component addresses the fate and transport of contaminants (mercury, plastics, and pharmaceuticals) in the sea up to biota (mercury) using spatially explicit models that integrate different approaches to simulate the contaminant pathways from coastal inputs to marine biota.

Sampling and analytical activities provide critical data and approaches to characterize contaminant sources, distributions, and effects. Themes addressed in the Deliverable include:

- Monitoring and modeling of macro and micro litter in coastal zones;
- Assessment of MPs in surface waters and benthic fish, with evaluation of human exposure via seafood
- Investigation of sediment contamination in port areas, accounting for marine dynamics and riverine inputs
- High-resolution mapping and modeling of plastic and bioplastic transport using drone-based and in situ observations with integrated uncertainty quantification;
- Hyperspectral imaging techniques for precise identification and classification of plastics in various environmental matrices;
- Evaluation of physiological responses of aquatic plants exposed to MPs, and potential use of phytoremediation in contaminated waters.

In detail, the contribution of the OGS group focuses on spatially explicit models for simulating the fate and transport of coastal pollutants, including mercury, plastics, and pharmaceuticals, up to their bioaccumulation in marine organisms. Multiple modeling approaches are employed, such as Lagrangian transport, biogeochemical cycles, food web modeling, and genomics. UNIBA activities are focused on the analysis and distribution of macro and micro litter in coastal zones through multi-technology monitoring and modeling, with a focus on beach litter and MPs found in sediments and the water column. UNIFI group assesses the presence of MPs in surface waters and benthic fish (e.g., red mullet) across Mediterranean ports, with a specific evaluation of human exposure and MP intake in different population groups from contaminated fish. In addition, the UNIFI team examines the physiological effects of MPs in model aquatic plants (*Spirodela polyrhiza*) grown in water with blue-fluorescent MPs, investigating the role of root exudates in MPs aggregation and exploring phytoremediation potential in contaminated waters. UNIGE investigates the presence of MPs in port sediments to analyze the influence of marine hydrodynamics and freshwater inputs. Sediments are treated with H_2O_2 with different methods to better remove plant material and extract MPs. Water dynamics and physical parameters were acquired with ADCP and CTD probes. UNIPA group conducts high-resolution mapping of plastic and bioplastic transport through drone and in situ surveys, coupled with multiscale modeling approaches, incorporating uncertainty quantification. UNIROMA1 develops innovative HSI-based strategies to identify and classify macro- and microplastics in complex matrices such as sandy beaches and marine sediments, including the use of a custom HSI micro-scanner for improved MPs detection.

In line with the aims of WP 4.3, activities envisaged in Task 4.3.2 are focused on the analysis processes related to pollutants distribution, transport, and their bioaccumulation and magnification in marine and coastal areas and related matrices (i.e., sediments, water column, and biota). By combining field surveys, analytical strategies, and innovative modeling tools, the activities envisaged in the frame of this Task contribute to the definition of an integrative framework for the analysis of contaminant behavior and environmental risks in marine coastal systems, supporting both environmental and public health protection.

Task participants, who belong to six institutions (OGS, UNIBA, UNIFI, UNIGE, UNIPA, and UNIROMA1), have contributed to the Deliverable preparation by summarizing the proposed methodological approaches and their scientific results in the form of a dedicated thematic chapter. The document is therefore composed of seven thematic chapters referring to a single research group. Ongoing collaborations and joint activities among two or more research groups are also highlighted in the text.

3. Table of contents

List of Figures

4. Multiscale modeling framework for contaminants transport and reaction with uncertainty quantification in marine coastal systems

4.1 Fate, transport, and bioaccumulation of contaminants: modeling tools for coastal-marine environments (OGS)

4.1.1 Introduction

The Northern Adriatic Sea is a shallow, semi-enclosed marine basin characterised by strong land–sea interactions, marked physical variability and the co-occurrence of multiple natural and anthropogenic pressures. Its geomorphological setting, intense riverine influence, high productivity and dense human presence make it particularly vulnerable to environmental degradation and to the cumulative effects of pollutants, maritime activities, and climate-related stressors.

Over the last decade, the OGS research team has developed a comprehensive set of tools for analysing the transport and transformation of tracers and contaminants in the Northern Adriatic Sea and its lagoons. These capabilities have been built through several major research projects, including HARMONIA, SHAREMED, NAMIRS, ICCC, and NECCTON, and rely on advanced hydrodynamic and biogeochemical modelling systems.

In the present work, these consolidated modelling tools have been applied and further extended, benefiting from new developments carried out within parallel initiatives such as the PNRR National Biodiversity Future Centre (NBFC) "Zero Pollution" activities and the Horizon Europe project NECCTON. These complementary efforts have enabled basin-scale assessments of pollutant loading, fate, and transport for both traditional and emerging contaminants, including oil, mercury, microplastics, and selected pharmaceuticals. The resulting high-resolution simulations provide spatially explicit distributions of multiple pollutants under variable oceanographic conditions, supporting integrated multi-risk assessments for the Adriatic Sea.

In particular, the MITgcm ocean circulation model (Querin et al., 2016) the SHYFEM hydrodynamic model for coastal seas and lagoons (Umgiesser et al., 2003; Rosati et al., 2024), the OGSTM-BFM-Hg model (Rosati et al., 2022) and the Lagrangian particle-tracking model LTRANS-Zlev (Laurent et al., 2020) have been used to reproduce multi-scale transport patterns, and dispersion and transformation processes, also coupled to biogeochemical modules.

The lagrangian computation relies on the LTRANS-Zlev particle tracker (Laurent et al., 2020) coupled to OILTRANS (Berry et al. 2011) and to other modules that simulate the fate of specific substances. In this framework particles are transported and subjected to transformation processes such as weathering and chemical degradation which are explicitly resolved also including dependence to environmental conditions (seawater temperature, light penetration…). Within this system, pollutants transport and transformation are simulated under dynamically varying ocean conditions (Melaku Canu et al., 2019). These conditions are provided by a high-resolution implementation of the MITgcm hydrodynamic model, at a spatial resolution of 1/128° (850 m × 600 m) with 27 vertical levels, which supplies three-dimensional currents, temperature fields, and meteorological forcing (Marshall et al., 1997; Querin et al., 2016).

Together, these tools allow the simulation of pollutants distribution in time and of their pathway from point sources, and they provide spatial maps of hazard to target organisms or habitats, including socio-economic targets (Melaku Canu et al., 2015, Melaku Canu et al., 2019, Bandelj et al., 2024)

4.1.2 Case study description

The Northern Adriatic is a shallow marine area bordered by Italy, Slovenia, and Croatia, characterized by wide continental shelves, sandy coastlines, and strong seasonal and interannual variability driven by atmospheric and land-based forcing. Its coastal zone hosts dense human activities and major industrial centres, making it highly exposed to multiple pressures.

4.1.3 Methodology

4.1.3.1 Analytical methods

n.a.

4.1.3.2 Experimental methods

n.a.

4.1.3.3 Modelling approaches

Models to simulate fate and transport of pollutants in the Adriatic Sea

The plastic, oil and pharmaceutical transport simulations were performed using the LTRANS-Zlev (Laurent et al., 2020) modeling framework. The Lagrangian model simulates the release of particles from the point sources and tracks their trajectories byapplying advection and diffusion processes driven by three-dimensional hydrodynamic fields provided by the MITgcm ocean circulation model. In addition to velocity fields, the Lagrangian simulations use relevant physical and chemical seawater properties, such as temperature and salinity, to represent substance-specific behaviours and transformation processes.

The hydrodynamic forcing was derived from a high-resolution MITgcm hindcast covering the Northern Adriatic Sea for the period 2017–2021 (Giordano et al., 2025a). The model configuration employs a horizontal resolution of 1/128° (approximately 600 × 850 m in the longitudinal and latitudinal directions) and 29 vertical layers with thicknesses ranging from 1 to 11 m. Initial and open boundary conditions are provided by the CMS Mediterranean Physics Reanalysis (Escudier et al., 2022), while surface atmospheric forcing is supplied by COSMO-2I products from ARPAE. Further details on the hydrodynamic setup are reported in Giordano et al. (2025b).

Oil spill was simulated by explicitly modelling transport and transformation processes, including spreading, evaporation, emulsification, and vertical dispersion, following the approach described in Melaku Canu et al. (2019). The modelling chain reproduces the evolution of oil spills released at specific locations along major shipping routes, accounting for the probability of spill occurrence. Each simulation provides spatial distributions of oil at the sea surface, within the water column, and along the coastline (Melaku Canu et al., 2015; Bruschi et al., 2021). Simulations were performed for each day of the simulated years to capture the full range of meteorological and oceanographic conditions and to account for different oil types (Bandelj et al., 2024).

Plastic pollution was simulated by considering macroplastic inputs from riverine sources and microplastic inputs from both rivers and wastewater treatment plants (WWTPs). Two particle categories were defined: (i) near-surface buoyant particles, representing macroplastics and buoyant microplastics, and (ii) passive particles, vertically mixed within the upper water column, representing neutral or slightly negatively buoyant microplastics. A mass-based approach was adopted, whereby a specific mass of macro- and microplastics was associated with each particle based on the release frequency at each source, the corresponding water discharges ($m^3\ s^{-1}$), and plastic concentrations ($g\ m^{-3}$) from rivers and WWTPs. The combined contributions from all sources were used to estimate plastic concentrations in surface waters (0–3 m depth), expressed in $g\ km^{-2}$.

Pharmaceutical pollution was represented by modelling the dispersion and transformation of Ibuprofen and Diclofenac. The modelling framework was developed within the PNRR National Biodiversity Future Centre (NBFC), Spoke 2, Activity 1.2 “Zero Pollution”, building on observational datasets and internal project collaborations. In the present study, this framework was applied to support a multi-risk assessment for the Adriatic Sea. In addition to transport processes, the Lagrangian model accounts for pharmaceutical degradation mechanisms, including photolysis and microbial degradation, modulated by environmental forcings such as irradiance and temperature.

Mercury speciation, transport, transformation and bioaccumulation of MeHg in Adriatic plankton were simulated using the OGSTM-BFM-Hg model (Rosati et al., 2022). This model couples mercury dynamics with hydrodynamics and biogeochemical cycles of carbon and nutrients, extending to a planktonic food web composed of four phytoplankton functional groups, four zooplankton groups, and one bacterioplankton group (Vichi et al., 2015).

Models implementation and runs

The spatial distribution and magnitude of potential **oil** releases were derived from marine traffic density and vessel typology along the main shipping routes of the Adriatic Sea (Bandelj et al., 2024).

Each spill event was represented by an ensemble of 200 Lagrangian particles, whose trajectories were computed by applying advection and diffusion processes using a second-order Runge–Kutta scheme, including wind drag and a constant horizontal diffusivity of 10 $m^2\ s^{-1}$. Oil weathering sub-processes—spreading, evaporation, emulsification, and vertical dispersion—were dynamically parameterised following standard formulations of oil behaviour (Jokuty et al., 2022). Particles were considered stranded when approaching within 10 m of the coastline. Model outputs were stored at 3-hour intervals for ten days after release, allowing the assessment of both short- and medium-term exposure patterns.

Oil types were selected to represent the main traffic classes (bunker C, diesel, and Arabian Light crude). Their physical and chemical properties (API gravity, viscosity, SARA fractions) and evaporation laws were assigned according to established reference datasets (see Bandelj et al., 2024 for details). Each release scenario was simulated repeatedly over a full meteorological year to ensure statistical robustness across seasonal circulation regimes. Aggregated exposure fields (surface, subsurface, and stranded oil) were summarised at operational time horizons corresponding to 30% and 50% cumulative stranding, typically occurring within 68–185 hours after release depending on oil type, and used to generate exposure maps.

Riverine **plastic** emissions were derived from the global probabilistic model of Meijer et al. (2021) and complemented with estimates from the WWF (2018) report. River inputs were partitioned using a mass-based approach assuming 65% macroplastics and 35% microplastics. Macroplastics were represented as buoyant floating particles, while microplastics were simulated as particles with a range of densities, affecting both their buoyancy and release depth at river mouths. Wastewater treatment plants (WWTPs) were included as point sources of microplastics, released at the depth of sewage diffusers, down to a maximum depth of 50 m.

Microplastic emissions from WWTPs were estimated by combining average mass loads expressed in mg $PE^{-1}\ yr^{-1}$ with discharges proportional to population equivalent and effluent concentrations dependent on treatment level, accounting for the large variability reported in the literature. An average target emission of 200 mg $PE^{-1}\ yr^{-1}$ was adopted and obtained through an iterative calibration procedure, whereby population-equivalent emission factors for each treatment category were adjusted according to their cumulative removal efficiencies.

The simulations yielded average surface microplastic concentrations of approximately 112.5 g km^{-2}, lower than the ~217 g km^{-2} reported for the Adriatic Sea. To account for external inputs and legacy plastics, a uniform background concentration of 105 g km^{-2} was added. Final concentration maps were computed by combining floating and neutrally buoyant microplastics within the upper 3 m of the water column, consistent with available observational evidence on sampling depth and vertical distribution, and expressed as surface mass per unit area (g km^{-2}).

Emerging pollutants: Lagrangian particles representing Ibuprofen and Diclofenac were released from WWTP locations at the depth of sewage diffusers, down to a maximum of 50 m. For river sources, particles were released both at the surface and at the estimated local river depth (up to 30 m). In rivers with estimated depths between 10 and 30 m, additional releases were distributed along the water column at 10 m intervals. Particles were released daily from each source over a five-year simulation period (2017–2021), and their trajectories, driven by prescribed hydrodynamic fluxes, were followed for one year after release.

Pharmaceutical loadings from rivers and wastewater treatment plants (WWTPs) were defined using concentration data provided by the University of Ancona within the framework of the National Biodiversity Future Centre (NBFC). Measured concentrations in river waters and in WWTP effluents were combined with source-specific water discharge data to estimate the total pharmaceutical inputs from each point source to the Adriatic Sea.

The first year of the simulation (2017) was used as a spin-up phase, allowing the system to reach stable concentration levels, while modelled pharmaceutical concentrations were computed by averaging the remaining four years (2018–2021).

4.1.4 Results

The **oil spill** modelling framework provides spatially explicit exposure and hazard maps by combining the probability of spill occurrence along shipping routes with hydrodynamic and meteorological conditions. As an illustrative example, Figure 4.1.1 shows the evolution of a representative bunker oil spill released along a major shipping route under specific environmental conditions. In this case, shortly after the release (11 hours), oil is transported over large offshore areas and reaches coastal zones both at the surface and within the water column. The most exposed coastal segments in this case are located along the Italian coast between Venice and the Po River delta, extending southward towards Ravenna and Ancona, as well as along the northern part of the Croatian island of Cres and the adjacent mainland coast near Rijeka. As transport and weathering processes evolve: after two days from the release, stranded oil affects most of the northern Italian coastline and along the Istrian Peninsula.

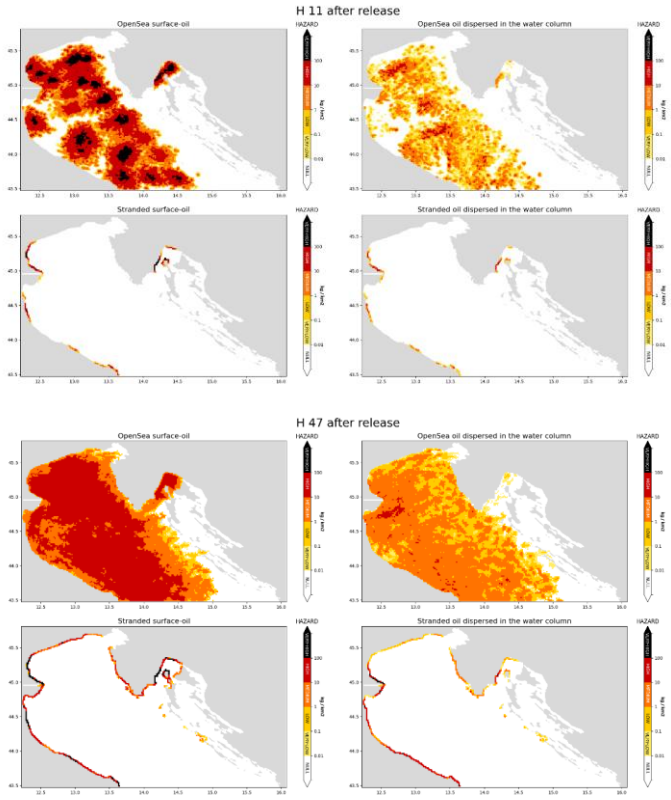

Figure 4.1.1: Potential bunker oil slicks released along the main shipping routes of the northern Adriatic (expert set of release sites) pose a threat to coastal areas at short time scales (11 hours after release), both at the surface and in the water column.

The simulated distributions of **macroplastics** and microplastics in surface waters (0–3 m depth), averaged over four years following a one-year spin-up, show marked spatial heterogeneity across the Adriatic Sea (Figure 4.1.2). Higher concentrations are consistently found in proximity to major river mouths and along coastal regions influenced by riverine inputs, while offshore concentrations decrease due to dilution and dispersal.

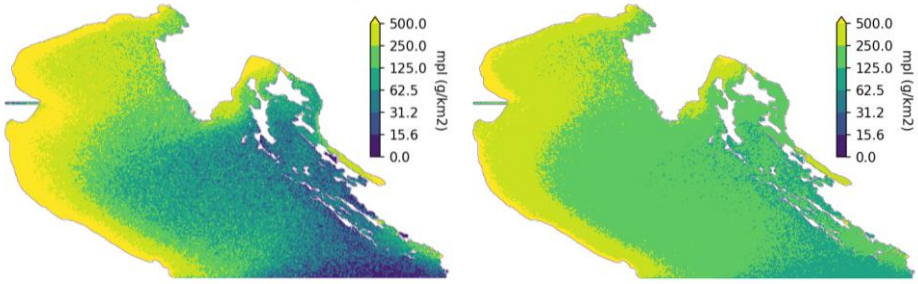

Figure 4.1.2: Macroplastics (left) and b) Microplastics (right) modelled concentrations in surface waters (0-3 meters depths).

Rivers dominate the microplastic inputs to surface waters, accounting for approximately 111 g km^{-2}, whereas wastewater treatment plants contribute less than 1 g km^{-2}. Floating microplastics from rivers represent the largest fraction, followed by neutrally buoyant microplastics, while contributions from WWTPs are negligible at the basin scale. When including an additional uniform background concentration to account for external sources and legacy plastics, the total mean surface microplastic concentration reaches approximately 217 g km^{-2}. These results suggest that a substantial fraction of microplastics present in the Adriatic Sea originates from sources outside the model domain or from releases predating the simulated period, highlighting the long residence times of plastic debris in the marine environment.

To the best of our knowledge, this work represents the first attempt to model the fate of **emerging pollutants** in the Adriatic Sea. The modeled distributions of Ibuprofen and Diclofenac in the surface (0 – 5 m depth) and deeper water (< 5 m depth) of the Adriatic Sea, averaged over the four years of simulation, are shown in Figures 4.1.3. Concentrations tend to be higher at the surface than in deeper waters, with a few exceptions in close coastal areas such as the central Croatian coast. A general decreasing gradient moving offshore is predicted for all drugs investigated, consistent with dilution and degradation processes. However, modeled concentrations of ibuprofen are generally much higher than those of diclofenac, due to the different degradation rates combined with different levels of loadings. These contrasting behaviors agree with available observations in the Gulf of Trieste and the Ancona coast. More field data would be needed to better address the spatial and temporal variability of different compounds and carry out a robust validation of the model results. Nonetheless, at the state of the art, the capability to reproduce the main differences among different drugs through the model demonstrates that the approach adopted is conceptually robust and can be informative for this class of chemicals.

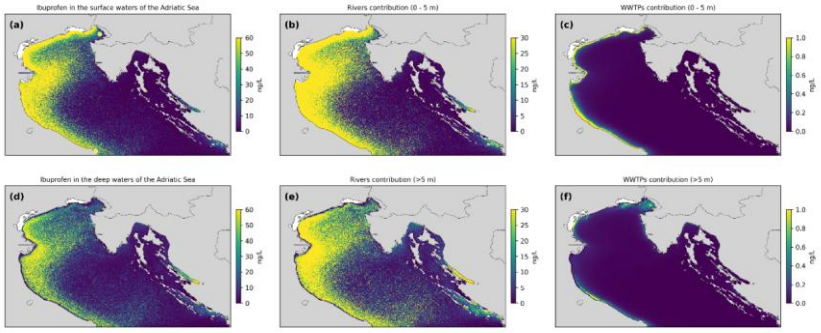

Figure 4.1.3: Average distribution of Ibuprofen in (a) the surface (0 – 5 m depth) and (d) deeper water (< 5 m depth) of the Adriatic Sea. Contributions from rivers (b, e) and wastewater (c, f) are shown for the same water layers.

The OGSTM-BFM-Hg **mercury** model provided key insights into the spatial, seasonal, and interannual variability of Hg species concentrations in the Adriatic Sea, providing a solid background to support environmental monitoring and risk assessments. The modeled concentrations of MeHg in different phytoplankton and zooplankton functional types are shown in Figure 4.1.4. The highest MeHg concentrations were predicted in the plankton food web of the coastal areas of the North Adriatic and in the open water of the South Adriatic.

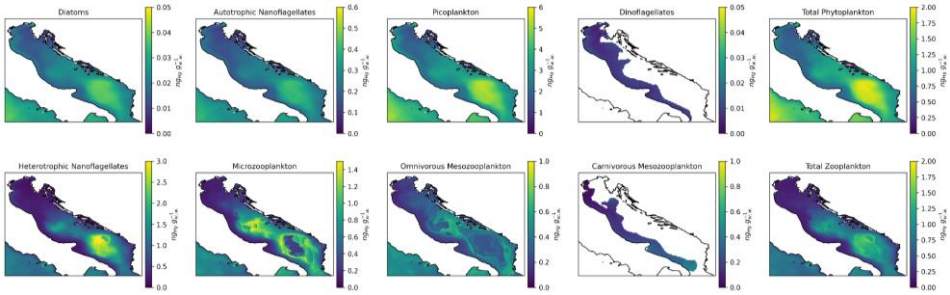

Figure 4.1.4: Average MeHg concentrations in different functional groups of phytoplankton and zooplankton in the upper 100 m depth from a multi-year simulation.

4.1.5 Scientific products and dissemination

Published papers:

Rosati, G., Solidoro, C., Laurent, C., Aveytua Alcázar, L., Umgiesser, G., & Canu, D. (2024). Mercury cycling in contaminated coastal environments: modeling the benthic-pelagic coupling and microbial resistance in the Venice Lagoon. Water Research, 261, 121965. https://doi.org/10.1016/j.watres.2024.121965

Ginevra Rosati, Cosimo Solidoro, Celia Laurent, Leslie Aveytua Alcàzar, Donata Canu. Mercury in the Venice lagoon from sources to receptors: a modelling study. In Sfide scientifiche e gestionali per una società resiliente ai rischi ambientali in un clima che cambia. Tognolli, A., Fonti, V., Lipizer, M., & Solidoro, C. Conference proceeding del convegno di disseminazione RETURN. Trieste, 4-6 March 2025

Célia Laurent, Gaia Buccino, Ginevra Rosati , Cosimo Solidoro, Donata Canu. Pollutants modelling with LTRANS-Zlev. In Sfide scientifiche e gestionali per una società resiliente ai rischi ambientali in un clima che cambia. Tognolli, A., Fonti, V., Lipizer, M., & Solidoro, C. Conference proceeding del convegno di disseminazione RETURN. Trieste, 4-6 March 2025

Ginevra Rosati, Cosimo Solidoro, Donata Canu. Modelling Mercury Bioaccumulation in Reared Clams from a Temperate Polluted Lagoon. International Conference on Mercury as a Global Pollutants ICMGP2024, Capetown (SA), 21-26 July, 2024.

Dissemination:

Organization and co-chair of the special session “Hg and MeHg in marine food webs” at the ICMGP2024 conference, Capetown, Sud Africa.”. Capetown (SA), 21-26 July, 2024.

Rosati, G. "Un mare di inquinanti", webinar on pollution in marine ecosystems for the artists participating in the project MareDireFare 2025, festival of Art and Science. https://www.maredirefare.it/. Online, 05 February, 2025.

Rosati, G. Modelling Mercury Cycling in a Contaminated Coastal Environment. DANUBIUS Workshop on Coastal Ecological Modelling. Online, 29 October, 2024.

4.2 Analysis and distribution of macro and micro litter as a function of marine and coastal environments and dynamics (UNIBA)

4.2.1 Introduction

Marine and beach litter, which is defined as "any persistent, manufactured or processed solid material discarded, disposed of or abandoned in the marine and coastal environment" (UNEP, 2009), constitutes a constantly growing worldwide environmental issue for managers and researchers due to the million tons of litter entering every year oceans and seas from different sources. In this context, the high density of beach litter (BL (items >2.5 cm) and microplastics (MPs - particles < 5 mm) poses a constant environmental risk to coastal areas and related ecosystems. Effective monitoring programs and management plans are therefore required to enhance coastal conservation and protection. The Mediterranean region represents one of the areas most affected by the presence of ML and BL (UNEP-MAP, 2015), due to the semi-closed conformation of the basin and limited water exchange, thus favoring the litter accumulation both on the sea surface and along the coasts. For this reason, monitoring activities are carried out at the national level by countries facing the Mediterranean Sea. By way of example, in Italy, the Institute for Environmental Research and Protection (ISPRA), on behalf of the Environmental Ministry, coordinates the national beach monitoring activities that are locally carried out by the Regional Environmental Agencies (ARPA). Data derived from the in-situ monitoring activities are then elaborated to calculate the linear density and the CCI values, which are therefore used as indicators for the beach characterization in the frame of the United Nations Sustainable Development Goals and the European Marine Strategy Framework Directive (2008/56/EC). The most updated data show that the BL linear density along the Italian beaches remains very high (median of 250 litter/100 m) compared to the threshold value (20 objects/100 m) set at the European level for achieving Good Environmental Status (Hanke et al., 2025). As highlighted by Rizzo et al. (2024), the integrated analysis of BL, MPs, and shoreline evolution should be considered a mandatory requirement for the integrated geo-environmental characterization of any coastal site. For this reason, the activities performed in the frame of Task 3.2 were aimed at proposing a multi-technology approach to identify, characterize, and model BL and MPs in the different coastal and marine sub-environments (i.e., beach sediments, marine sediment from the upper shoreface, lower shoreface, and offshore) and on the water surface, allowing the definition of the beach quality state from a multi-disciplinary perspective.

Field surveys and laboratory analyses, coupled with the exploitation of UAV images, hyperspectral data, and machine learning tools, contribute to assessing the level of pollution and the consequent environmental quality. Furthermore, based on BL and MPs densities, a numerical model has been applied to simulate the litter dispersion in the marine environment.

The assessment of BL distribution was carried out by applying both standard in-situ procedures and innovative methods based on the use of drones and imaging classification approaches (both manual and automatic) that solve the logistic limitations related to the in-situ surveys. Furthermore, the analyses were integrated with the assessment of the predominant morphodynamical processes (in terms of coastal erosion and/or accretion processes) and with the occurrence of storm events. Such kind of data provided useful informative layers for identifying coastal sectors prone to be affected by BL accumulation and burial.

The assessment of the MPs content in coastal and marine sediments and sea water has required the definition of tailored sampling procedures. Furthermore, both standard (e.g., µRaman) and innovative techniques (e.g., based on the exploitation of the oil olive) are applied for the MPs classification.

In Figure 4.2.1, a schematic representation of the procedures proposed for the monitoring and analysis of the BL and MPs in marine and coastal environments is proposed. Field activities are performed to analyze the

abundance and typology of BL items estimated by both in situ direct activities and indirect analysis by UAV images exploitation. MPs analyses are performed on both marine and beach sediments and seawater samples. Then, specific environmental indices are calculated to define the environmental quality of the investigated sites, i.e., the Clean Coast Index (CCI - Alkalay et al., 2007) and the Microplastics Pollution Index (MPPI - Rangel-Buitrago et al., 2020, 2021; Abelouah et al., 2022). Obtained data enable the identification of litter accumulation hotspots, for which tailored management practices are needed.

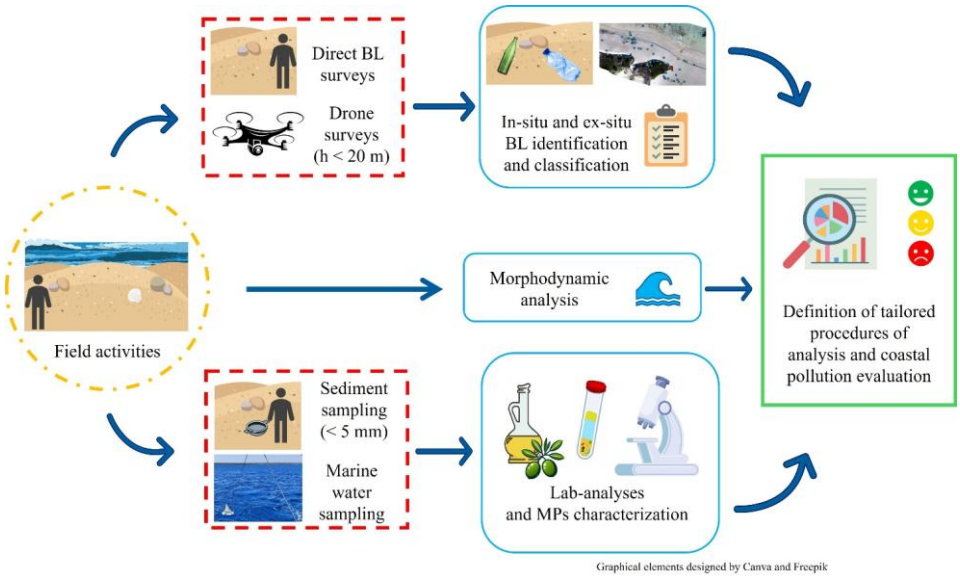

Figure 4.2.1: The flow chart shows the procedures for the MPs and BL analysis in coastal environments.

It is worth noting that during the project, the UNIBA team has also worked in collaboration with the UNIROMA1 and UNIGE teams. Activities performed in the frame of the collaboration with UNIROMA1 were focused on the testing of innovative procedures for automatic polymer classification based on the hyperspectral imaging (HSI) approach. For what concerns the collaboration with UNIGE, sediment samples from the port of Genoa have been analysed by different research groups involved in the task activities by applying different procedures to allow the comparison among the obtained results.

4.2.2 Case study description

Field and sampling activities were carried out in several coastal sites of the Apulia Region, Southern Italy, including both Adriatic and Ionian sides (Figure 4.2.2). The investigated areas were selected for their significant economic value, as they are popular tourist destinations during the summer months. Furthermore, the area of Taranto is also characterized by a high level of urbanization and the presence of several industrial sites.

In detail, the BL monitoring activities were performed on the Adriatic coast at Capitolo beach (Bari province) and Torre Guaceto beach (Brindisi province) while sediment samples were collected both in emerged and submerged environments, on the Adriatic side (Torre Guaceto beach, the Adriatic offshore area) and the Ionian side (Gulf of Taranto and Pino di Lenne beach) of the Apulian coast.

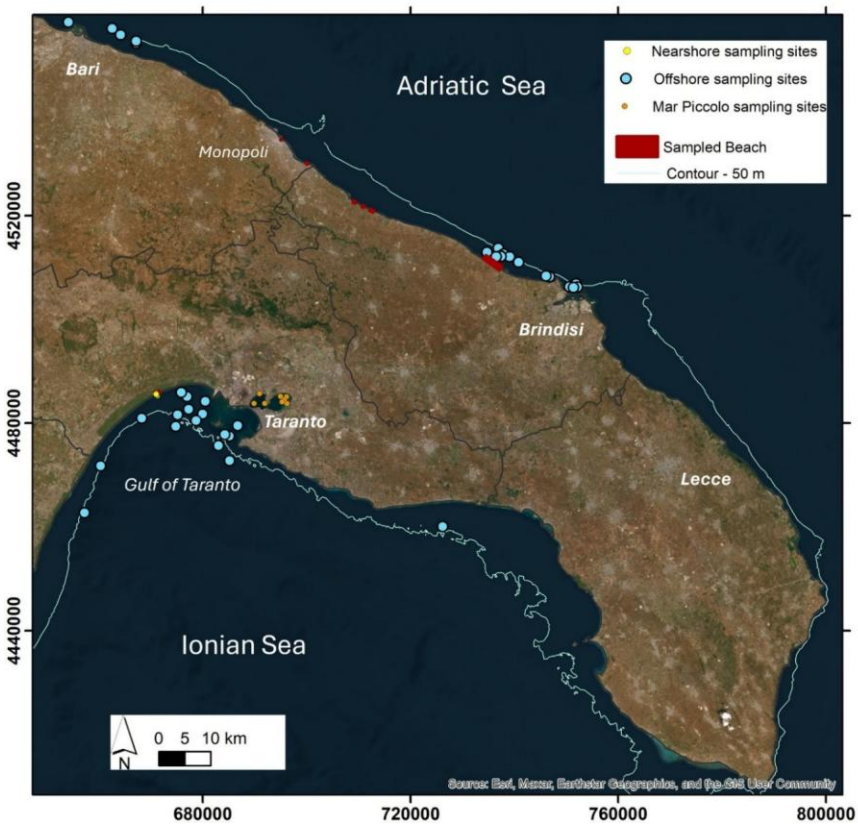

Figure 4.2.2: Investigated sites in the Apulian region.

Torre Guaceto beach is included in a natural protected area established to preserve the local habitat biodiversity and protect a wide wetland separated from the sea by the dune system. The area was selected as a test site since not subject to scheduled cleaning activities, due to the lack of touristic and recreational services. Furthermore, the investigated coastal sector is characterized by the presence of the mouth of "Canale Reale", which is a 48 km long creek that acts as a potential litter source, especially during the occurrence of heavy rain events.

Capitolo beach is is located along the Adriatic coast of Apulia and it characterized by a predominant erosion process with a shoreline retreat ranging from a minimum value of – 8.24 to a maximum value of -2.47 m in the last 10 years, with an average value of -5.09 m. Recently, Scarrica et al. (2022) conducted a preliminary study on the environmental conditions of this area, which revealed that most of the identified macroplastics included bottles, caps, food containers, and fishing nets (or fragments of nets), mostly deriving from mariculture and fishing industry. The presence of these items is closely linked to beach recreational use, which significantly increases during the summer months when the beach attracts many national visitors, and fishing activities.

The Gulf of Taranto, and in particular the Mar Grande and the Mar Piccolo basins, are semi-enclosed basins characterized by the presence of high-density anthropogenic activities, including industrial districts, shipyards and arsenals, and intensive mussel aquaculture plants, which have led to major environmental modifications. For this reason, the marine and coastal area of Taranto is included in the list of Sites of National Interest, for which urgent remediation activities are required.

The sandy beach of Pino di Lenne, along the Gulf of Taranto, features small *Sabellaria alveolata* bioconstructions and the mouth of a minor stream from a karstic spring (Lenne River). Located within the Stornara Nature Reserve, a SIC and SPA protected area, the site is largely free from human disturbance. It represents a typical segment of the Taranto Ionian coast, offering a natural laboratory for studying coastal and ecological dynamics.

4.2.3 Methodologies

To assess the density and spatial distribution of both microplastics (MPs – i.e., particles < 5 mm) and beach litter (BL – items > 2.5 cm) along the investigated beach, international procedures were applied for items' collection and classification as well as MPs sampling and analysis (Fleet et al., 2021; Galgani et al., 2023). Furthermore, tailored environmental indices were used to define the environmental quality of the beach sector investigated. the following sub-sections detail on the analytical, experimental, and modelling approaches are provided.

4.2.3.1 Analytical methods

BL and MPs sampling activities

The in-situ BL visual assessment was conducted following the international guidelines (Hanke et al., 2013; Vlachogianni, 2017), which suggest investigating a 100 m long coastal sector, from the shoreline to the inland natural or anthropic limit (Figure 4.2.3a). All BL items bigger than 2.5 cm were classified according to the Joint List of Litter Categories for marine macro-litter monitoring proposed by the European Commission (Fleet et al., 2021). In-situ surveys were performed mainly in spring, during favorable weather conditions. Furthermore, monitoring activities were also carried out pre- and post- the occurrence of marine storms, to investigate the potential effects of waves and currents on the litter displacement and accumulation.

Innovative BL assessment procedures were based on the exploitation of images acquired by UAV photogrammetric images and their analysis. In detail, photogrammetric images were acquired by using the multirotor quadcopters "DJI Inspire 2" equipped with a "DJI Zenmuse X5S" optical camera (20.8 MP, DJI MFT 15 mm/1.7 ASPH supported lens, 4/3" CMOS sensor, FOV 72◦ and image resolution 5280×3956 pixel) and "DJI Phantom 4 Pro" equipped with a "DJI Phantom" optical camera (20.8 MP, 1" Exmor R CMOS sensor, FOV 84° and image resolution 5472× 3648 pixel). To define the best setting, UAV surveys were carried out at flight heights ranging from 5 to 20 m Above Ground Level (AGL) of the take-off location. Furthermore, the high-precision georeferencing procedure was ensured by the use of the Ground Control Points (GCP) coordinates acquired with the "Stonex S9III-N" Global Navigation Satellite System receiver in Real Time Kinematic (GNSS-RTK) mode to ensure vertical and horizontal accuracy of about 0.02 m and 0.01 m, respectively. To comply with monitoring guidelines, 100 m long sectors were surveyed (Figure 4.2.3a). Then, image post-processing was executed using Agisoft Metashape Professional, which allowed for obtaining the digital elevation model and the orthomosaics of the investigated sites.

BL identification and classification on orthomosaics were performed by applying both a manual visual screening approach and an automatic procedure. Visual screening, carried out in a GIS environment, allowed to obtaining a database of detectable elements and to produce BL distribution and density maps (Figure 4.2.1). The automatic BL identification was performed based on a tailored system of analysis described in section 4.2.3.3.

To assess the MPs content in beach sediments, samples were collected at different points along the backshore (Figure 4.2.3a). The sampling points were selected along transects perpendicular to the shoreline, at the morphological steps of the berms, and at the base of the dune. By using an ASTM Sieve (4000 microns), a first sieve was carried out directly on the beach to collect the sediment fraction representative of the MPs size (Figure 4.2.3b). Using a steel sampling spoon, two samples of sediment were collected for each sampling point, with a variable weight ranging from 400 to 500 g, both at the beach surface and at a depth of approximately 5-10 cm.

The offshore sampling activities were supported by the Marina Militare Italiana (Italian Navy) and Lega Navale Italiana (LNI) who made their vessels available to support sampling activities. Marine sediment samples were collected using a sediment grab installed on board of ship (Figure 4.2.3c) while sea water samples were collected with a manta net (Figure 4.2.3d).

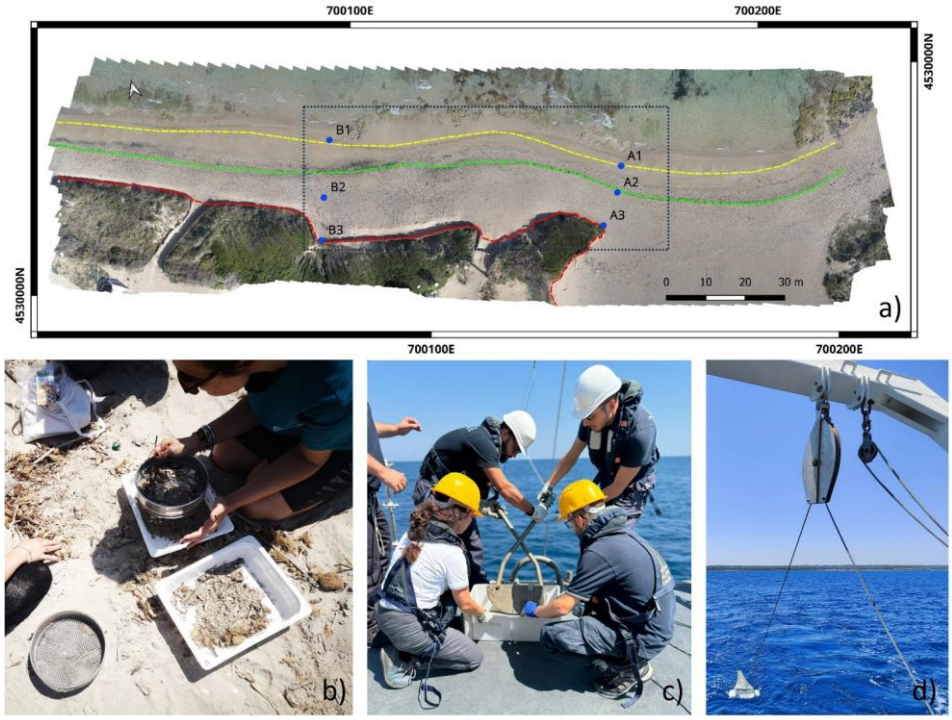

Figure 4.2.3: a) Sampling points for MPs analysis are indicated in blue, while the area monitored for BL analysis is delimited by a white dotted rectangle. Coloured lines represent the main beach morphologies. b) Example of beach sampling activities. c) Example of offshore sediment activities d) Manta net used for marine surface water sampling.

Offshore sampling sites were selected based on the location of the main harbors and river mouths (c.f., Figure 4.2.2). Sampling sites in the Gulf of Taranto were selected based on a preliminary analysis of the marine substrate derived by the interpretation of morpho-acoustic data, while in the Mar Piccolo basin, sites were identified mainly accounting for the distribution of the mussel farm plants, which limit ship navigation.

MPs Analyses

To evaluate the MPs concentration, the collected samples were dried in an oven for approximately 48 hours at a temperature not exceeding 45 °C. Once this phase was completed, the samples were weighed using a precision balance to determine their dry weight. Then, the procedure proposed by Scopetani et al. (2020), which is based on the use of olive oil, was applied to extract MPs from sediment samples. To avoid contamination, all the analysis steps were carried out by using glass bakers, also cleaned with compressed air, stainless-steel accessories, and wearing laboratory clothing.

Organic matter digestion

Before separating MPs from the sediment, a digestion phase was performed to eliminate the organic matter present in the samples. Following the marine plastic monitoring guidelines published by Galgani et al. (2023), Hydrogen peroxide (H_2O_2) was used as an oxidizing agent. During the digestion phase, a sediment sample from each size class was placed in a glass beaker, and then approximately 25 mL of 30 % H_2O_2 was added for 24 hours. After digestion, the remaining oxidized organic matter in the beaker was eliminated by rinsing the sample thoroughly with distilled water using a sieve with a mesh size of 100 µm, which is the smallest particle analyzable size.

MPs Extraction

To apply the method proposed by Scopetani et al. (2020) for the MPs separation, 15 g of sample and 30 mL of pure water were put in a 50 mL conical test tube in polypropylene. This mixture was mixed by sealing the top of the test tube. Then, 5 mL of olive oil was added, and the mixture was remixed to ensure that sediment and water came into contact with the oil and was left to rest for 5 minutes. This procedure was applied twice; therefore, for each sample, a total of 30 g of sediment was analyzed. Because oil has a lower density than water, it floated to the top, carrying MPs particles. This was made possible by the oleophilic property of plastic polymers, as they repel water and have an affinity for oil, adhering to their surface (Crichton et al., 2017). The prepared sample was placed in a freezer at -4 °C for 24 hours to prevent the oil from dispersing. Freezing the sample was useful as it allowed easier extraction of the accumulated oil layer. Once the ice-oil mixture was separated from the sample, the filtration phase started. Using a vacuum pump and a glass flask system, the sample was filtered through a Whatman GF/D glass microfiber filter with a diameter of 70 mm, which retained the solid particles while allowing the liquid to pass through. To remove any traces of oil from the filter and retained particles, the sample was rinsed with 50 mL of ethanol, as described by Mani et al. (2019) and Battaglini et al. (2024). To recover any MPs that may have been trapped in the oil residues still clinging to the walls of the beakers used for used to contain the extracted ice oil portion, the beakers were rinsed with pure water and ethanol. The resulting solution was then filtered through the same filter.

MPs Characterization

To conduct a careful and precise observation of the filtered sample, each filter was examined using a reflected light optical Opticka microscope (with 2x, 3x, and 4x objectives). By the use of the optical microscope and an integrated camera, it was possible to capture high-resolution images for each filter and identify MPs particles up to 100 µm. To allow each acquired image to have a reference scale, the imageJ software was used. Furthermore, the counting was organized by categorizing the MPs according to their type, colour, and morphological classes, following the classification proposed by Galgani et al. (2023). In detail, the following classes were taken in consideration: fibers, filaments, fragments, films. The obtained quantities were subsequently converted into density values expressed as MPs per kilogram (MPs/kg).

Granulometric Analysis

The samples were analyzed for grain size distribution following standard procedures, combining two methodologies. ASTM sieves were used for the coarser fractions, ranging from the largest particle present in the sample down to 4φ (0.063 mm), while the Beckman Coulter Multisizer 4 and laser sedigraph analysis were employed for the finer fractions, from 5φ (0.032 mm) down to 9φ (0.002 mm). The grain-size scale applied has an interval of 1φ, where $\varphi = -\log_2 d$ and d is the sieve mesh size in millimeters.

Before analysis, samples were oven-dried at 80°C for 24 hours, quartered, and placed into the sieve column. To enhance sieving efficiency, particularly for the finer fractions, the stack of sieves was placed on a vibrating shaker for 20 minutes. Each retained fraction was then weighed, and the results processed using the GRADISTAT software (v8, Blott & Pye, 2001), which generates cumulative particle-size distribution curves, histograms, and calculates key textural parameters.

The statistical parameters obtained include:

- Mean ($\bar{x}$) – the center of gravity of the particle-size distribution, calculated as a weighted average.
- Sorting (σ) – indicating the degree of uniformity or selection in particle diameters.
- Skewness (Sk) – describing the asymmetry of the distribution curve.
- Kurtosis (K) – indicating the peakedness or flatness of the distribution curve.

This integrated approach allows for a comprehensive characterization of both coarse and fine sediment fractions and the extraction of the main textural parameters (mean grain size, sorting, skewness, and kurtosis) according to ASTM and British Standard methodologies.

Pollution Indices calculation

To assess the environmental quality of the analyzed beach based on BL and MPs abundance, the Clean Coast Index (CCI - Alkalay et al., 2007) and the Microplastics Pollution Index (MPPI - Rangel-Buitrago et al., 2020, 2021; Abelouah et al., 2022) were used. These indices evaluate the environmental quality of a beach by examining the relationship between the quantity of BL and MPs and the extent of the surveyed area. Once the indices are calculated, they are classified according to the classification proposed in the literature (Rangel-Buitrago et al., 2020, 2021; Akarsu et al., 2022).

4.2.3.2 Experimental methods

Innovative methods are applied for the characterization of polymers identified in sediment samples and are based on the application of hyperspectral imaging (HSI) approaches developed by the UNIROMA1 team, which are described in Thematic Chapter 4.6.

4.2.3.3 Modelling approaches

BL automatic identification

This subsection reports the procedures proposed for the automated identification and classification of BL items by using orthomosaics derived from UAV images.

A first algorithm exploited Mask Region-based Convolutional Neural Network (Mask-RCNN). As described in Scarrica et al. (2022) and Sozio et al. (2023), its architecture is based on Faster-RCNN and performs an instance segmentation based on a pre-training phase on the COCO dataset (Lin et al., 2014). The automatic identification was conducted by splitting the available dataset into training and test sets, which consisted of multiple tiles obtained from orthomosaics with associated polygon shapefiles, relative to the BL items. In detail, the training phase consisted of manually labeling litter objects on images and cataloging them in 5 classes. The manually labeled objects were used by the algorithm to produce a train model file, containing all information to differentiate objects of each class. In the testing phase, the algorithm exploited the train model file to automatically identify and classify objects in images not used before. To evaluate the performance of the proposed method, the mAP@IoU (Everingham et al., 2010) was used. This parameter expresses the overlapping area between the predicted masks produced by the algorithm and the manually digitized reference polygon (adopted as ground truth). Finally, the script of the proposed algorithm was also implemented with a further feature for georeferencing the segmentation outputs.

The second model is based on the exploitation of Computer Vision techniques. In detail, the proposed procedure leverages the Segment Anything Model (SAM; Kirillov et al., 2023) for segmentation and the Vision Transformer (ViT; Dosovitskiy et al., 2021) for the subsequent classification of segmented objects. SAM, developed by META AI, is a panoptic segmentation system that can be applied to any image without requiring additional training. Its training dataset includes over 1.1 billion masks collected from approximately 11 million images, enabling accurate and comprehensive segmentation of all recognizable elements within an image. SAM is employed in the first stage of image processing, where panoptic segmentation is performed. The outcome of this operation consists of the masks corresponding to the beach litter items present in the image and identified by SAM. The individual masks were then selected by an operator and organized into specific folders associated with the categories of beach litter, in order to filter out irrelevant or extraneous masks and to balance, as much as possible, the number of masks for each category. At this stage, 11 categories were proposed. A Vision Transformer (ViT) is a type of machine learning model that uses processing blocks capable of analyzing input data in parallel. ViT required a tailored training phase. At the end of the training phase, a model file was generated, containing the weights computed during training. During the subsequent testing phase**,** ViT used the information stored in the model file to classify object masks that had not been used during the previous training and validation stages. The result of the testing phase is represented by the confusion matrix along with the accuracy, precision, Recall, and F1-score value. This procedure of analysis has been developed in the framework of the collaboration agreement with the Department of Science and Technology of the University of Naples "Parthenope".

A Lagrangian Framework for Simulating the Dispersal and Fate of Marine Plastic Debris

This subsection reports the joint analysis of meteo-marine parameters with floating plastic distribution along the Apulian coasts. Here, two kinds of datasets were selected to analyze the floating and transportation of plastic debris from the offshore to the nearshore/foreshore zones:

- Current dataset derived from Copernicus reanalysis considering eastward (u0) and northward (v0) sea water velocities up to 10 m of the water column.
- Density of marine plastic debris derived from manta net surveys and subsurface water samples.

The main results obtained are referred to the main tracks followed by marine plastic debris based on the current fields and maps of particle density.

The transport and dispersion of marine plastic debris were modelled in “plastiparcels” for the Apulian offshore zones. The “plasticparcels” is an open-source, Python-based software package designed for the simulation of the transport, dispersal, and environmental fate of marine plastic debris. It is a highly specialized extension built upon the foundational Parcels (Probably A Really Computationally Efficient Lagrangian Simulator) framework. The core innovation of plasticparcels lies in its translation of the complex physical and biogeochemical processes affecting plastic particles in the marine environment into a customizable Lagrangian particle-tracking model. In this paradigm, individual plastic items or aggregates are represented as discrete, virtual particles ("parcels") whose trajectories are computed through numerical integration of velocity fields derived from oceanographic models.

The model operates through a modular structure that governs particle advection and a suite of state-transformation processes:

- **Advection:** The primary driver of movement is oceanic and atmospheric circulation. Particles are advected by 2D or 3D current fields. A key feature is the incorporation of **wind drag** acting on the exposed surface of floating debris, parameterized through a wind drift factor (often a percentage of surface wind velocity), which is critical for accurately simulating the transport of buoyant plastics.
- **Particle Characterization:** Particles are defined by a set of initial properties (e.g., size, density, shape, polymer type). These properties are not static; they evolve dynamically based on environmental conditions, driving the model's state-transformation processes.

Further processes are parameterized to obtain the plastic persistence in the water column and along the coast:

- **Vertical Mixing:** Simulates the effect of wind-driven mixing and turbulence, moving particles between the surface layer and the water column. This is often implemented as a random walk or deterministic mixing parameterization.
- **Biofouling:** A central and sophisticated process within plasticparcels. The model simulates the colonization of particle surfaces by algae and bacteria, which increases their density. This can trigger a **vertical velocity** (sinking or rising), moving particles out of the wind-driven surface layer and into deeper, differently flowing water masses. The rate of biofouling growth can be a function of water temperature and nutrient availability.
- **Degradation:** Models the fragmentation and mass loss of particles due to UV radiation (photo-degradation) and mechanical weathering, potentially altering their size and buoyancy over time.
- **Beaching:** Particles are removed from the active simulation when they interact with coastlines. Parameterizations can determine whether beaching is permanent or temporary (resuspension after a time period).

Here, we considered the reanalysis dataset of MEDSEA_MULTIYEAR_PHY_006_004 (Clementi et al., 2019; Escudier et al., 2020) to assess the advection processes. The dataset reports the u0 and v0 hourly current components in a netCDF file with 0.04x0.04 degrees of cell resolution. The current speed was assessed through the following relationship, for each cell in a given time:

The particle characterization was obtained from direct sampling performed in the offshore areas of the Apulia coasts (Table 4.2.1). The particle characterization is represented by density in the sample point and radius of the debris.

Table 4.2.1: Particle characterization for the different surveys considered for the model simulation.

ID	Lat and Lon of sample points	Time of simulation	Kind of surveys	Density (items/m2)	Radius of debris (m)
Survey-02042016	1) 40.24N 17.8E 2) 40.23N 17.87E 3) 40.18N 17.79E 4) 40.47N 17.17E 5) 40.45N 17.18E 6) 40.38N 17.13E	01/02/2016-01/04/2016	Manta net (Dalle Mura et al., 2022)	1) 0.325 2) 0.325 3) 0.325 4) 0.325 5) 0.325 6) 0.325	1) 0.001 2) 0.001 3) 0.001 4) 0.001 5) 0.001 6) 0.001
Survey-09112016	1) 40.24N 17.8E 2) 40.23N 17.87E 3) 40.18N 17.79E 4) 40.47N 17.17E 5) 40.45N 17.18E 6) 40.38N 17.13E	01/09/2016-31/10/2016	Manta net (Dalle Mura et al., 2022)	1) 0.501 2) 0.501 3) 0.501 4) 0.501 5) 0.501 6) 0.501	1) 0.001 2) 0.001 3) 0.001 4) 0.001 5) 0.001 6) 0.001
Survey-09112017	1) 40.24N 17.8E 2) 40.23N 17.87E 3) 40.18N 17.79E 4) 40.47N 17.17E 5) 40.45N 17.18E 6) 40.38N 17.13E	01/09/2017 26/11/2017	Manta net (Dalle Mura et al., 2022)	1) 0.43 2) 0.43 3) 0.43 4) 0.43 5) 0.43 6) 0.43	1) 0.001 2) 0.001 3) 0.001 4) 0.001 5) 0.001 6) 0.001
Survey-092019	1) 41.5N 16.15E 2) 41.2N 17.4E 3) 40.9N 18E	01/09/2019-30/09/2019	Niskin	1) 0.26 2) 0.08 3) 0.08	1) 0.001 2) 0.002 3) 0.0005
Survey-10122020	1) 40.24N 17.8E 2) 40.23N 17.87E 3) 40.18N 17.79E 4) 40.25N 17.3E 5) 40.26N 17.3E 6) 40.22N 17.3E	01/10/2020 30/11/2020	Manta net (Trani et al., 2023)	1) 2.33 2) 2.33 3) 2.33 4) 2.33 5) 2.33 6) 2.33	1) 0.001 2) 0.001 3) 0.001 4) 0.001 5) 0.001 6) 0.001
Survey-02042021	1) 40.3N 18.55E 2) 40.25N 18.55E 3) 40.27N 18.5E	01/02/2021 20/04/2021	Manta net (Trani et al., 2023)	1) 1.9 2) 1.9 3) 1.9	1) 0.001 2) 0.001 3) 0.001
Survey-01102024	1)41.16N 18.63E 2) 41.16N 18.66E	01/10/2024 31/10/2024	Manta net	1) 1.8 2) 1.1	1)0.002 2)0.002

4.2.4 Results

Regarding the BL analysis, direct surveys allowed for defining the litter density along the investigated coastal sectors (Figure 4.2.4). Obtained density values ranged from 0.03 items/m^2 (estimated at Capitolo beach by the visual screening of orthophoto) to 0.47 (estimated at Torre Guaceto beach by direct in situ surveys). In all the investigated sites, most of the detected elements were artificial polymers (>80 %).

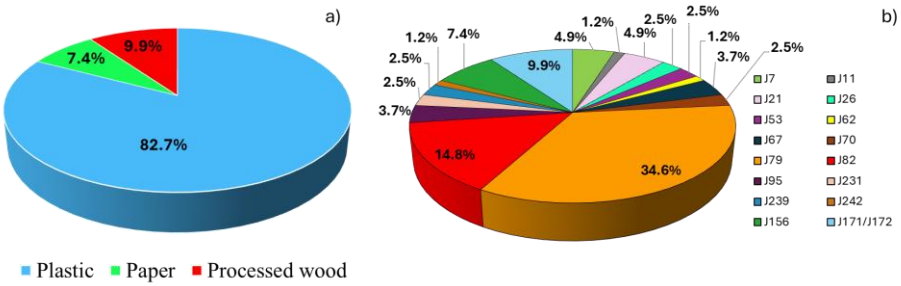

Figure 4.2.4: Graphs reporting a) the percentage of BL materials and b) BL categories detected through the visual screening task (BL codes refer to the classification proposed in Galgani et al., 2021). Data refer to the monitoring activities carried out at Capitolo.

According to the Clean Coast Index (CCI) classification, the BL density of 0.03 items/m² places Capitolo beach in the "very clean" category. However, it is worth noting that the screening performed on UAV images is unable to detect objects smaller than 2.5 cm, such as cigarette butts, which are responsible for significant beach pollution and ecological impacts (Loizidou et al., 2018; Araújo and Costa, 2019; Asensio-Montesinos et al., 2021). Therefore, the density value can be considered understated. By analysing the spatial distribution of BL litter items along the beach profile, it emerged that the BL concentration is highest between the storm berm and the dune toe, particularly in the south-eastern sector along the vegetation line, reflecting the hydrodynamic and morphological setting of the beach. The spatial distribution of the BL is consistent with the effects of recent storm events, as evidenced by the presence of a well-developed storm berm (Andriolo et al., 2020a, 2020b). Furthermore, both short-term and medium-term indicators of coastal morphodynamics confirm a predominantly erosive trend of the beach, significantly influencing the distribution and burial/exhumation of BL. The erosion process may remobilize previously buried litter. These interactions between erosion, sediment dynamics, and litter mobility highlight the need to integrate BL monitoring with coastal geomorphology investigations (Rizzo et al., 2023; Anfuso et al., 2024). The characterization of collected items highlighted that several items have a foreign origin (e.g., from Albania and Greece). This latter aspect emphasizes the role played by the longshore drift in the marine litter dispersion and its accumulation on the beach and the role of regional circulation in transboundary litter transport (UNEP/MAP, 2015; United Nations Environment Programme, 2021).

Activities focused on the analysis of BL distribution and movement during storms have highlighted that, on average, for the same storm intensity, small pocket beaches are characterized by higher average CCI values than larger beaches and tend to retain waste for longer. Furthermore, it should be noted that more intense storm surges generally lead to an increase in CCI values, while less intense ones lead to random and, in any case, limited variations compared to the previous situation, with numerous cases of improvements in the CCI. Finally, the first intense autumn storm surges are characterized by the greatest increases in beach litter on beaches.

The approach based on the indirect analysis of orthophots derived from aerophotgrammetric surveys proved to be a suitable alternative solution for the in-situ BL monitoring action for the identification of litter items falling in the macro-litter category (>2.5 cm). Overall, the findings underline the importance of

implementing a harmonized and spatially explicit monitoring framework that combines in situ observations with indirect analysis exploiting the UAV image manual interpretation.

The results obtained from the application of the proposed algorithms allow to state that, although the Mask-RCNN-based algorithm turned out to be more suitable for the detection task compared with the analysis tools already available in QGIS, its performance was not good enough to support operative beach litter monitoring programs and still requires improvements to increase the automatic classification performance (Sozio et al., 2024). On the other hand, preliminary results obtained by the application of the SAM-VIT model showed that, at the current stage of implementation, it allows to yield image classification with an accuracy of 0.93 and an F1-score of 0.6. Therefore, the method demonstrated high reliability in detecting beach litter and thus represents a robust and effective approach for assessing its spatial distribution and identifying major accumulation zones.

For what concerns MPs, the analysis carried out on the sediment samples collected at Capitolo beach revealed that a total of 274 MPs were found in sediment samples collected along the first transect (Transect A), while 116 MPs were found in samples from the second transect (Transect B), corresponding to 3045 MPs/kg and 1289 MPs/kg, respectively. The detailed quantitative results are indicated in Table 4.2.2 and Table 4.2.3.

Table 4.2 2: MPs identified in each sample collected at Capitolo beach expressed as quantitative value (number of MPs) and density value (MPs/kg). ("S" refers to surface samples and "P" refers to those collected at 5-10cm depth).

Sample	Sector	Total MPs	MPs/kg	Fibers (MPs/kg)	Fragments (MPs/kg)	Foams (MPs/kg)	Pellets (MPs/kg)
A1S	Foreshore	22	488.89	377.8	88.889	22.222	0
A1P	Foreshore	40	888.89	866.7	88.889	22.222	0
A2S	Berm	41	911.11	755.6	155.56	0	0
A2P	Berm	23	511.11	466.7	44.444	0	0
A3S	Dune limit	83	1844.4	1444	177.78	200	22.222
A3P	Dune limit	65	1444.4	1444	0	0	0
B1S	Foreshore	18	400	333.3	44.444	22.222	0
B1P	Foreshore	19	422.22	422.2	0	0	0
B2S	Berm	15	333.33	311.1	22.222	0	0
B2P	Berm	23	511.11	466.7	22.222	22.222	0
B3S	Dune limit	19	422.22	333.3	0	44.444	44.444
B3P	Dune limit	22	488.89	488.9	0	0	0

Table 4.2.3: MPs identified in each sampling point expressed as quantitative value (number of MPs) and density value (MPs/kg).

SAMPLING POINT	Sector	Total MPs	MPs/kg	Fibers (MPs/kg)	Fragments (MPs/kg)	Foams (MPs/kg)	Pellets (MPs/kg)
A1	Foreshore	62	688.89	622.22	55.56	11.11	0
A2	Berm	64	711	611	100	0	0
A3	Dune limit	148	1644	1444.44	88.89	100	11.11
B1	Foreshore	37	411.13	377.8	22.22	11.11	0
B2	Berm	38	422.23	388.9	22.22	11.11	0
B3	Dune limit	41	455	411	0	22	22

In both analyzed transects, the concentrations of fibers were very high (about 90 %) compared to the other types of MPs. In contrast, fragments and foam presented much smaller percentages (6.7 and 3.6 %), with pellets being < 1 %. The microscope observations also allowed for the distinction of MPs particles into 9 different colours. The most abundant colours in both transects were black and transparent, representing respectively 45.6 and 26.7 % of the total amount of particles. Regarding Transect A, observations revealed a high presence of dark fibers (with a maximum of 52 MPs in sample A3P) and transparent fibers in large numbers at sampling point A3S. Blue, pink, and white fibers were also visible. Various fragments were noted, characterized by different colours (transparent, red, blue, purple, green, and black). Furthermore, a significant quantity of white foam (9 MPs) was observed in sample A3S, corresponding to the largest size class (4999-1000 µm). Examining the filters obtained from Transect B, an abundance of fibers was observed in all collected samples, totalling 106 particles, including red, blue, and white fibers. Among these, 40 dark and 40 transparent fibers were identified. The presence of white foam was noticed. The analysis revealed a total of four fragments in different colours, including transparent, green, and black. A transparent and an orange pellet, as well as a grey foam, were also present. Finally, in Figure 4.2.5, the relative abundance of the MPs particles in each sample is shown in relation to the sampling position along the beach profile. According to data, fibers represent the most abundant typology in all the samples, characterizing the whole beach profile. On the contrary, the presence of pellets has been highlighted only in the samples collected in proximity to the dune limit (samples A3 and B3), being absent in all the other samples.

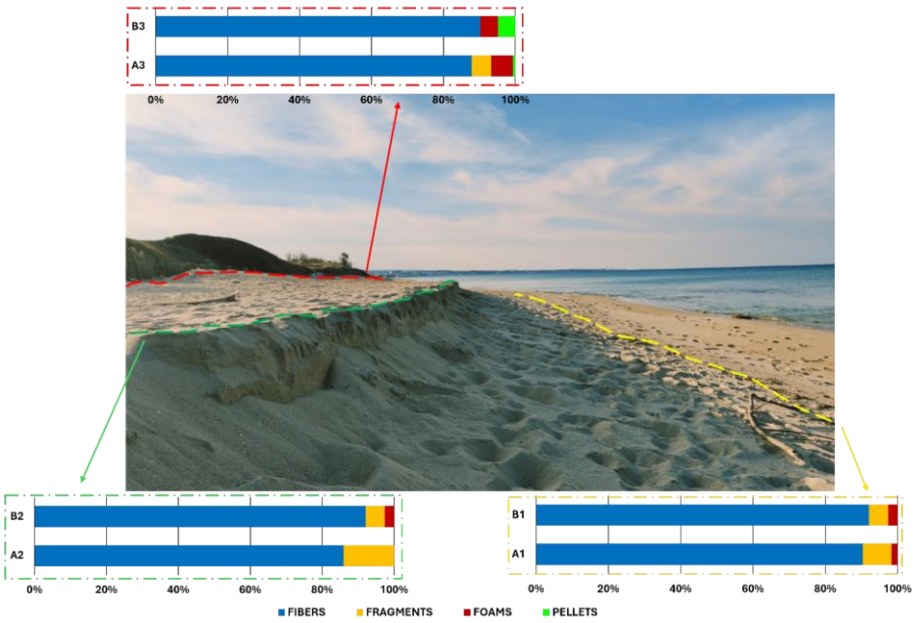

Figure 4.2.5: Graphs reporting the percentage of MPs for each sampling point subdivided by shape. Each dash-dot rectangle corresponds to a different sector of the beach profile: foreshore (yellow), storm berm (green), and dune limits (red).

The analysis of MPs collected along the Pino di Lenne coastal system provides a detailed picture of how microplastics are transported, retained, and redistributed within a morphodynamically stable Mediterranean beach. The use of an eco-friendly extraction protocol based on olive oil enabled the effective isolation of MPs across all 40 sediment samples and ensured the recovery of plastics with varying densities without introducing harmful reagents into the workflow. Visual examination under optical microscopy confirmed fibres as the dominant morphology—mainly black and blue—followed by fragments, while films and pellets were comparatively rare. This pattern is consistent with the contribution of both marine and terrestrial sources, as well as with the reworking processes typical of microtidal wave-dominated beaches.

Quantitative results reveal strong spatial heterogeneity across the investigated sub-environments. The highest microplastic concentrations were found in the submerged sandbar (2435 MPs/kg), the *Sabellaria alveolata* bioconstructions (2324 MPs/kg), and the dune base (2065 MPs/kg). These hotspots correspond to areas characterized by sediment trapping, lower current velocities, or biological structures capable of incorporating particulate material. In particular, the *Sabellaria* bioconstructions act as efficient biological filters, capturing MPs both actively—through particle selection—and passively, as fibres and fragments become embedded within the tube matrix. Conversely, the estuarine channel exhibits the lowest concentrations (718 MPs/kg), reflecting elevated hydrodynamic energy, continuous flushing, and limited potential for long-term deposition. Intermediate concentrations were detected in the backshore, offshore, and offshore transition zones, where MPs may be temporarily stored but are not consistently retained due to active sediment reworking. Statistical analysis corroborates the environmental significance of these differences.

ANOVA results show that microplastic concentrations vary significantly among the ten depositional settings, with hydrodynamic regime, sediment texture, and biological mediation emerging as the main controlling factors. The grouping of environments into homogeneous subsets further highlights a clear dichotomy between high-retention zones—such as the dune base, sandbar, and *Sabellaria* reef—and dynamic environments like the channel and offshore transition, where MPs are more likely to be transported rather than accumulated. As shown by the distribution analysis, MPs exhibit a distinct spatial organisation, with

higher concentrations in depositional settings and in areas where biological structures—such as *Sabellaria* bioconstructions—enhance the capacity of the substrate to retain particulate matter. These zones function as effective accumulation hotspots due to reduced flow energy, sediment stability, and biologically mediated trapping. In contrast, the channel and offshore transition behave as high-energy corridors, where frequent resuspension and export processes limit long-term storage. Seasonal variability further shapes these dynamics: winter storms mobilise plastic debris and drive its burial at the dune base, establishing this sector as a persistent storage environment, while summer calm conditions stabilise previously deposited particles. Submerged areas show slightly higher MPs abundances, likely due to continuous low-intensity reworking that promotes fragmentation and redistribution, as well as the ability of deeper sedimentation processes to incorporate MPs into the offshore transition.

Overall, this conceptual framework illustrates how hydrodynamic forcing, sediment transport pathways, and biological mediation jointly control the selective trapping and seasonal redistribution of MPs across the beach system (Figure 4.2.6). Overall, the Pino di Lenne coastal system demonstrates the value of such kind of sites as excellent natural laboratories for evaluating beach morphodynamic processes, including the influence of anthropogenic inputs and their interaction with natural sedimentary and ecological dynamics.

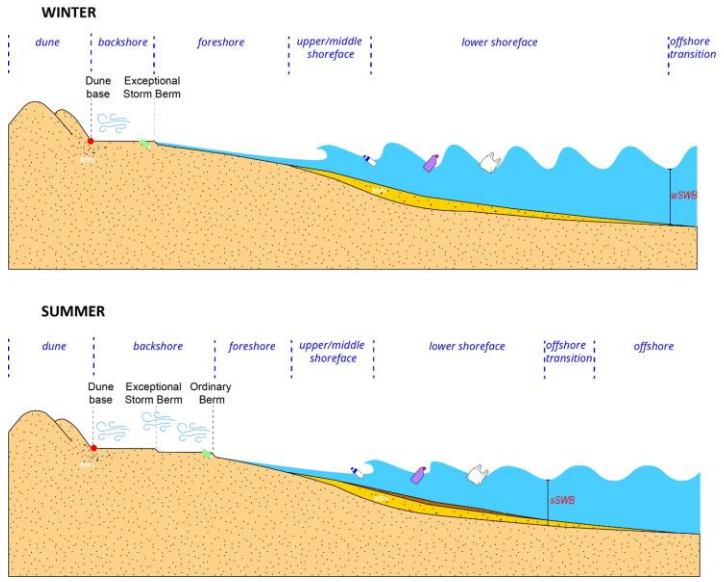

Figure 4.2.6: Seasonal variability in beach morphology, sediment dynamics, and microplastic (MP) distribution along a cross-shore beach profile (after Walker and Plint, 1992). The diagram highlights the contrasting spatial extent of sediment transport under winter and summer wave regimes, together with the preferential accumulation of macrolitter on storm-related or ordinary berms. Microplastics are shown to concentrate near the dune toe in both seasons, while deeper sedimentary deposits associated with winter conditions extend offshore beyond the zone affected by summer reworking.

The main results of the modelling approaches reported the tracks of floating plastic debris on the sea surface and the particle distribution density (Figures 4.2.7 and 4.2.8). The trajectories for different kinds of plastic debris are strictly dependent on the surface current distribution, which follows the seasonality of the Mediterranean basin.

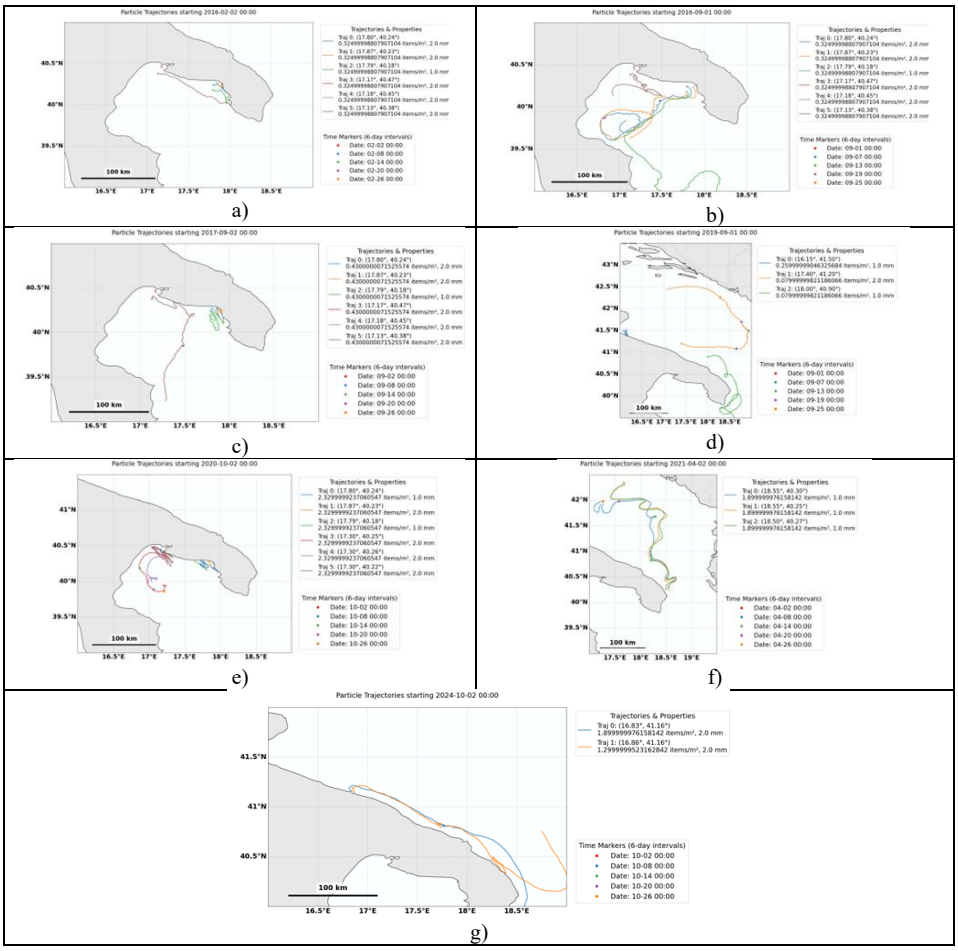

Figure 4.2.7: Simulation of plastic trajectories based on surface currents derived from Copernicus reanalysis; a) trajectory February 2016; b) trajectory September 2016; c) trajectory September 2017; d) trajectory September 2019; e) trajectory October 2020; f) trajectory April 2021; g) trajectory October 2024.

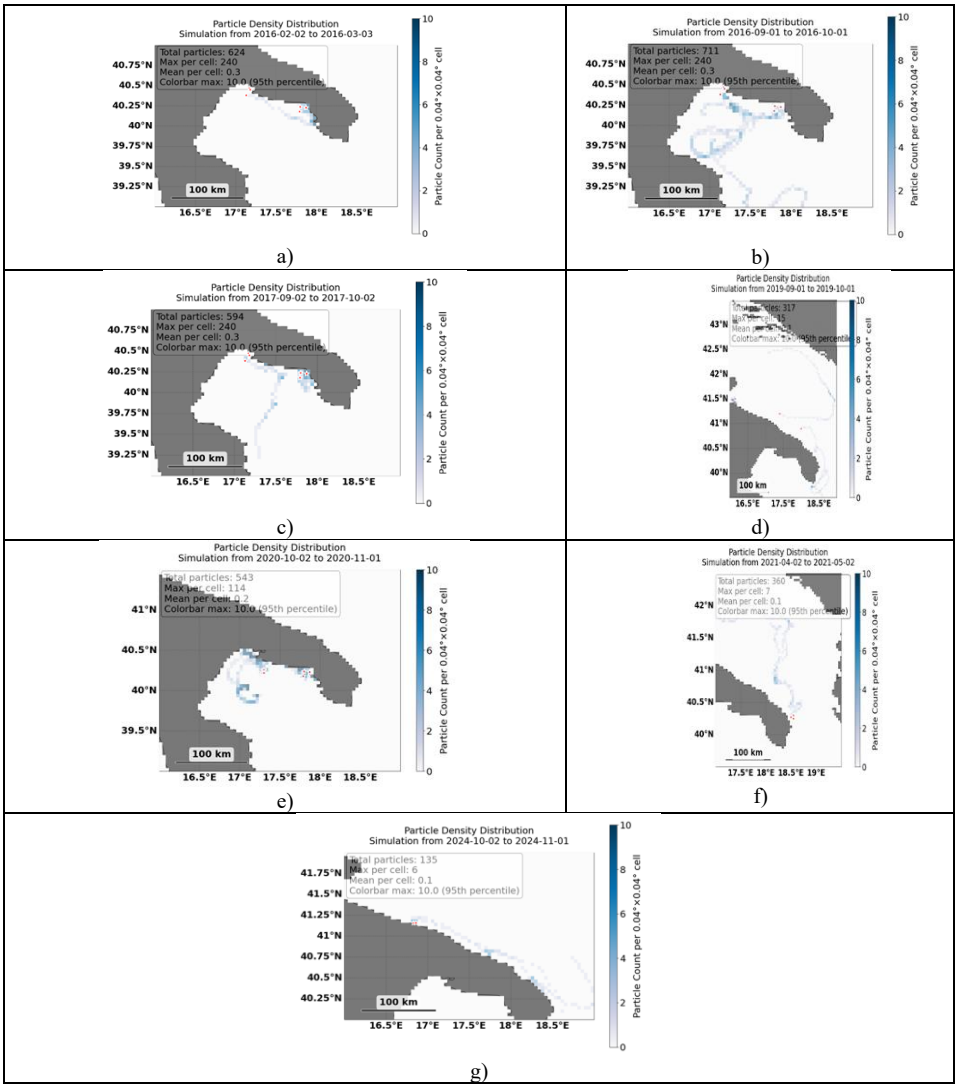

Figure 4.2.8: Simulation of the plastic density distribution in the Apulia region; a) density distribution in February 2016; b) density distribution in September 2016; c) density distribution in September 2017; d) density distribution in September 2019; e) density distribution in October 2020; f) density distribution in April 2021; g) density distribution in October 2024.

In particular, the distribution of plastic debris along the Ionian and Adriatic coasts revealed that low-lying sandy areas, such as alluvial plains and pocket beaches, are highly impacted by plastic pollution. The model results revealed high concentrations of plastic debris beached along the pocket beaches of the Salento peninsula (Figure 4.2.9).

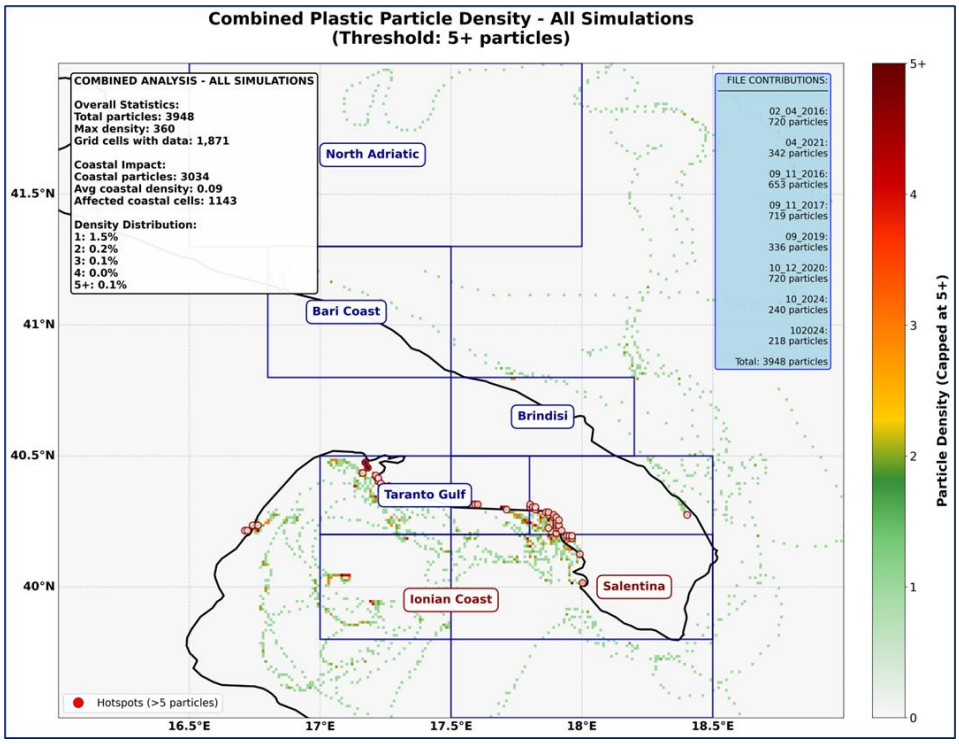

Figure 4.2.9: Results of plastic distribution from all simulations at different time steps, highlighting hotspot areas where floating plastics were stranded on the beaches.

4.2.5 Scientific products and dissemination

Publications (international journal 2023-2025):

Serranti S., Capobianco G., Gorga E., Cucuzza P., Bonifazi G., Rizzo A., Lapietra I., Mastronuzzi G., Mele D - Direct identification of microplastics in marine sediments by hyperspectral imaging and machine learning (Manuscript under review).

Lo Bue, G.,Musa, M., Marchini, a., Riccardi, M.P., Dubois,S.F., Lisco, S., Moretti, M., de Luca, A., Mancin, N. (2025). Microplastic pollution in the littoral environment: insights from the largest Mediterranean Sabellaria spinulosa (Annelida) reef and shoreface sediments Marine Pollution Bulletin 217 (2025) 118132

Sasso, C., Rizzo, A., Mastronuzzi, G. Anfuso, G., Lapietra, I., Liso, I.S., Marsico, A., Sozio, A., Scicchitano, G. (2025). Unveiling coastal pollution: A multi-technology approach to micro and macro litter assessment for the environmental characterization of beaches, *Marine Pollution Bulletin*, 220, 118423

Scarrica, V. M., Cocozza, P., Anfuso, G., Staiano, A., Bonifazi, G., Rizzo, A., Serranti, S. (2025). Cost-effective approaches for microplastic pellets characterization using a machine learning tool. *Ecological Informatics*, 103230.

Cocozza, P., Scarrica, V. M., Rizzo, A., Serranti, S., Staiano, A., Bonifazi, G., Anfuso, G. (2025). Microplastic pollution from pellet spillage: Analysis of the Toconao ship accident along the Spanish and Portuguese coasts. *Marine Pollution Bulletin*, 211, 117430.

Sozio, A., Scarrica, V. M., Rizzo, A., Aucelli, P.P.C., Barracane, G., Dimuccio, L. A., Ferreira, R., La Salandra, M., Staiano, A., Tarantino, M.P., Scicchitano, G. (2024). Application of Direct and Indirect Methodologies for Beach Litter Detection in Coastal Environments. *Remote Sensing*, 16(19), 3617.

Rizzo, A., Scicchitano, G., Mastronuzzi, G. (2024). A set of guidelines as support for the integrated geo-environmental characterization of highly contaminated coastal sites. *Scientific Reports*, 14(1), 8198.

Anfuso, G., Álvarez, O., Dilauro, G., Sabato, G., Scardino, G., Sozio, A., Rizzo, A. (2024). A First Attempt to Describe the Real-Time Behavior and Fate of Marine Litter Items in the Nearshore and Foreshore under Low Energetic Marine Conditions. *Water*, *16*(3), 409.

Marsico, A., Rizzo, A., Capolongo, D., De Giosa, F., Di Leo, A., Lisco, S., Mastronuzzi, G., Moretti, M., Scardino., G., Scicchitano, G. (2023). Spatial distribution of trace elements in sub-surficial marine sediments: New insights from bay I of the Mar Piccolo of Taranto (Southern Italy). *Water,* 15(20), 3642.

Conference proceedings indexed in Scopus:

Rizzo, A., Serranti, S., Cucuzza, P., Lisco, S., Marsico, A., Bonifazi, G., Mastronuzzi, G. (2024). Application of hyperspectral imaging and machine learning for the automatic identification of microplastics on sandy beaches. In *Algorithms, Technologies, and Applications for Multispectral and Hyperspectral Imaging XXX* (Vol. 13031, pp. 181-193). SPIE (extended abstract)

Sozio, A., Scarrica, V. M., Aucelli, P. P., Scicchitano, G., Staiano, A., Rizzo, A. (2023). Comparing Meanshift/SVM and Mask-RCNN algorithms for beach litter detection on UAVs images.Conference paper in: 2023 IEEE International Workshop on Metrology for the Sea; Learning to Measure Sea Health Parameters (MetroSea) (pp. 483-487) (extended abstract)

Published papers (national journal 2023-2025)

Sasso C., Rizzo A., Scardino G., Pellegrino L., Mastronuzzi G. (2025). “La barca della Legalità “EROS” per lo studio delle microplastiche nel porto di Bari”, Rivista della Lega Navale Italiana.

Rizzo A., Scardino G. (2024). “Il progetto nauticAttiva per il monitoraggio dell’ambiente marino-costiero”. Rivista della Lega Navale Italiana.

Rizzo A., Fracchiolla T., Lapietra I., Lisco S., Liso I. S., Marsico A., Sasso C., Sozio A., Veneziano F. (2024). “Analisi della distribuzione di plastiche e microplastiche in ambiente di spiaggia” in: Le Dune Costiere, Monografia di Geologia Ambientale a cura di F. Stragapede (SIGEA)

Scardino G., Mancino S., Romano G., Patella D., Scicchitano G. (2024). “Rilevazione dello stress idrico sulle dune costiere attraverso il telerilevamento” in: Le Dune Costiere, Monografia di Geologia Ambientale a cura di F. Stragapede (SIGEA)

Presentations at International Conferences:

Capobianco, G., Cucuzza, P., Gorga, E., Serranti, S., Rizzo, A., Lapietra, I., Mastronuzzi, G., Mele, D., Bonifazi, G. - Hyperspectral imaging applied to microplastic monitoring in marine sediments from a highly contaminated coastal site (Taranto, southern Italy) - 11th International Conference on Sustainable Solid Waste Management (19-22 June 2024, Rhodes, Greece).

Rizzo A., Barracane G., Bonifazi G., Capobianco G., Gorga E., Mele D., Scardino G., De Santis V., Lapietra I, La Salandra M., Lisco S., Liso S., Marsico A., Mastronuzzi G., Parise M., Serranti S., Scicchitano G., Sozio A. - Litter distribution in marine and coastal sediments: highlights from ongoing research projects - SGI-SIMP: Geology for a sustainable management of our Planet (3-5 September 2024, Bari, Italy).

Rizzo A., Anfuso G., Barracane G., Bonifazi G., Capobianco G., Cucuzza P., Gorga E., Lapietra I., Lisco S., Liso S., Marsico A., Mastronuzzi G., Mele D., Parise M., Scardino G., Serranti S., Sozio A., Scicchitano G. - Litter distribution in marine and coastal environments: case studies from the Apulia region (Southern Italy) – LITTORAL 2024: European Coastal Challenge Summit (24-27 September 2024, Constanta, Romania).

Capobianco G., Cucuzza P., Rizzo A., Bonifazi G., Mastronuzzi G., Serranti S. - Ground-based hyperspectral imaging for the detection of plastic waste on coastal areas - CSI2025: XLIV. Colloquium Spectroscopicum Internationale (27-31 July 2025, Ulm, Germany).

Rizzo A. "Litter distribution in marine and coastal environments: case studies from Apulia region (southern Italy).IV Workshop "*Women in Geomorphology"* (8-3-2024, online)

Bonifazi G., Capobianco G., Cocozza P., Mastronuzzi G., Rizzo A., Serranti S. - Identification of plastic debris on beaches by ground-based hyperspectral imaging - ECDS 2023: Emerging Concepts & Design for Sustainability (8-11 October 2023, Villers-sur-Mer, Calvados, France).

Presentations at national events:

25/10/2024: "Mare di Legalità a Taranto" organized by Lega Navale Italiana (Taranto, Italia). Oral presentation: "Il monitoraggio ambientale delle aree marino-costiere". Authors: Rizzo A., Scardino G.

12/10/2025 (online): "Seconda Giornata Regionale della Costa" organized by SIGEA e Ordine dei Geologi della Puglia. Oral presentation: "La caratterizzazione geoambientale come strumento di protezione delle spiagge". Authors: Rizzo A., Lisco S.

12/4/2024 (online): "Notte Internazionale della Geografia (GeoNight)". Oral presentation: "Approcci metodologici multidisciplinari per la valutazione dell'impatto antropico in ambiente costiero". Authors: Rizzo A., Lisco S., Liso S.

SGI e SIMP 2024 "Geology for a sustainable management of our Planet". Fracchiolla T., Veneziano F., de Luca A., D'Abbicco V., Trani R., Moretti M. & Lisco S. - Evaluation of microplastics in coastal and marine sediments of the Ionian Sea (Southern Italy).

XVI GEOSED MEETING (Rende, 10-14/06/2025) Titolo della presentazione: Tracking Microplastics in Coastal Environments: A Case Study from Pino di Lenne, Taranto (Southern Italy). Autori: Lisco, S., T. Fracchiolla, A. Rizzo , A. De Luca , C. Sasso , R. Trani , F.A. Veneziano , M. Moretti.

Dissemination:

Rizzo A., Bonifazi G., Capobianco G., Gorga E., Mele D., Scardino G., De Santis V., Lapietra I., La Salandra M., Lisco S., Liso S., Marsico A., Mastronuzzi G., Parise M., Serranti S., Scicchitano G., Sozio A. - Litter distribution in marine and coastal sediments: case studies from Apulia Region - RETURN Dissemination Workshop (1-2 February 2024, Turin, Italy).

Pagliaccia B., Santini G., Lubello C., Maisto G., Gori R., Francalanci S., Polettini A., Falzarano M., Cincinelli A., Sforzi L., Serranti S., Capobianco G., Gorga E., Falsini S., Colzi I., Rizzo A. - Microplastics: from the detection to the characterization of their effects into the environment - RETURN Dissemination Workshop (19-21 June 2024, Bari, Italy).

Rizzo A., Capobianco G., De Santis V., Gorga E., Lapietra I., Lisco S., Liso S., Marsico A., Mastronuzzi G, Mele D., Parise M., Scardino G., Scicchitano G., Serranti S. - Macro and Micro Litter distribution in marine and coastal sediments: highlights from ongoing research activities - RETURN Dissemination Workshop (19-21 June 2024, Bari, Italy).

4.3 Presence of microplastics in the Mediterranean through the analysis of surface waters and benthic fish, with assessment of human MPs intake (UNIFI)

4.3.1 Introduction

Over the last three years, our research has concentrated on microplastic (MP) contamination in marine ecosystems, with a specific focus on the Mediterranean Sea. By combining chemical analyses with microbiological investigations, we explored MPs distribution, composition, and how interaction with marine organisms and environmental processes.

The Mediterranean Sea is widely regarded as one of the world's most affected regions in terms of plastic pollution, since its semi-enclosed configuration, together with intense commercial activity, makes it particularly susceptible to MP accumulation (Mancuso et al., 2023). Various maritime activities, such as fishing, commercial shipping, and tourism, represent major contributors to MP inputs at sea (Sharma et al., 2021). Additionally, the basin's hydrodynamic features indicate that the Mediterranean may act as a terminal sink for debris entering from the Atlantic Ocean. The presence and distribution of macro- and microlitter on the seafloor, in the water column, and along coastlines, together with their ingestion by marine fauna and associated impacts such as entanglement or mortality, remain critical targets for environmental management.

Our initial investigation, conducted in collaboration with the Department of Biology of the University of Florence, assessed the spatial variability of MPs and their associated microbial assemblages in Mediterranean surface waters. This study not only quantified particle abundance and characteristic but also highlighted the role of MPs as vectors for diverse microbial communities, including specific bacterial groups. A subsequent study focused on the Mediterranean red mullet (*Mullus barbatus*), a species of high ecological and commercial relevance (Santonicola et al., 2023). By employing advanced analytical methodologies, we identified and quantified ingested MPs and evaluated potential implications for human consumers.

Collectively, these complementary studies provide a holistic insight into MP pollution across the marine trophic network, from open-water occurrence to biological uptake and potential human exposure, and offer valuable scientific support for the development of evidence-based policies aimed at safeguarding Mediterranean marine ecosystems and ensuring sustainable resource management.

4.3.2 Case study description

Case studies included the investigation of MP abundances in surface seawater and benthic fish samples, collected from 22 commercial harbors across the Central, Western, and Eastern Mediterranean, covering a broad area of the basin. The correlations between MP concentration and type with the composition of surface water microbial communities were explored.

In parallel, another study was conducted with the aim to provide a large-scale assessment of MPs in the red mullet, Mullus barbatus, a species of ecological and commercial significance in the Mediterranean. Fish were sampled across different environmental conditions and gradients of human influence to evaluate spatial variability in MP ingestion and identify potential contamination hotspots. A dedicated sample processing procedure was used to examine MPs within the intestinal tracts of the fish. Red mullet is a demersal fish with high ecological and economic importance in the Mediterranean (Cocci et al., 2022). It primarily feeds on sediment, thus making it particularly vulnerable to ingesting marine debris. Due to its benthic feeding habits and small size, red mullet serves as an effective bioindicator for monitoring MP presence and impacts in marine benthic habitats. Moreover, being a commercially important species red mullet also represents a potential route for MPs to enter the human food chain, highlighting its relevance for food safety considerations.

4.3.3 Methodologies

The lack of harmonized protocols remains one of the main obstacles in the field of MP analysis, leading to inconsistencies in data generation and limiting the comparability of results between studies. From sampling to extraction and identification, each methodological step can significantly influence the reported concentrations and polymer profiles. This problem is particularly critical in biological matrices such as fish and food products, where complex organic components complicate isolation and purification processes, often requiring strong chemical or enzymatic treatments that can alter or degrade plastic polymers. The lack of standardized and validated procedures not only hinders the accurate quantification of MP in edible organisms but also compromises the robustness of food safety and human health risk assessments. Therefore, the development of harmonized analytical frameworks and validation protocols is essential to ensure data reliability, promote comparability, and ultimately support regulatory actions aimed at mitigating MP exposure through the food chain (Figure 1).

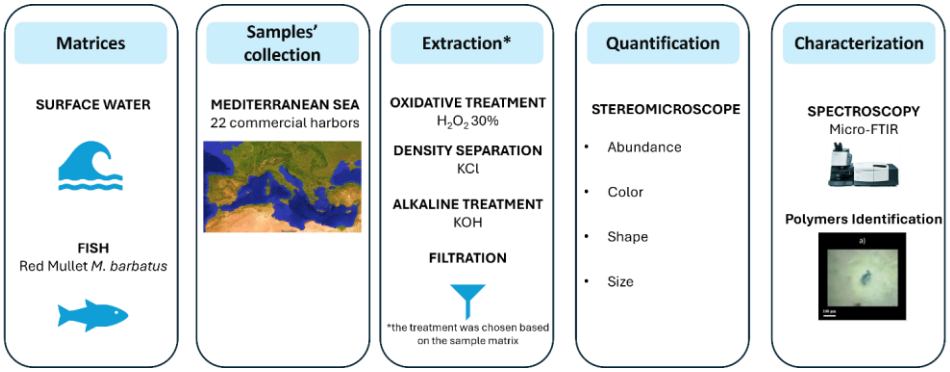

Figure 4.3.1: Schematic of the followed protocol.

4.3.3.1 Analytical methods

MPs were visualized and quantified using a Leica S9iper stereomicroscope equipped with a FLEXACAM C1 digital camera. Items were classified according to morphological features, size, and color. Following stereomicroscopy, the samples were analyzed using microFTIR 2D imaging to chemical characterized the polymers. Spectral analysis was performed by comparison of characteristic absorption bands and full spectral profiles to reference spectra from the literature.

Strict quality control and quality assurance measures were applied throughout sampling and sample processing. Operators wore gloves and laboratory coats of known composition and color. Only glassware and stainless-steel equipment were used, cleaned sequentially with distilled water, ethanol, and ultrapure water, wrapped in aluminum foil. All sample handling was conducted in a controlled environment. Procedural blanks were included at all stages of sample processing and digestion, with filters positioned near the filtration system to monitor airborne contamination, ensuring the reliability of results.

4.3.3.2 Experimental methods

The sampling campaign was carried out in 22 areas of the Mediterranean Sea. For each site, 1 L of surface seawater was collected directly, and 4 specimens of red mullet were purchased from coastal commercial fisheries.

Water samples were directly filtered on the glass fiber filter under vacuum. The digestion protocol of the fish intestine involved a first freeze-drying step, and chemical treatment using 1:10 w/v of 30% hydrogen peroxide, at 60°C for 96 h. A saturated KCl solution was used as density separation medium, after the digestion step, to maximum recovery of all polymeric items. Finally, the filters were put in Petri dishes, covered, and stored inside desiccators. If the organic matter impaired the chemical characterization, a second digestion step was performed, using 0.05 M KOH. Statistical analysis was performed to assess significant differences between data.

4.3.3.2 Modelling approaches

n.a.

4.3.4 Results

MPs were detected in all but one water sample (n=21), at varying concentrations. The predominant form was fragments, followed by fibers, and the greatest abundance of MPs was in the size range of 1-0.1 mm. Fragments and fibers were mainly characterized by black, red, and blue colours. Several polymers were identified in surface seawater, mainly polyethylene (PE), polyethylene terephthalate (PET), and polyamide (PA).

In the overall intestine of the Mediterranean mullet analysed, the frequency of MP detection was 77.3%. Fulton condition factors (K), a parameter related to fish metadata, were calculated. No significant correlations were found between K and abundances expressed as items/individual at the sampling site, while significant differences were found between sampling sites for abundances expressed as both items/g ww and items/individual. Variability in MP ingestion rates was detected, probably attributed to the location of the sampling points and the sampling period. The dominant form ingested was fiber, followed by fragments, with a prevalence of dark and transparent colors. The most frequently identified polymers were polymethyl methacrylate (PMMA), ethyl vinyl acetate (EVA), and polyethylene terephthalate (PET). The ingestion of microplastics by commercial fish species highlights their dual importance as bioindicators of marine plastic pollution and as a potential food safety concern.

4.3.5 Scientific products and dissemination

Publications

Stefano Nenciarini, Saul Santini, Laura Sforzi, Alessandro Russo, Aldo D'Alessandro, Sonia Renzi, Lorenzo Cipriani, Tania Martellini, Alessandra Cincinelli. Distribution of microplastics and associated microbial communities in Mediterranean surface waters. Submitted to *Journal of Hazardous Materials Advances*

Laura Sforzi, Saul Santini, Stefano Nenciarini, Tania Martellini, David Chelazzi, Lorenzo Cipriani, Alessandra Cincinelli, Duccio Cavalieri. Microplastics in Mediterranean red mullet (Mullus barbatus): advanced analytical approaches and food safety assessment. *Under revision*

Dissemination

Poster presentation "Distribution and characterization of microplastics in the coastal areas of the Mediterranean Sea" L.Sforzi, S.Santini, L.Santi, S.Nenciarini, A.Russo, D.Chelazzi, T.Martellini, A.Cincinelli, D.Cavalieri- 05/05/2024 – 09/05/2024 Sevilla (Spain), 34th Congress SETAC

Oral presentation “Crossing Aquatic Systems: Insights into Microplastic Pollution in the Mediterranean Sea”. Sforzi L., Martellini T., Cincinelli A. PhD Symposium in Chemical Science PiCSU 4th ed., Florence (Italy), January 14-17, 2025

4.4 Presence of microplastics in port sediments: influence of marine dynamics and stream inputs – The case of the Port of Genoa (UNIGE)

4.4.1 Introduction

In the field of research applied to the presence and spread of microplastics (MPs) in the marine environment, the initial data on the type of items (in terms of shape and polymer) present in a study area, together with the dynamic characteristics of it, they are the basis for a mathematical models to understand the mechanisms of MPs dispersion, and identify the main transport routes and areas of deposition (Cai et al., 2023; Simantiris et al., 2022). Furthermore, in a port marine environment, knowledge of both the quantity and type of MPs contained in bottom sediments and the dynamics of the water masses is also the starting point for understanding the mechanisms of MPs release from bottom sediments subject to resuspension due to the action of propellers during ship transit or maneuverings, or as a result of sediment movement, as occurs during dredging (Ji et al., 2021).

When MPs enter the marine environment, their composition (polymer with specific density) and shape (fragment, granule, sphere, film, etc.) play a fundamental role in determining their behavior along the water column in terms of buoyancy, sedimentation time, resistance to chemical and mechanical degradation, etc. (Waldschläger et al., 2022). Similarly, the velocity and direction of currents typical of the area where MPs are dispersed, as well as the physical stratification of the water column, play a fundamental role in the path the items will follow and the time it will take to settle.

In this section, we present the sampling carried out and the results obtained within the Port of Genoa (NW Italy), regarding both the MPs present in the bottom sediment and the dynamics and the physical-chemical characteristics of the water column. The results obtained are the starting point for the application of microplastic diffusion modeling in the port environment.

Data of the water masses of the port were acquired in collaboration with WP4.2 “Setting the scene on environmental degradation stressors in terrestrial and marine environment”.

4.4.2 Case study description

The Port of Genoa (Figure 4.4.1) is a complex basin in which commercial, industrial, recreational and port service functions coexist. It is a leader in the traffic of conventional goods, transported by ships with differentiated characteristics (traditional, ro-ro, specialized). It is also an important port of the Mediterranean Sea for cruise traffic, serving as a departure point or stopover for numerous cruise ships, but also ferries. There are numerous marinas inside, and the inner part of the port is very popular with tourists. The entire port basin is dominated by the city of Genoa (600,000 inhabitants) and includes the mouths of numerous small city streams and two important major streams (Polcevera and Bisagno streams) as well as civil and industrial waste. Because of these characteristics, there are many possible sources of pollution in the port waters and sediments, including plastic pollution. One contributor certainly comes from rain that causes runoff from the streets of Genoa, and, within the port, from all the commercial and industrial activities.

Two study sites within the Port of Genoa were chosen for sediment sampling for the quantification of MPs and acquisition of dynamics and water parameters data: Site 1 and Ste 2, at the western and eastern entrance to the port, respectively (Figure 4.4.1).

Site 1 is located near the western entrance to the port, in front of the mouth of the Polcevera stream, and is therefore directly affected by the stream flow. It is also subject to the influence of the open sea and sea storm from the southeast. Ship traffic in this area is very limited.

Site 2 is located near the eastern entrance to the port; it is subject to the influence of open-sea waters and sea storms from the southeast; it is affected by solid and freshwater contributions from the Bisagno stream; both commercial and tourist shipping traffic affect it.

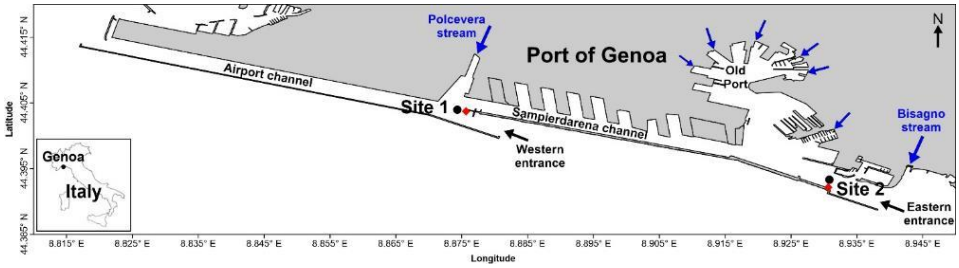

Figure 4.4.1: The Port of Genoa: localization of sampling (black dot) and measuring (red rhombus) Site1 and Site 2; blue arrows show the position of streams; in black the main parts of the port.

4.4.3 Methodologies

4.4.3.1 Analytical methods

Dynamics and physical-chemical parameters of the water masses were measured by fixed and mobile instruments.

Fixed monitoring stations (Site 1 and Site 2) are deployed on the internal part of the port breakwater at 7 m-depth and continuously measure. Fixed stations are equipped with a multiparametric probe (CTD, Idromarambiente) with temperature (in °C) and a horizontal acoustic Doppler current profiler (H-ADCP WorkHorse 300 kHz, RD Instruments) for current velocity (in m s^{-1}) and direction (in ° N) measurement. The instruments were programmed to take a measurement every 15 minutes, 24 hours a day, continuously. For the data return, bin #15 of the ADCP was taken into consideration, which measures currents at a distance of approximately 65 m from the breakwater towards the center of the channel.

Periodically (approximately once a week, weather and sea conditions permitting, and depending on shipping traffic), a portable CTD (Idromarambiente) was used by monitoring vessel for measurements of temperature, salinity, density (in kg m^{-3}) and turbidity (in Formazin Turbidity Units – FTU) in the water column (from the sea surface to the bottom) near the fixed station. This was done to identify any stratification in the water column during different seasons, caused by heavy rainfall and the presence of river mouths or the warming of surface waters typical of summer. Data was acquired from May 2023 to April 2025.

4.4.3.2 Experimental methods

Sediment from the Port of Genoa were sampled on 12 January 2024 and 14 October 2024 with a stainless-steel 5-L Van Veen grab in two different sites (Site 1 and Site 2). Sediment was collected with a metal spoon and placed in a glass jar. All materials used were previously rinsed with microfiltered water. The samples were kept in a refrigerator at +4 °C until analysis.

The weather and sea conditions during the January 2024 sampling were characterized by calm seas, clear skies and no wind. The period was characterized by generally stable weather.

The weather and sea conditions during sampling of October 2024 were characterized by rough seas from south-east, strong winds from south-east and rain. The period was characterized by heavy rainfall. In fact, in the days prior to the measurements, large quantities of rain fell on the territory (Figure 4.4.2), affecting in particular the western area (Weather Alert was issued on 8 October 2024 by the Liguria Region), resulting in large quantities of organic material and debris being carried into the Port of Genoa basin. The sea was also rough, with a warning for heavy sea storms on 9 and 10 October.

The bottom sediment was sampled on 14 October 2024 also for the various research groups involved in WP3 for the application of different methods of extraction and characterization of MPs from marine sediments (Deliverable 4.3.3 - Improved methodologies for contaminant monitoring in marine coastal area). The samples collected in HDPE jars (to facilitate transport to the various locations), which had been previously rinsed with filtered water, were then sent to the laboratories of the Universities of Bari, Florence and Rome for analysis.

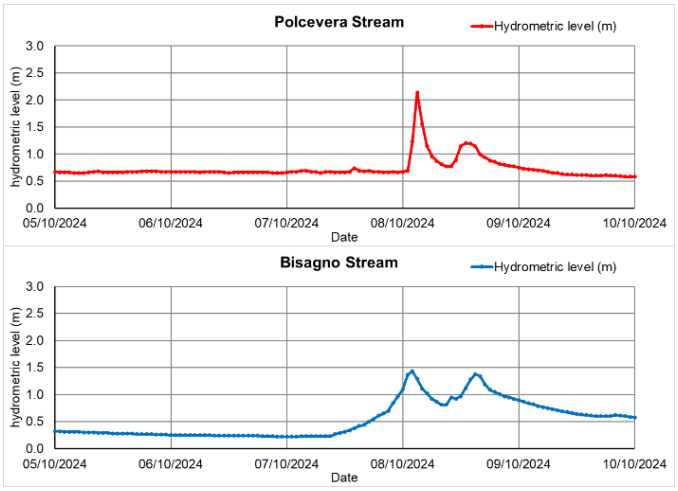

Figure 4.4.2: Hydrometric levels of Polcevera Stream (above) and Bisagno Stream (below) during the days before the sediment sampling campaign of 14 October 2024.

- *Sample processing and item extraction*

I) Sediment samples collected during the campaign on 12 January 2024 (S1 and S2) underwent the following preliminary treatment in order to degrade material composed of carbonates, strongly present in the sediment (sediment grains, fragments of mollusk shells, foraminifera). In this regard:

- 25 mL of samples S1 and S2 were pre-treated with HCl (4%) in a glass beaker.

Inside each beaker, 200 mL of microfiltered super-saline water with a density of 1.3 g cm^{-3} was added. The super-saline water was obtained by dissolving 2400 g of $MgCl_2$ in 1 L of fresh water. $MgCl_2$ was used because it produces a non-toxic solution with a higher density than that obtained with the more common NaCl (Cutroneo et al., 2021).

The mixtures of sediment and super-saline water thus obtained for each sample (S1 and S2) were stirred for 2 minutes with a glass rod in order to homogenize and suspend the sediments and then left to settle for 48 hours. At the end of the sedimentation period, 10 mL of supernatant containing floating particles was collected using a glass pipette and transferred to glass jars. The operation was repeated three times for each sample, obtaining a total volume of 30 mL of supernatant. The supernatants were then filtered on GF/F glass microfiber filters (diameter 47 mm, pore size 0.7 µm; Whatman™, GE HealthCare UK Limited, Little Chalfont, UK) and rinsed with 2 L of pre-filtered fresh water to remove salt residues and prevent crystal formation. Finally, the filters were placed inside Petri dishes. The sample treatment and extraction carried out in this way led to the collection of a large amount of material on the filter, as can be seen from the photos of the filters shown in Figure 4.4.3.

II) Sediment samples collected during the campaign on 14 October 2024 (S1 and S2) were divided in two aliquots (S1.1 and S1.2, S2.1 and S2.1) and underwent different preliminary treatments in order to assess the effectiveness of hydrogen peroxide (H_2O_2) on the sediment, particularly with regard to its ability to degrade organic matter. In this regard:

- 25 mL of samples S1.1 and S2.1 were not pre-treated but were directly dried in a thermostatic oven at 60°C for 24 hours and then weighed.
- 25 mL of samples S1.2 and S2.2 were pre-treated with 50 mL of H_2O_2 solution 40% w-v, in order to increase the degradation of the organic substance present. The reagent was left to act for 48 hours.

In subsequent operations, all samples (S1.1, S1.2, S2.1 and S2.2) underwent the same procedures and treatments aimed at studying the microplastic content, as reported below.

Inside each beaker containing 25 mL of sediment sample, 200 mL of microfiltered super-saline water with a density of 1.3 g cm^{-3} was added. The mixtures of sediment and super-saline water thus obtained from all the samples (S1.1 and S1.2, and S2.1 and S2.2) were stirred for 2 minutes with a glass rod in order to homogenize and suspend the sediments and then left to settle for 48 hours. At the end of the sedimentation period, 10 mL of supernatant containing floating particles was collected using a glass pipette and transferred to glass jars. The operation was repeated three times for each sample, obtaining a total volume of 30 mL of supernatant.

Five mL of H_2O_2 solution 40% w-v was then added to each sample in order to degrade the organic substance in supernatant. Addition of H_2O_2 was repeated for 4 times per sample. At each stage, the H_2O_2 was added gradually to prevent the degradation reaction from causing the supernatant to spill out of the containers. The supernatants were then filtered on GF/F glass microfiber filters (diameter 47 mm, pore size 0.7 µm; Whatman™, GE HealthCare UK Limited, Little Chalfont, UK) and rinsed with 3 L of pre-filtered fresh water to remove salt residues and prevent crystal formation. Finally, the filters were placed inside Petri dishes. The effect of H_2O_2 was visible in the supernatant inside the glass jars, as samples S1.2 and S2.2 had less floating material on the surface than the untreated samples (S1.1 and S2.1), but it became evident once filtration was performed on the filters (Figure 4.4.3).

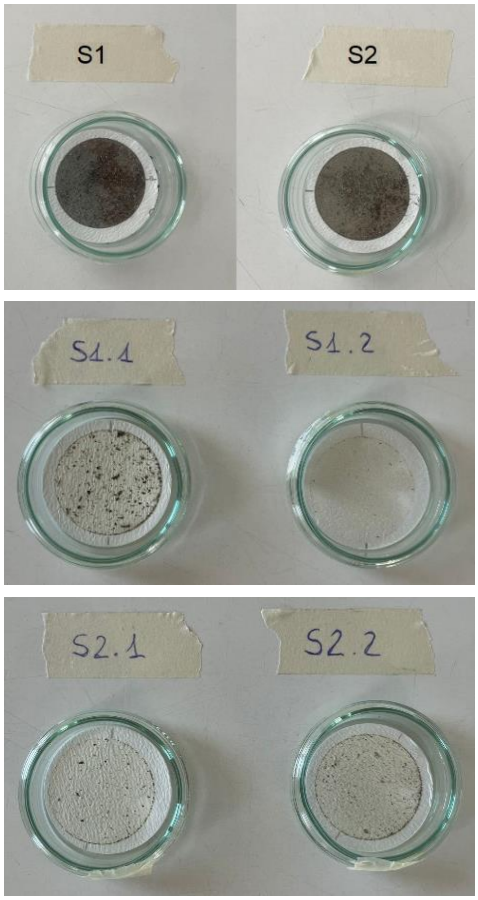

Figure 4.4.3: Filters inside Petri dishes: on top, filters Si and S2 obtained from the first sampling campaign without the use of H_2O_2; below, filters S1.1, S1.2, S2.1, and S2.2 obtained from the second sampling campaign after the use of the H_2O_2 to eliminate organic matter.

- *Items analysis*

Filters were observed using a Leica Z16 APO optical microscope (5x magnification) operated by Leica Application Suite 3 analysis software (Leica Microsystems, Mannheim, Germany), which allowed for image acquisition, counting, and morphological and dimensional characterization of the items collected on the filters. The items identified were then classified according to shape (fragment, pellet, fiber, film, granule, and other), color (white, red, orange, blue, black, grey, brown, green, pink, yellow and other) and size. Items smaller than 30 µm were not taken into consideration due to the optical resolution of the instrument used.

Between 20% and 40% of the items identified on the filters were subsequently chemically analyze using the XploRA™ PLUS micro-Raman (µRaman) spectrometer (Horiba Scientific, Ltd., Kyoto, Japan) and the associated LabSpec 6 Spectroscopy Suite software (Horiba Scientific, Ltd., Kyoto, Japan). The following instrument settings were used: laser 785 nm, filter 10%, range 100-3800 cm^{-1}, grating 600 g mm^{-1}, acquisition time 30 s, and accumulation 3 times. The µRaman spectra resulting from the analysis of the items were compared with those in the µRaman spectral library of Wiley's KnowItAll® Software (version 24.2.72.0; John Wiley & Sons, Inc., Hoboken, NJ, USA) and considered valid only when the match was greater than 70%. Particles smaller than 30 µm were not taken into consideration, as was previously done during characterization under the optical microscope.

Given the large amount of material collected on filters S1 and S2, the cataloging of items under the optical microscope, as well as µRaman analysis, was reduced to only those items with clearly identifiable shapes and colors (e.g., fibers and pellets), leaving out everything else. This still allowed us to obtain preliminary information on any foreign materials present in the sampled sediment.

- *Precautions*

During all stages of sample handling in the laboratory, strict precautions were taken to minimize the risk of microplastic contamination. Operations were performed under a fume hood with the exhaust flow turned off, using only glass or steel utensils, which were rinsed beforehand with microfiltered fresh water (obtained by filter paper), and whenever operations did not require exposure of the samples to air, they were covered with a glass cap. Operators wore cotton gowns and coats to avoid the release of synthetic fibers.

To monitor potential environmental contamination, a GF/F control glass filter was used, identical to those used for sample filtration. This filter was exposed to the air each time the samples were handled without lids in laboratory. The analysis of the control filter proved to be fundamental during morphological observation under an optical microscope, as it allowed the identification and exclusion from the final count of any particles that may have been introduced during the laboratory phases and not attributable to the original samples. Since the filters were exposed to air during µRaman analysis, an additional GF/F control filter was also exposed to air during measurements. Both control filters were then analyzed using both optical microscopy and µRaman spectroscopy in order to identify and remove any environmental contamination from the final dataset (Figure 4.4.4).

The following diagram shows the sequence of actions performed on the samples and the related anti-pollution precautions taken. Specifically, the diagram refers to samples from October 2024.

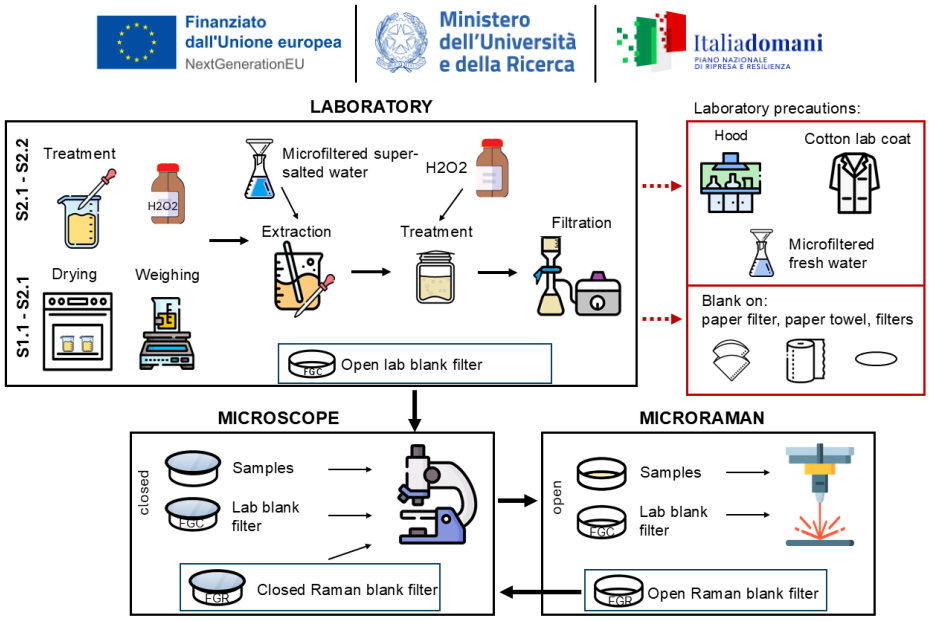

Figure 4.4.4: Schematic representation of the steps performed in the laboratory for samples of 14 October 2024 under the optical microscope and with µRaman (black boxes) and the precautions taken to limit environmental contamination (red box).

4.4.3.3 Modelling approaches

An initial study of microplastic modelling was carried out in recent years by the University of Genoa (Department of Civil, Chemical and Environmental Engineering) thanks to the SPlasH! and SPlasH & Co projects, as part of the France-Italy Interreg Maritime 2014-2020 Programme. In the simulations (deliverable of the SPlasH & Co project: "SPlasH & Co T1.2.2 Scenari di dispersione di rifiuti galleggianti.pdf"; https://interreg-maritime.eu/web/splash-co), for each selected weather-sea scenario, 10,000 virtual particles representing potential plastic objects were released within the port and their preferred paths of movement were identified. The main scenarios selected were those characterized by winds from the N, SE and SW. The results obtained with wind and sea from the SW are shown below as an example (Figure 4.4.5).

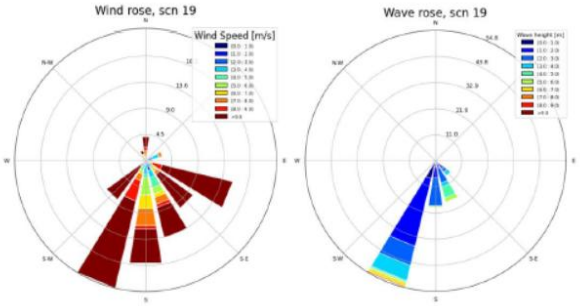

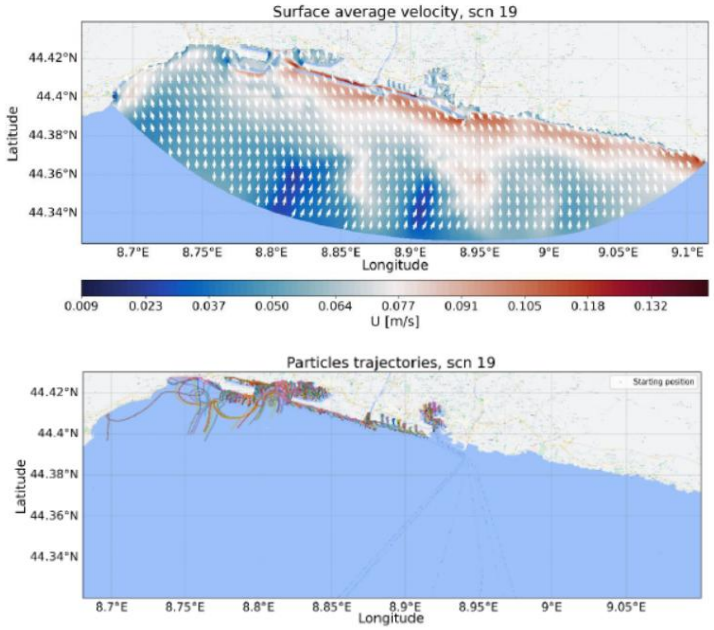

Figure 4.4.5: Example of simulation of plastic dispersion in the presence of SE wind and resulting trajectories.

The data collected within the Port of Genoa and presented in this deliverable represent important basic information in the long term for the application of numerical models, which simulate the behavior of plastic items from the point of release in the port environment, under the various forcing that characterize the port (sea currents, input from streams, characteristics of the water column).

4.4.4 Results

Regarding dynamics and chemical-physical parameters of the water column, below are the results of the data collected by both fixed stations and mobile stations from May 2023 to April 2025. The interruptions in the parameter profiles of the fixed stations are due to the removal of instruments for extraordinary maintenance necessary for the upkeep of the equipment. Please note that, by convention, the direction of the current indicates the direction where the water masses move (as opposed to the direction of the wind, which indicates the direction from which it is coming).

Dynamics measured by fixed ADCP

Currents measured at the fixed station at Site 1 showed speeds between 0 and 0.74 m s^{-1}, with the highest values occurring during SE sea storms or ship transits. The prevailing directions alternate between ESE and WNW (Figure 4.4.6 and Figure 4.4.7).

Currents measured at the fixed station at Site 2 showed speeds between 0 and 0.95 m s^{-1}, with the highest values occurring during SE sea storms or ship transits. The prevailing directions alternate between ESE and WNW (Figure 4.4.6 and Figure 4.4.7).

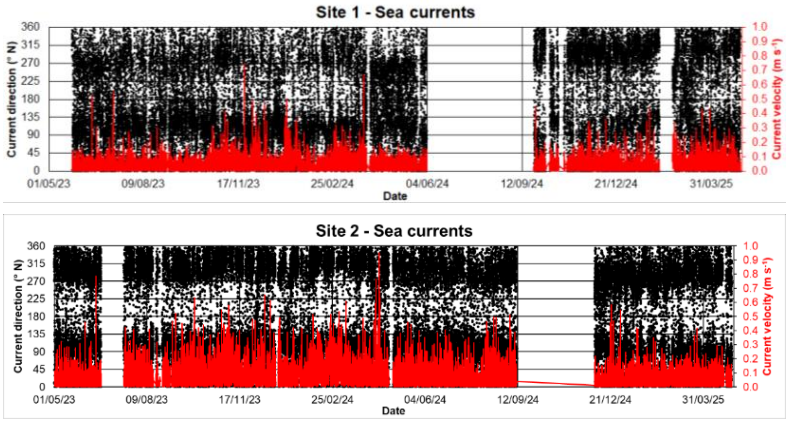

Figure 4.4.6: Velocity (in red) and direction (in black) of currents measured by the fixed station at Site 1 (above) and Site 2 (below) (reference bin #15).

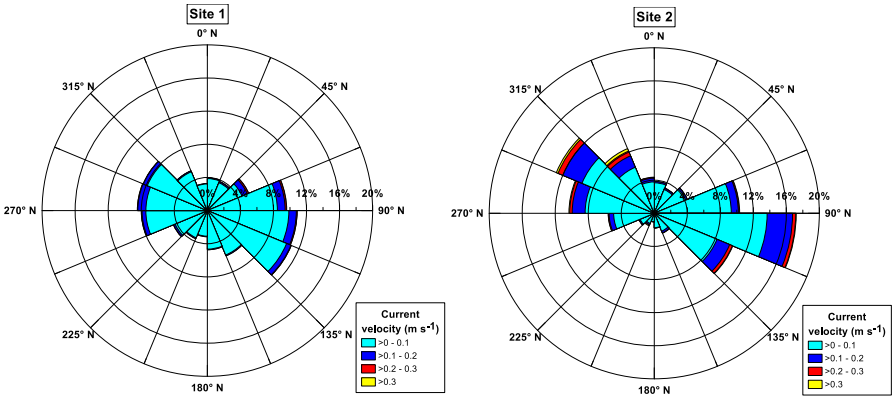

Figure 4.4.7: Polar diagram of the main directions of the current based on the measured velocity (colors in the legend) at Site 1 (left) and Site 2 (right) (reference bin #15).

Chemical-physical parameter measured by fixed CTD

Regarding chemical and physical parameters of the water masses, temperature was taken into account at the fixed stations, and temperature, salinity, turbidity and density in the measurements taken from the boat. In particular, water turbidity is an indicator of any plume that can be generated by various natural and anthropogenic factors (river flooding, resuspension of bottom sediment generated by wave motion or the action of ship propellers and tugs in transit and maneuvering in port, port dredging) and can carry not only sediment particles but also MPs, thus promoting their spread in the marine environment.

Temperatures at 7-m depth at Site 1 (Figure 4.4.8) were between the minimum of 13.1 °C measured on 19 February 2025 and the maximum of 28.3 °C measured on 20 July 2023. The summer of 2023 was characterized by a heatwave that brought record temperatures both in the air and at sea. August 2023 saw the highest maximum air temperature (37.9 °C) since temperature measurements began in 1833 by the Historical Meteorological Observatory of the University of Genoa (https://life.unige.it/agosto-2023-record-caldo). This record value is associated with the high-water temperature measured by the fixed station of

Site 1. Temperatures at 7-m depth at Site 2 (Figure 4.4.8) were between the minimum of 12.7 °C measured on 20 January 2025 and the maximum of 28.7 °C measured on 14 August 2024. Maximum temperature measured in summer 2023 was 28.5 °C on 20 July, confirming values measured at Site 1.

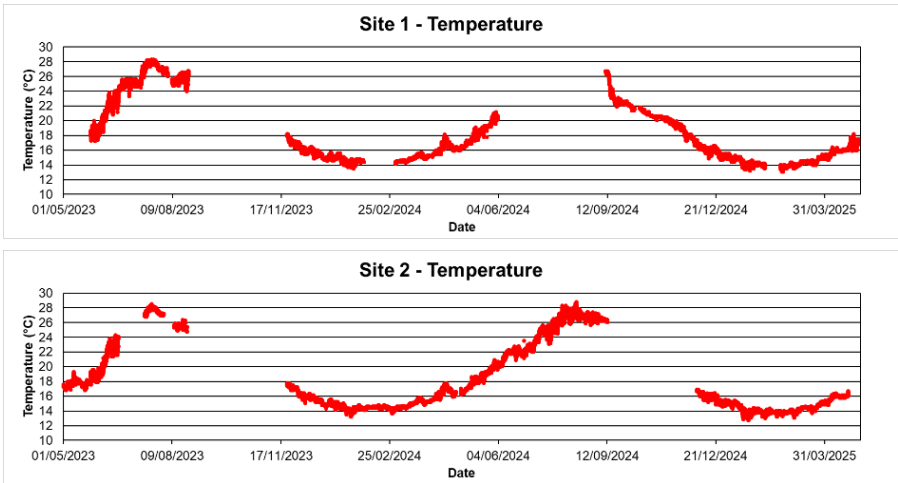

Figure 4.4.8: Temperature (°C) at the fixed station of Site 1 (above) and Site 2 (below).

Chemical-physical parameter measured by mobile CTD

Minimum and maximum water temperature, salinity, turbidity and density measure by the mobile CTD at Site 1 and Site 2 during the study period are reported in the following table:

Table 4.4.1: Summary of parameters measured at Site 1 and Site 2 by mobile CTD.

Site 1				
Parameter	**Minimum (date)**	**Depth (m) of minimum (layer in the water column)**	**Maximum (date)**	**Depth (m) of maximum (layer in the water column)**
Temperature (°C)	12.0 (14/02/2025)	1 (surface)	28.3 (01/08/2024)	1 (surface)
Salinity	21.1 (25/03/2025)	0 (surface)	40.3 (30/11/2023)	0 (surface)
Turbidity (FTU)	0.3 (06/07/2023)	9 (intermediate)	21.0 (31/08/2023)	14 (bottom)
Density (kg m^{-3})	15.3 (25/03/2025)	0 (surface)	30.2 (30/11/2023)	0 (surface)
Site 2				
Parameter	**Minimum (date)**	**Depth (m) of minimum (layer in the water column)**	**Maximum (date)**	**Depth (m) of maximum (layer in the water column)**
Temperature (°C)	12.6 (21/01/2025)	17 (bottom)	28.4 (05/08/2024)	0 (surface)
Salinity	31.3 (02/05/2024)	0 (surface)	39.8 (01/08/2024)	8 (intermediate)
Turbidity (FTU)	0.2 (21/02/2025)	1 (surface)	13.1 (02/05/2024)	0 (surface)
Density (kg m^{-3})	23.0 (02/05/2024)	0 (surface)	29.6 (12/01/2024)	0 (surface)

The following figures show the frequencies of the values (Figure 4.4.9) and the temporal distributions in the water column (Figure 4.4.10) of the different parameters acquired at Site 1 and Site 2.

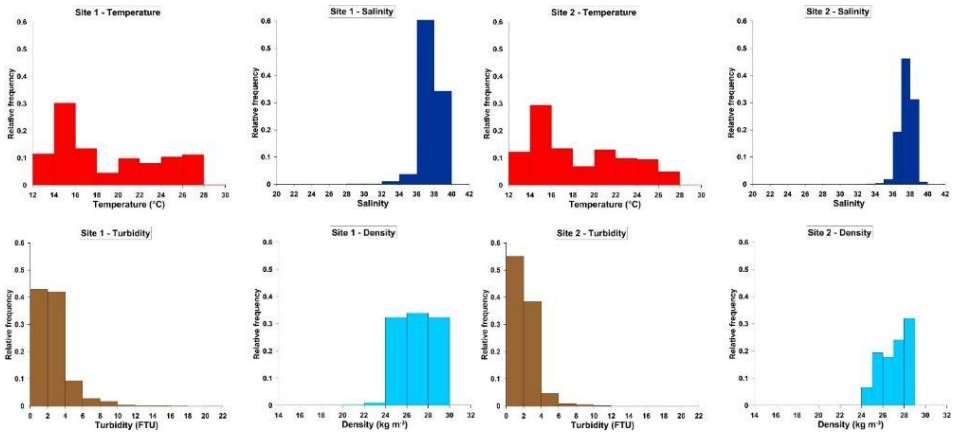

Figure 4.4.9: Frequency of temperature, salinity, turbidity, and density data measured with mobile probe at Site 1 (left) and Site 2 (right).

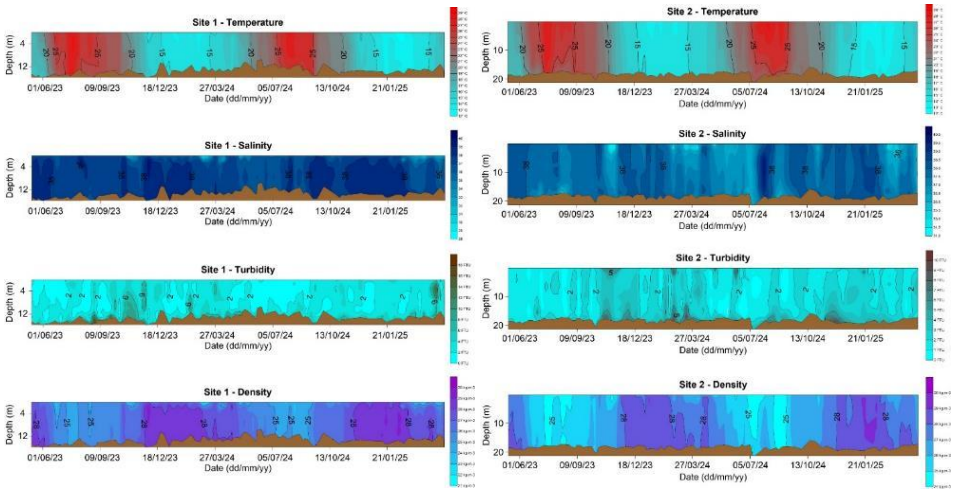

Figure 4.4.10: Vertical profile of temperature, salinity, turbidity and density at Site 1 and (left) and Site 2 (right).

The differences between the two measurement sites highlight the complexity of the marine environment in the Port of Genoa, due to the morphology of the basin, but also to the characteristics of the territory in which it is located and the climatic and meteorological conditions that characterize it (described in Deliverable 4.2.2 - Design of dataset). Differences show also how both the different dynamic conditions and the uneven distribution of rainfall and related contributions from streams can create peculiar conditions that could theoretically have a significant influence on the transport and spread of microplastics in the port marine environment. Below (Figure 4.4.11) are the vertical profiles of the characteristics of the water column (salinity and turbidity) measured after rainfall at Site 1, in front of the mouth of the Polcevera Stream, and

at Site 2, at the eastern entrance to the port near the mouth of the Bisagno Stream. In the first case, relatively fresh water is visible in the surface layer, along with a turbid layer generated by the input of the Polcevera Stream; in the second case, there are no indications of the influence of the Bisagno Stream.

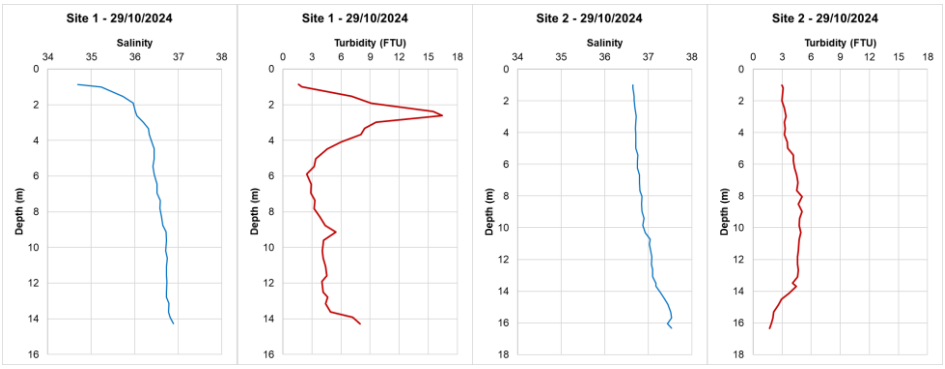

Figure 4.4.11: Vertical profiles of salinity (in blue) and turbidity (in red) at Site 1 (left) and Site 2 (right) measured on 29 October 2024 after rain.

Results obtained from the analysis of items extracted from sediment samples are shown below. Items collected on the filters were first counted and classified under an optical microscope according to shape, color and size, and then analyzed using µRaman to determine their composition. The results can provide very important information about the shape of MPs and the polymer they are made of. These two characteristics are fundamental pieces of information for applying MP dispersion models, as both determine how the MP will behave once it enters the marine environment.

- *Results of the first sampling (12 January 2024)*

Due to the large amount of organic material of vegetal origin present in the samples taken on 12 January 2024, which was extracted together with possible MPs and collected on the filters, the counting and characterization of the items in these samples can only be considered partial, as many items were probably hidden from view by the organic material deposited on top of them. We therefore only considered fibers with an easily identifiable shape and fragments of striking colors that were difficult to attribute to natural materials (such as pink, blue or yellow). The results for filters S1 and S2 are therefore indicative of the possible MPs present in the sediment samples but can still provide valuable information in terms of their shape, size, color and composition, which is useful for understanding the environmental impact on the marine environment of the Port of Genoa.

Observation under optical microscope (Figure 4.4.12) allowed for the identification of 39 items in S1, 82% fibers, 10% fragments and 8% granules, with 62% items white, 18% blue and 10% green. Sizes are mostly between 250 and 1000 µm. Forty-four items were considered in samples S2 divided in 68% fibers, 18% fragments and 14% granules; colors identified are white, blue, black and green; sizes are mostly between 250 and 1000 µm.

MicroRaman analysis of items revealed pink, blue and black fibers and blue and green fragments characterized by the presence of dyes or additives (such as TiO_2 or N_2). The orange and white granules were found to be minerals.

Figure 4.4.12: Significant items found in samples S1 (blue granules; above) and S2 (blue and green fibers; below).

Figure 4.4.13: Fibers found in the control filter.

- *Results of the second sampling (14 October 2024)*

Observation under optical microscope allowed for the identification of 64 items in S1.1 (Table 4.4.2 and Figure 4.4.14), divided into 45% fibers and 42% fragments. Item sizes are divided into all the size classes, while predominant colors are blue, black and white. S2.1 shows the presence of 88 items, divided into 61% fragments and 28% fibers. Sizes are mainly fine, below 250 µm. Prevailing colors are blue, black, white and grey.

For sample S1.1, 24 items were analyzed with µRaman, only 10 returned spectra with appreciable peaks and 8 were recognized: 2 fibers composed of plastic material [p-(Ethylene terephthalate) – PET, and polyester – PES], 4 fibers for which only the dye was determined, 1 fiber of cellulose and 1 fragment of calcium carbonate. For sample S2.1, 27 items were analyzed with µRaman, only 13 returned spectra with appreciable peaks and 13 were recognized: 1 fiber composed of plastic material [p-(Propylene)], 4 fibers and 1 fragment for which only the dye was determined, 1 fiber of cellulose and 6 fragment/pellets of calcium carbonate or quartz.

Table 4.4.2: Classification of items from samples S1.1 (left) and S2.1 (right) by shape, size and color.

Site 1 - Sample S1.1		
Item shape	**n. items**	**%**
Fibers	29	45.3
Sphere	0	0.0
Granules	1	1.6
Fragments	27	42.2
Other	7	10.9
Total	64	100

Site 2 - Sample S2.1		
Item shape	**n. items**	**%**
Fibers	25	28.4
Sphere	0	0.0
Granules	3	3.4
Fragments	54	61.4
Other	6	6.8
Total	88	100

Site 1 - Sample S1.1		
Item size	**n. items**	**%**
Ø ≥ 2000 µm	8	12.5
1000 µm ≤ Ø < 2000 µm	6	9.4
500 µm ≤ Ø < 1000 µm	8	12.5
250 µm ≤ Ø < 500 µm	13	20.3
125 µm ≤ Ø < 250 µm	9	14.1
63 µm ≤ Ø < 125 µm	12	18.7
Ø < 63 µm	8	12.5
Total	64	100.0

Site 2 - Sample S2.1		
	n. items	**%**
Ø ≥ 2000 µm	3	3.4
1000 µm ≤ Ø < 2000 µm	1	1.1
500 µm ≤ Ø < 1000 µm	13	14.8
250 µm ≤ Ø < 500 µm	6	6.8
125 µm ≤ Ø < 250 µm	14	15.9
63 µm ≤ Ø < 125 µm	29	33.0
Ø < 63 µm	22	25.0
Totale	88	100

Site 1 - Sample S1.1		
Item color	**n. items**	**%**
White	9	14.1
Cream	3	4.7
Red	2	3.1
Orange	5	7.8
Blue	22	34.4
Black	14	21.9
Grey	4	6.3
Brown	0	0.0
Green	3	4.7
Pink	1	1.5
Yellow	1	1.5
Other	0	0.0
Total	64	100

Site 2 - Sample S2.1		
Item color	**n. items**	**%**
White	11	12.5
Cream	5	5.7
Red	1	1.1
Orange	7	8.0
Blue	37	42.0
Black	13	14.8
Grey	9	10.2
Brown	0	0.0
Green	1	1.1
Pink	4	4.6
Yellow	0	0.0
Other	0	0.0
Total	88	100

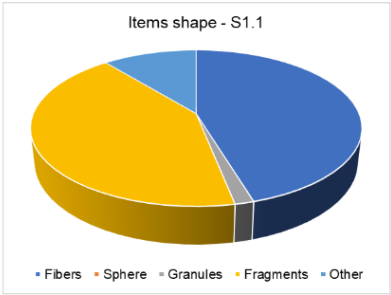

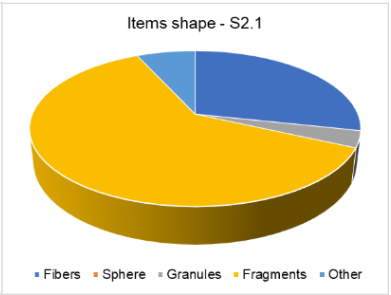

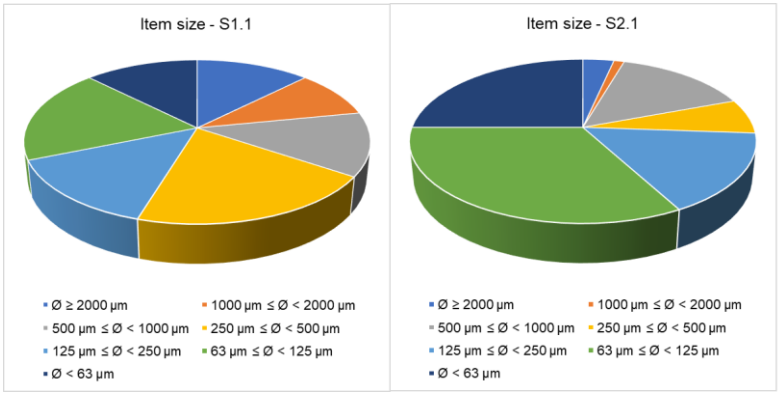

Figure 4.4.14: Item shape (above) and size (below) for S1.1 (left) and S2.1 (right).

Below are some photographs of the items identified in samples S1.1 and S2.1 (Figure 4.4.15).

Figure 4.4.15: Significant items found in samples S1.1 (green fiber and yellow fragment; above) and S2.1 (orange fiber and blue granule; below).

Observation under optical microscope allowed for the identification of 68 in S1.2 (Table 4.4.3 and Figure 4.4.16), divided into 49% fragments, 24% granules and 15% fibers. Item sizes are mostly less than 250 µm, while predominant colors are black, blue and grey. S2.2 shows the presence of 119 items, divided into 45% fragments, 20% granules and 14% fibers. Sizes are mainly between 63 and 250 µm. Prevailing colors are black, white, grey and blue.

For sample S1.2, 16 items were analyzed with µRaman, only 8 returned spectra with appreciable peaks and 4 were recognized: 2 granules and 1 fiber composed of dye or additives ($CaCO_3$ and TiO_2), 1 granule of calcite. For sample S2.2, 31 items were analyzed with µRaman, only 16 returned spectra with appreciable peaks and 13 were recognized: 4 dyes of fibers and fragments, 1 fiber of cellulose and 8 fragments/granules of calcium carbonate or carbon black.

Table 4.4.3: Classification of items from samples S1.2 (left) and S2.2 (right) by shape, size and color.

Site 1 - Sample S1.2		
Item shape	**n. items**	**%**
Fibers	10	14.7
Sphere	0	0.0
Granules	16	23.5
Fragments	33	48.5
Other	9	13.3
Total	68	100

Site 2 - Sample S2.2		
Item shape	**n. items**	**%**
Fibers	17	14.3
Sphere	2	1.7
Granules	24	20.2
Fragments	53	44.5
Other	23	19.3
Total	119	100

Site 1 - Sample S1.2		
Item size	**n. items**	**%**
Ø ≥ 2000 µm	0	0.0
1000 µm ≤ Ø < 2000 µm	2	2.9
500 µm ≤ Ø < 1000 µm	4	5.9
250 µm ≤ Ø < 500 µm	7	10.3
125 µm ≤ Ø < 250 µm	18	26.5
63 µm ≤ Ø < 125 µm	24	35.3
Ø < 63 µm	13	19.1
Total	68	100.0

Site 2 - Sample S2.2		
	n. items	**%**
Ø ≥ 2000 µm	1	0.8
1000 µm ≤ Ø < 2000 µm	7	5.9
500 µm ≤ Ø < 1000 µm	7	5.9
250 µm ≤ Ø < 500 µm	13	10.9
125 µm ≤ Ø < 250 µm	43	36.1
63 µm ≤ Ø < 125 µm	41	34.5
Ø < 63 µm	7	5.9
Totale	119	100

Site 1 - Sample S1.2		
Item color	**n. items**	**%**
White	1	1.5
Cream	3	4.4
Red	2	2.9
Orange	6	8.8
Blue	13	19.1
Black	19	28.0
Grey	10	14.7
Brown	3	4.4
Green	3	4.4
Pink	5	7.4
Yellow	1	1.5
Other	2	2.9
Total	68	100

Site 2 - Sample S2.2		
Item color	**n. items**	**%**
White	23	19.4
Cream	7	5.9
Red	1	0.8
Orange	7	5.9
Blue	15	12.6
Black	43	36.1
Grey	18	15.1
Brown	2	1.7
Green	1	0.8
Pink	2	1.7
Yellow	0	0.0
Other	0	0.0
Total	119	100

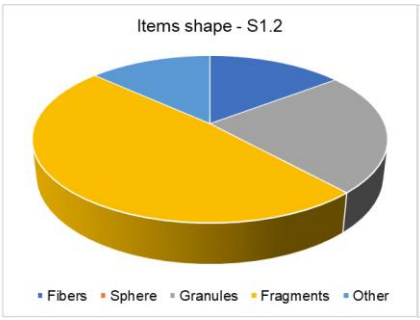

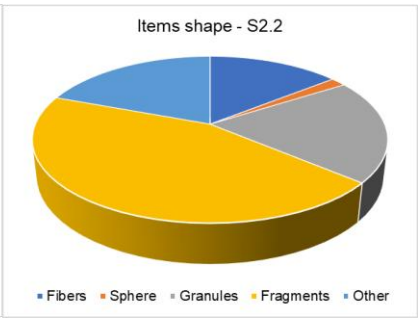

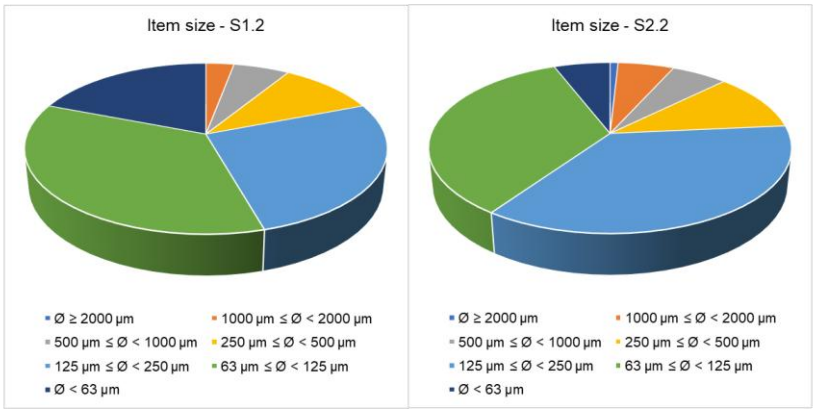

Figure 4.4.16: Item shape (above) and size (below) for S1.2 (left) and S2.2 (right).

Below are some photographs of the items identified in samples S1.2 and S2.2 (Figure 4.4.17).

Figure 4.4.17: Significant items found in samples S1.2 (yellow and black fibers; above) and S2.2 (blue-white fibers; below).

Figure 4.4.18: Significant items found in control filter (black fiber on the left and).

The green fibers (Figure 4.4.19) found first in the east (sample S1) and then in the west (S1.1) of the port were found to be composed of PE. Their presence at both sites and at different times can indicate widespread contamination of the sediments by this type of MP. Therefore, several hypotheses can be drawn from these results: either the contamination extends throughout the port and is therefore caused by a widespread source and thus by the use of a material widespread throughout the port and/or the area behind the basin (city of Genoa and hinterland); or the source is localized, but the effect of sediment dredging, sediment resuspension due to the action of ship and tugboat propellers, and transport due to sea currents has caused it to spread within the port basin; or a combination of the above. An internet search on the possible sources of these fibers based on the material composition and color has revealed a number of hypotheses, such as PE nets frequently used in the land for fencing or to support horticultural activities, or green PE ropes that can be used both in the nautical sector and for land-based activities (Figure 4.4.19).

Figure 4.4.19: Example of green fibers found in sediments of the Port of Genoa and possible match with industrial products: on the left, a PE net used in various settings (gardens, farming, terraces, etc.; www.plastic-netting.org), on the center, a PE rope used both in boating and for activities on land (www.suntengroup.en), and, on the right, green PE net for agricultural use (crop cover, greenhouses, shading) or industrial use (ground cover, sheds, etc.; www.PE-nets.com).

Another peculiarity found in the sediments of Genoa consists of multicolored fragments measuring around 100 µm (Figure 4.4.20). These fragments could derive from plastic recycling processes; in fact, during the production of recycled plastic, the original materials of different colors are ground and then combined to create mixed-color pellets. Although the plastic composition has not been identified, the presence of carbonates within the granules confirms its industrial origin and reinforces the hypothesis that it is recycled plastic. In fact, calcium carbonate ($CaCO_3$) is one of the most widely used mineral fillers in the plastics industry. Thanks to its physical and chemical properties, it is added to polymer formulations to improve the performance of the final material (increase in stiffness, opacity and color), reduce costs and increase the stability of the extrusion process (www.bausano.com; www.europlast.com).

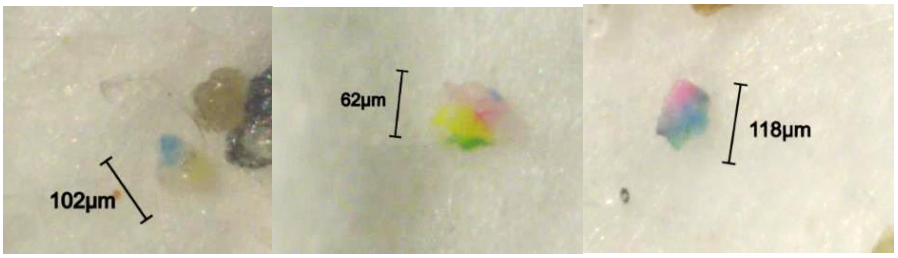

Figure 4.4.20: Example of multicolor fragments found in the samples.

4.4.5 Scientific products and dissemination

Presentations at International Conferences:

Cutroneo L., Benedetti B., Caiazzo L., Cecchi G., Di Bella G., Di Carro M., Di Piazza S., Di Trapani D., Gaggero L., Geneselli I., Magi E., Manzo S., Montereali M.R., Parrella L., Schiavo S., Serranti S., Zotti M., Capello M. (2024, poster, 3-minutes presentation). The Italian National Recovery and Resilience Plan (PNRR) RETURN Project: proposal of new monitoring and bioremediation protocols in the pilot site of the Port of Genoa. 11th International Conference on Sustainable Solid Waste Management, Rhodes, Greece, 19-22/06/2024

4.5 Observing Plastic and Bioplastic Fate in Coastal Systems through Multiscale Observations and Modelling (UNIPA)

4.5.1 Introduction

Plastic pollution is recognized as one of the major global issues, with negative effects on the environment, human health, and socio-economic activities (Strain et al. 2022). Recently, the demand for biodegradable polymers has grown significantly, being a sustainable alternative to conventional plastics (Joseph et al. 2023). The present research activity aims to investigate the hydrodynamic processes that influence the fate and transport of plastic and bioplastic debris in shallow coastal lagoons. The study integrates field measurements, drone-based mapping, and advanced numerical simulations for predicting the dispersion of plastic and bioplastic materials under varying hydrodynamic and meteorological conditions. The Stagnone Lagoon (Marsala, Sicily) was selected as the case study due to its ecological and economic importance, complex circulation patterns, and exposure to anthropogenic inputs. Recent research activities have focused on improving the characterization of the lagoon's bathymetry, velocity fields, and surface circulation patterns using an Uncrewed Surface Vehicle (USV) equipped with sonar and GNSS systems. The APACHE 4 USV surveys provide high-resolution bathymetric data that are being used to update existing maps and to validate the digital elevation model used in hydrodynamic simulations.

4.5.2 Case study description

The Stagnone Lagoon extends along the western coast of Sicily (Figure 4.5.1). The lagoon's geometry is about 2200ha of surface; it is characterized by shallow waters with average depth below 1 m, and tidal exchange through two mouths creates a dynamic environment where transport processes are highly sensitive to meteorological forcing, tidal oscillations, and bathymetric features.

The area is characterized by shallow waters, extensive seagrass meadows, several salt-harvesting plants, and important archeological sites like Mothia island. Water exchange occurs mainly through two tidal inlets located at the northern and southern ends of the lagoon.

During July 2025, a specific experimental campaign was carried out involving the release of ten Stokes drifters. These drifters were deployed at different times and locations within the lagoon on 8 and 9 July 2025, allowing for the tracking of surface currents and the validation of the modelled velocity fields. Complementary field measurements have been collected at several monitoring stations. Water level sensors are operating at the northern and southern mouths and at Altavilla Est, while additional anemometers are installed at Altavilla Est and Mulino, providing continuous records of wind speed, and direction.

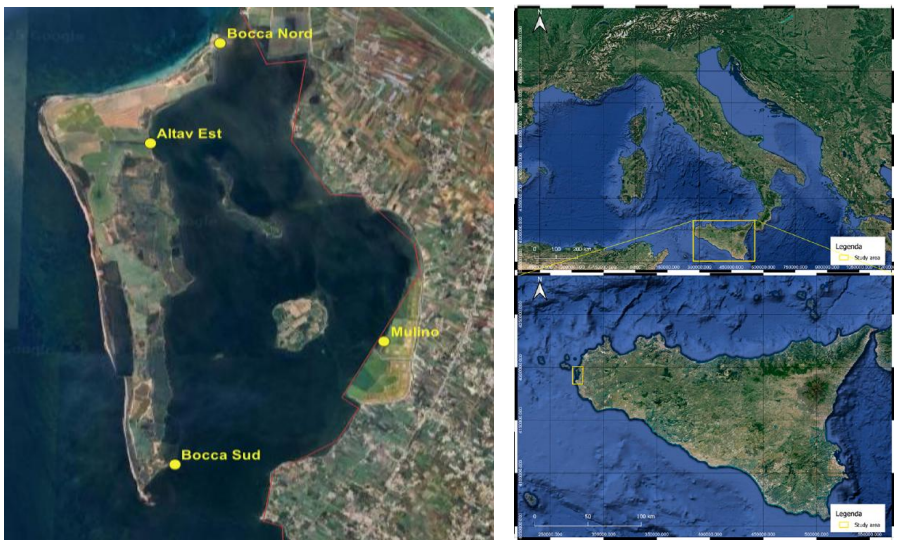

Figure 4.5.1: Study area - Stagnone Lagoon, water level and meteorological stations.

4.5.3 Methodologies

4.5.3.1 Analytical methods

n.a.

4.5.3.2 Experimental methods

The USV-based mapping provided dense spatial coverage of the lagoon's bathymetry and near-surface velocity. The system operates autonomously along predefined transects, collecting GNSS-referenced depth and flow velocity data. These measurements serve two purposes: (i) updating the digital elevation model and (ii) validating the hydrodynamic model outputs.

During the measurement campaigns conducted in the Stagnone Lagoon, the Uncrewed Surface Vehicle (USV) was employed for the simultaneous acquisition of velocity profiles using an ADCP (Acoustic Doppler Current Profiler) and for bottom tracking through a single-beam echosounder.

Subplot (a) of Figure 2 provides an overview of the transects covered by the USV within the lagoon, highlighting the spatial distribution of the surveys. Figure 4.5.2 (subplot b) presents a zoomed view of selected trajectories, showing the level of detail in the acquisition paths. The survey lines, planned along the main flow directions of the lagoon, provided a high-resolution georeferenced dataset, including both the vertical distribution of flow velocities and point-by-point depth measurements with a spatial resolution of approximately 1 m.

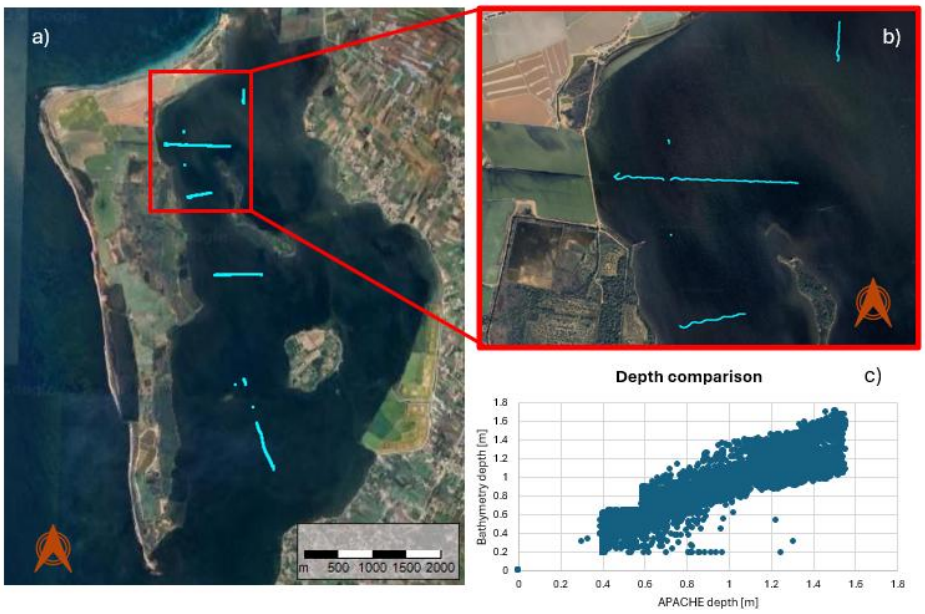

Figure 4.5.2: (a) Overview of the transects covered by the USV during the measurement campaigns, showing the spatial distribution of the surveyed areas across the lagoon. (b) Zoomed view of selected sections, highlighting the detail and density of the acquisition tracks used for ADCP and single-beam data collection. (c) scatterplot of bathymetry and Apache measures depth.

All measurements collected over the different survey days were merged into a single integrated dataset, while maintaining the exact temporal association between each point and its acquisition time. This approach allowed the subsequent tide correction of depth values according to the actual water level recorded at the time of each USV passage, thereby eliminating potential vertical misalignments caused by short-term water level variations within the lagoon.

In total, 13021 measurement points were collected, each containing geographic coordinates, measured depth, and acquisition timestamp. The tidal levels used for the correction were derived from monitoring stations located at the northern and southern inlets and at Altavilla Est, all referred to the same hydrometric zero adopted for the reference bathymetry.

In an initial comparison, carried out using uncorrected depth data, a noticeable dispersion was observed between the USV-measured depths ("APACHE depth") and the corresponding bathymetric values. This variability was primarily attributed to differences in water level during the acquisition period. Moreover, a larger variability was observed in the shallowest areas, where small fluctuations in water level and local bottom irregularities have a proportionally greater impact on the measured depth. Conversely, for deeper sections, the dispersion between measured and reference depths tends to decrease significantly, as the relative influence of tidal oscillations and positioning uncertainty becomes smaller compared to the total depth range. After applying the point-by-point tide correction, the depths were harmonized with respect to the common reference level, resulting in a clear improvement in consistency between the two datasets, as shown in Figure 2 subplot c).

The effectiveness of the correction procedure is evident in the post-correction comparison (Figure 4.5.3). The scatter plot (Figure 4.5.3b) displays an almost perfectly linear alignment between the USV (APACHE) and bathymetric depths, indicating a high level of agreement between the datasets.

A detailed analysis of the pointwise differences (Figure 4.5.3a) shows that most deviations fall within a narrow range, predominantly between +10 cm and −10 cm. The remaining discrepancies lie within the uncertainty range associated with acoustic measurements and the spatial resolution of the digital terrain model.

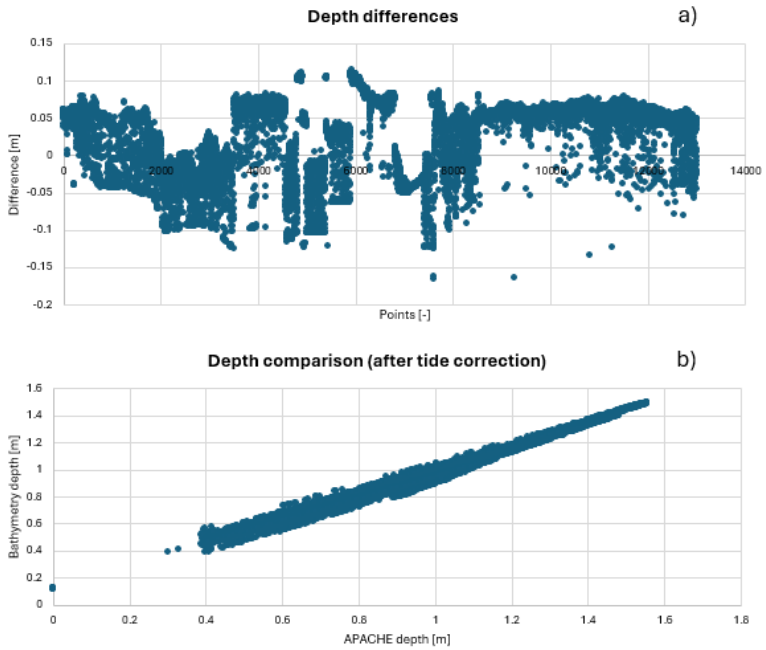

Figure 4.5.3: (a) Pointwise differences between APACHE-measured depths and reference bathymetry before and after tide correction. (b) Scatter plot showing the relationship between APACHE and bathymetric depths after tide correction, illustrating the strong linear correlation and improved consistency between the two datasets.

The results confirm the consistency between in situ measurements and the reference bathymetry for hydrodynamic modeling, ensuring the reliability of the boundary conditions. The integration of ADCP, single-beam, and tide-corrected data improves the quality of input data and provides a solid experimental validation of the model.

On the other hand, the drifter experiments were designed to capture real trajectories of passive particles driven by wind and current. The drifters recorded GPS positions at 1-minute intervals, enabling precise reconstruction of transport pathways and identification of recirculation zones.

Simultaneously, meteorological and hydrological monitoring at the fixed stations allowed for accurate boundary forcing in the model, ensuring that tidal and wind effects were realistically represented during the simulation period.

4.5.3.3 Modelling approaches

Hydrodynamic simulations have been developed using a numerical model. The model solves the depth-averaged shallow-water equations, which express the conservation of mass and momentum under hydrostatic and Boussinesq assumptions. Boundary conditions were defined using water level data

measured at the lagoon's northern and southern inlets, while spatially variable wind fields were applied based on local observations at Altavilla Est and Mulino.

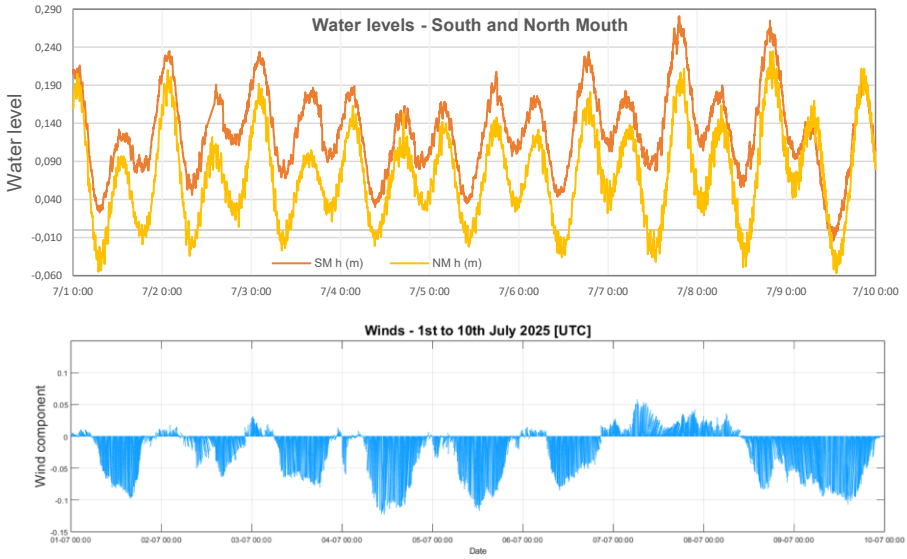

Figure 4.5.4: Measured water levels and wind conditions.

The model domain was discretized using an unstructured grid with variable resolution (5–25 m), allowing detailed representation of areas of interest. Model calibration is being developed tuning parameters as wind drag, bottom roughness and eddy viscosity, to reproduce the observed tidal range and current magnitudes.

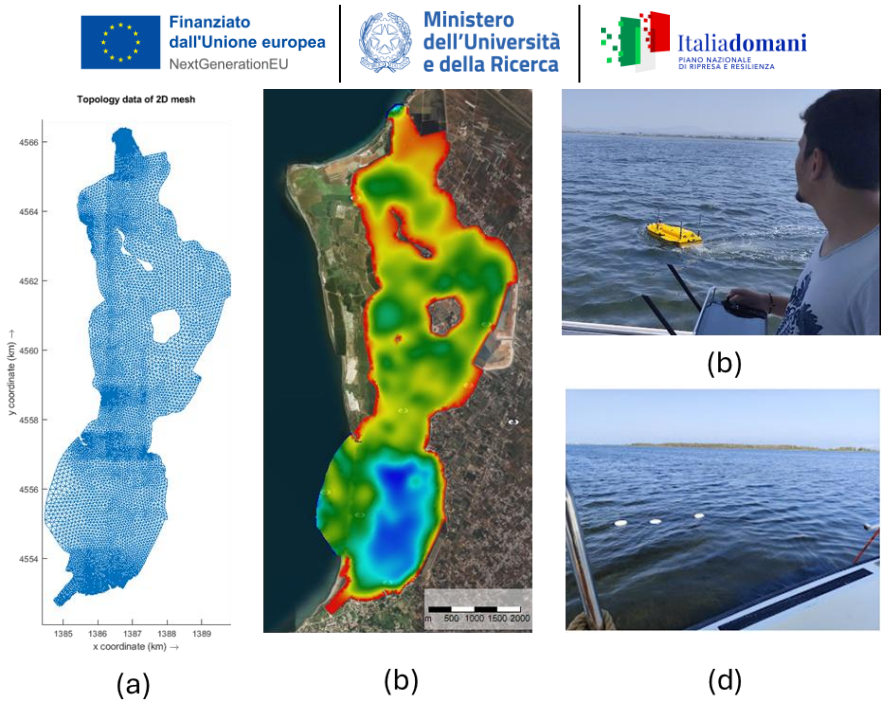

Figure 4.5.5: Stagnone lagoon. a) Mesh; b) bathymetry; c) USV drone; d) Stokes drifters.

4.5.4 Results

Preliminary outputs from the numerical model indicate that the numerical setup reproduces the dominant tidal dynamics and general circulation patterns of the Stagnone Lagoon.

Initial comparisons between simulated and observed water levels at the lagoon sensor at Altavilla Est show satisfactory agreement, with tidal amplitudes and phases closely matching field data. Early analyses of drifter trajectories also demonstrate promising consistency with modelled surface currents, though further tuning of wind forcing and bottom friction parameters is still ongoing.

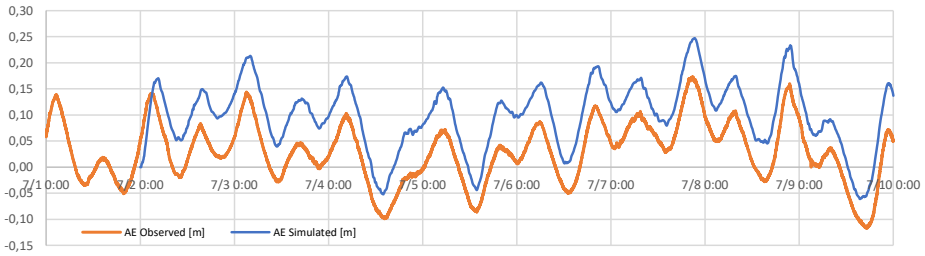

Figure 4.5.6: Comparison Altavilla Est water levels: observed and simulated.

The integration of USV-based bathymetric mapping is enhancing the accuracy of the model's digital terrain, especially in shallow and channel areas where previous data were limited. These updated bathymetries improved model stability and the accuracy of velocity predictions in subsequent runs.

Preliminary particle-tracking simulations have been executed to test the dispersion patterns of neutrally buoyant particles under different wind and tidal regimes. The results show clear dependence on wind direction and magnitude, confirming the expected sensitivity of surface transport to meteorological forcing.

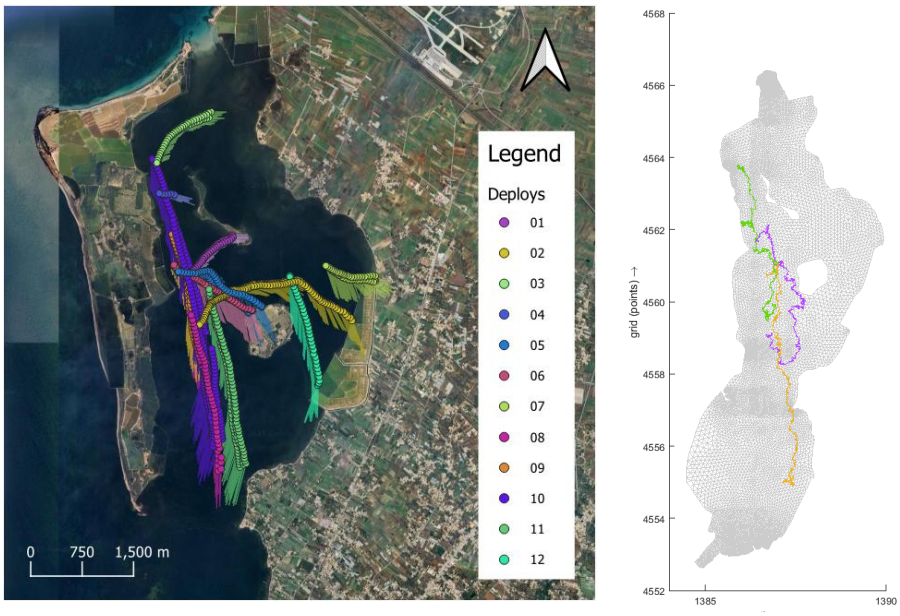

(a) *(b)*

Figure 4.5.7: (a) Stokes drifters deploys and (b) initial particle tracking simulation.

The model has been fully calibrated and validated using the complete dataset from the July 2025 campaign. Detailed analyses have quantified residence times, accumulation zones, and compared modelled dispersion patterns with field observations.

4.5.5 Scientific products and dissemination

Scientific outputs are currently in preparation, and dissemination activities are planned for the coming months as data processing and model validation progress.

The expected products include:

- A validated hydrodynamic model of the Stagnone Lagoon, integrating field and remote observations.
- A high-resolution bathymetric and hydrodynamic dataset to be made available through the UNIPA data repository upon validation.

These results were disseminated through:

- A scientific paper currently under preparation, provisionally titled “Multiscale Modelling and Validation of Surface Transport in a Shallow Coastal Lagoon Using USV and Drifters”.
- Planned presentations of intermediate results at national and international conferences.

The results obtained provided a comprehensive understanding of the hydrodynamic drivers governing the dispersion of plastic and bioplastic in shallow coastal systems.

4.6 Development of spectral sensing methodologies for monitoring and rapid identification and classification of macro- and microplastics dispersed in marine and coastal environments by fast and efficient spectral sensing technologies (UNIROMA1)

4.6.1 Introduction

The aim of this research was to develop spectral sensing strategies for environmental monitoring and rapid identification and classification of macro- and microplastics (MPs) dispersed in marine and coastal environments. The widespread diffusion of plastic litter represents a critical environmental concern, highlighting the need for effective monitoring tools to assess pollution levels and support sustainable management strategies. To achieve this goal, the research activities were divided into methodological strategies focused on the development and optimization of analytical methods based on hyperspectral imaging (HSI) technology and, in parallel, on the application of the developed spectral sensing strategies to several case studies representing different environmental matrices.

In particular, for methodological strategies, different acquisition parameters and classification models were evaluated to define an optimal analytical protocol for the rapid detection of MPs (*Analytical method 1*). Additionally, a custom micro-HSI scanner, specifically designed for MP analysis, was tested to evaluate its performance. The device allows for automatic scanning of areas up to 20 x 20 mm, significantly reducing analysis times compared to traditional techniques. The results demonstrated the device's ability to detect particles of different polymer types down to 150 µm (*Analytical method 2*).

Different innovative spectral sensing strategies were developed and applied to different case studies aiming at environmental monitoring and rapid identification and classification of macro- and MPs. Specifically, an innovative methodology was developed, based on HSI operating in the short-wave infrared range (SWIR: 1000-2500 nm), combined with chemometric data analysis, to directly detect and classify MPs both in sandy beaches (*Case study 1*) and marine sediments (*Case study 2*). The results demonstrated the feasibility of the analytical strategy to identify and classify polymers without prior extraction of MPs. Furthermore, laboratory-scale studies of plastic marine litter from various marine and coastal areas in Europe were conducted using HSI-based approaches for MP identification and classification (*Case study 3 and 4*). Moreover, to assess field applicability, a ground-based HSI device (*Case study 5*) and portable point-based spectrometer (*Case study 6*), both working in the near infrared range (NIR: 1000-1700 nm) were used for rapid monitoring of macroplastic litter in various coastal environments, enabling plastic debris mapping and in-situ screening directly at sampling sites, respectively. Finally, the research addressed the characterization of plastic pellets resulting from accidental spills (*Case study 7*) to validate rapid monitoring approaches and a low-cost methodology based on a machine learning tool for pellet classification was developed (*Case study 8*). In particular, the latter approach relies on morphological variables, avoiding the use of expensive instrumentation, providing a cost-effective solution for environmental monitoring and source traceability of plastic pellets.

4.6.2 Case study description

- **Case study 1: Application of hyperspectral imaging and machine learning for the automatic identification of microplastics on sandy beaches (Torre Guaceto, Brindisi, Italy).** Direct identification and classification of MPs in sandy beaches without prior extraction, in collaboration with UNIBA project partner (Rizzo et al., 2024).
- **Case study 2: Direct identification of microplastics in marine sediments by hyperspectral imaging and machine learning (Mar Piccolo, Taranto, Italy).** Direct identification and classification of MPs in

marine sediment samples without prior extraction, in collaboration with UNIBA project partner (Manuscript submitted).

- **Case study 3: Hyperspectral imaging for detecting plastic debris on shoreline sands to support recycling (Sabaudia, Latina, Italy).** MP litter classification on marine and coastal areas at laboratory-scale (Palmieri et al., 2024a).
- **Case study 4: Marine microplastic classification by hyperspectral imaging: Case studies from the Mediterranean Sea, the Strait of Gibraltar, the Western Atlantic Ocean and the Bay of Biscay.** MP litter classification on marine and coastal areas at laboratory-scale (Palmieri et al., 2024b).
- **Case study 5: Ground-based hyperspectral imaging for the detection of plastic waste on coastal areas (Torre Guaceto, Brindisi, Italy).** In-situ macroplastic litter classification by ground-based HSI sensor, in collaboration with UNIBA project partner (Manuscript under preparation).
- **Case study 6: Fast characterization of marine plastic litter by portable NIR spectroscopy for monitoring purposes (Cadiz, Spain).** In-situ macroplastic litter classification by portable NIR device (Manuscript under preparation).
- **Case study 7: Microplastic pollution from pellet spillage: Analysis of the Toconao ship accident along the Spanish and Portuguese coasts.** Plastic pellets characterization and degradation analysis, in collaboration with UNIBA project partner (Cocozza et al., 2025).
- **Case study 8: Cost-effective approaches for microplastic pellets characterization using a machine learning tool.** Plastic pellets characterization and degradation analysis, in collaboration with UNIBA project partner (Scarrica et al., 2025).

4.6.3 Methodologies

4.6.3.1 Analytical methods

Analytical method 1: Definition of the optimal analytical protocol for fast and efficient microplastic classification by HSI (Serranti et al., 2024)

The aim of this methodological study was to define the best analytical strategies for the characterization of MPs by HSI, testing different set up with reference to 1) spatial resolution, 2) wavelength range and 3) classification model. For these purposes, MPs dataset was created by shredding post-consumer plastic packaging samples selected among the most widespread polymers in the environment, i.e. PS, PP and PE. For each studied polymer, 3 size classes were prepared (i.e., size 1: -2 mm +1 mm; size 2: -1 mm +0.5 mm; size 3: <0.5 mm). The acquisition was carried out using the SisuCHEMA XL™ Chemical Imaging Workstation embedding an ImSpector™ N25E (Specim®, Finland) operating in the SWIR range. Hyperspectral images were acquired using two different objectives: a 31 mm lens, covering a 5 cm field of view (FOV) corresponding to a spatial resolution of 150 µm, and a macro lens, covering a 1 cm FOV, corresponding to a spatial resolution of 30 µm. Moreover, two spectral ranges were considered: 1000-1700 nm (NIR) and 1000-2500 nm (SWIR). Different classification models were tested on the same acquired images in order to evaluate their performances: PLS-DA, ECOC-SVM and NNPR. The HSI data processing was carried out using different tools running inside MATLAB® environment (version R2022b, The Mathworks, Inc., Natick, MA, USA). The classification models were evaluated by sensitivity and specificity values.

Analytical method 2: Custom micro-HSI scanner for microplastic detection and classification (Serranti et al., 2025)

The aim of the study was to test a custom micro-HSI scanner operating in the near-infrared range (NIR: 1000-1700 nm) for the detection of MPs. The prototype was designed by DV s.r.l. (Padua, Italy) as part of the PNRR RETURN project. The core of the system is an imaging spectrophotometer (XEVA-1696-XC130, Xenics Infrared Solution, Belgium) operating in the NIR range with a spectral resolution of 5 nm. Light enters through a slit of 30 µm × 9.6 mm, designed to optimize the compromise between resolution and intensity of the acquired signal. The system includes a dual-axis micro-positioning stage (X, Y) with a 20

mm travel range per axis and a displacement resolution of 160 nm to ensure precise sample placement. The movement is controlled by a management box with dedicated drivers and serial interface for connection to the computer. To ensure uniform illumination of the sample, the system is equipped with a microscope illuminator based on two 10 W halogen light sources positioned at a 45° angle relative to the sample. Complementing the spectrophotometer, the system also includes a CMOS camera (BASLER acA 1300-60gc, Germany) with a resolution of 1220 × 1024 pixels and a Gigabit Ethernet interface. This camera provides a visual reference for correct sample positioning and focus optimization prior to hyperspectral image acquisition. The system is mounted on a sturdy anodized aluminium structure, and 60 cm-high support column supports the entire optical system. Hyperspectral image acquisition is performed using SS4 software (Spectral Scanner, DV S.r.l., Padua, Italy). To evaluate the prototype's performance during its development, specific tests were performed on selected MPs of four different sizes and different types of polymers (high-density polyethylene - HDPE, polypropylene - PP, and polystyrene - PS) ground with an ultra-centrifugal mill (Retsch, ZM 300). The device allows for the automatic scanning of areas up to 20 x 20 mm. For each sample, a 3.37 x 3.37 mm area was scanned, taking approximately 1 minute per acquisition. To assess the spectral variance of the three polymers and understand their separability at different sizes, different combinations of preprocessing algorithms were tested on the acquired data hypercubes, on which principal component analysis (PCA) was subsequently applied. Furthermore, an Error Correcting Output Codes - Support Vector Machine (ECOC-SVM) model was developed to automatically and rapidly identify MPs based on their spectral signatures.

4.6.3.2 Experimental methods

n.a.

4.6.3.3 Modelling approaches

Different models have been developed for the identification and classification of macro- and microplastics and optimized to obtain the best performances when applied to the different case studies. The modelling approaches for the acquired hyperspectral images followed these main phases: preprocessing of spectra to highlight the differences between the various classes of materials, exploratory data analysis through Principal Component Analysis (PCA), development of the classification models using calibration datasets, application of the classification models to external validation datasets and, finally, evaluation of the classification model performance.

Specifically, on hyperspectral data, different algorithms have been applied depending on the specific needs. The most widely used pre-processing algorithms were scattering correction methods (i.e., Multiplicative Scatter Correction – MSC; Detrend; Standard Normal Variate – SNV; Normalization), spectral derivatives (i.e., Savitzky-Golay polynomial derivative filters), noise correction methods (i.e, Smoothing) and data centering (i.e., Mean Center – MC), typically applied at the end of preprocessing steps, to emphasize the differences between variables by removing the mean value.

After pre-processing phase, PCA was applied to spectral data for exploratory purposes. This technique is useful for providing an overview of the multivariate data and for evaluating the algorithms selected. The preprocessed data are decomposed into linear, orthogonal and independent combinations called principal components (PCs). The first few PCs are typically used to examine common features among samples and their clustering patterns. Indeed, samples with similar spectral signatures tend to group together in the score plots of the first two or three components. To build classification model, it is necessary to define the learning characteristics, that is, to define the classes of materials that constitute the calibration dataset. The classes setting occurs during the PCA phase.

Based on the results obtained in PCA, the type of classification model to be built was selected. The selection of the most appropriate classification model is a crucial aspect for material recognition by HSI. Linear models, such as partial least squares-discriminant analysis (PLS-DA), are simple, quick to train, and easy

to interpret. However, they are limited in handling the complexities of hyperspectral data, where relationships between variables can be nonlinear. Nonlinear models, such as nonlinear support vector machines (SVM) or neural networks, offer greater flexibility in capturing these complexities and improve recognition accuracy.

Finally, the performances of the developed classification model were evaluated using a pixel-based approach considering calibration and cross-validation for the calibration dataset and prediction for the validation dataset. The statistical metrics used were sensitivity and specificity. In particular, sensitivity expresses the ability of the model to correctly recognize samples belonging to the target class while minimizing the number of false negatives. On the contrary, specificity describes the ability of the model to correctly reject samples belonging to other classes while minimizing false positives. Both sensitivity and specificity range from 0 to 1, with a value of 1 indicating perfect predictive performance.

4.6.4 Results

Case study 1: Application of hyperspectral imaging and machine learning for the automatic identification of microplastics on sandy beaches (Rizzo et al., 2024)

The aim of this work was to apply and test SWIR-HSI strategy for direct identification and classification of MPs in beach sand samples, coupled with machine learning approaches (Figure 4.6.1). Sand samples were collected during a sampling campaign at Torre Guaceto beach (Brindisi, Italy), located along the Adriatic flank of the Apulia region, belonging to a natural protected area. A set of beach sand samples with the addition of known MPs particles (with an average diameter from 3 to 4 mm) composed of virgin and waste polymers was used to calibrate and validate a hierarchical classification model (Hi-PLS-DA) built for the recognition of 7 classes of materials: sand, natural material (plant and shells fragments), polyethylene terephthalate (PET), PP, PE, PS and expanded polystyrene (EPS). Parametric performances in prediction of the validation dataset show high-quality values ranging from 0.90 to 1.00 for sensitivity and from 0.91 to 1.00 for specificity. In addition, the classifier was applied on an external test dataset to verify the ability of the Hi-PLS-DA model in identifying MPs directly on sandy matrices. In total, the classifier identified 55 MPs. The most abundant polymer was EPS (38%), followed by PP (24%), PE (22%), PET (11%) and PS (5%). Overall, the results of the study demonstrated as the proposed approach represent a powerful, fast and effective alternative to the most common adopted analytical methods for MPs classification.

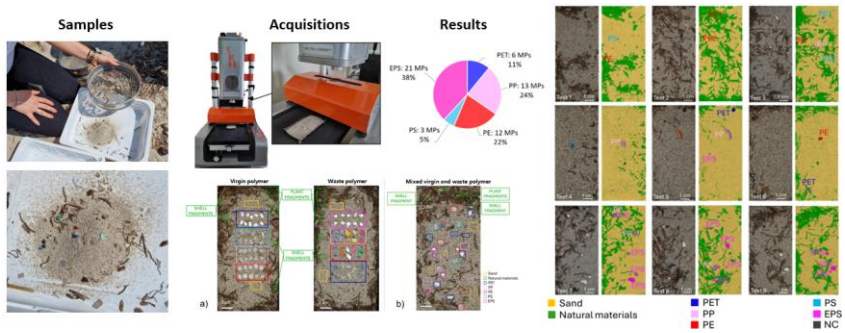

Figure 4.6.1: Schematic representation of Case study 1: Application of hyperspectral imaging and machine learning for the automatic identification of microplastics on sandy beaches.

Case study 2: Direct identification of microplastics in marine sediments by hyperspectral imaging and machine learning

The aim of this study was to apply an innovative methodology for identifying and classifying MPs in marine sediments, without preliminary extraction, thus significantly reducing analysis times (Figure 4.6.2). This approach was tested on marine sediment samples from the Mar Piccolo basin (Taranto, Italy), provided by UNIBA project partner. Samples were collected from eight different sites across both bays of Mar Piccolo using a grab sampler and then sieved. Nine granulometric classes (from -4 mm to +180 µm) were analyzed by SWIR-HSI using two instrumental setups based on particle size. Reference polymer particles were acquired and used to train classification models. Preprocessing algorithms were applied to enhance spectral differences between material classes. Principal Component Analysis (PCA) was employed to explore spectral variability and reduce data dimensionality. Two supervised classification models were developed: Hi-PLS-DA and ECOC-SVM. Both models successfully identified MPs of different polymers within sediment samples. Classification results were validated using Attenuated Total Reflectance Fourier Transform Infrared (ATR-FTIR) spectroscopy. MP concentrations ranged from 58 to 17,930 MPs/kg, with higher levels in finer sediment fractions and hotspot identified in MP_01 site, collected in proximity to the river mouth. PP was the most abundant polymer, followed by PE, PS, PET and PVC. PET was detected exclusively in the finest size classes, suggesting advanced fragmentation. The HSI-based strategy demonstrates high potential as a rapid tool for MP detection in complex environmental matrices, significantly reducing sample preparation and analysis time.

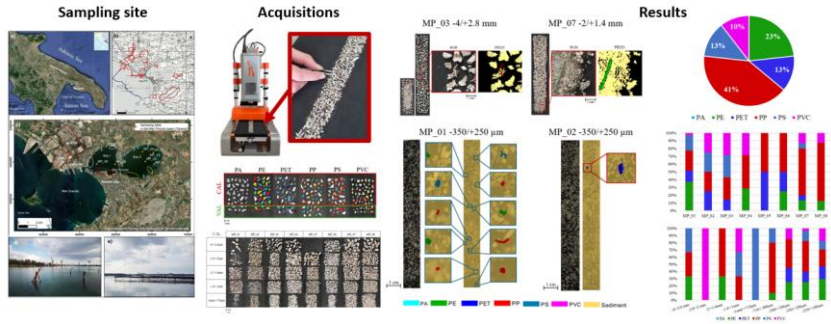

Figure 4.6.2: Schematic representation of Case study 2: Direct identification of microplastics in marine sediments by hyperspectral imaging and machine learning.

Case study 3: Hyperspectral imaging for detecting plastic debris on shoreline sands to support recycling (Palmieri et al., 2024a)

The aim of the study was to provide an operative tool finalized to perform an in-situ detection and characterization of plastic debris present in the coastal environment (i.e., beaches), adopting a NIR-HSI-based approach (Figure 4.6.3). In more detail, the possibility of identifying and classifying polymers of plastic debris by NIR-HSI in three different areas along the Pontine coastline of the Lazio region (Latina, Italy) was investigated. The study focused on three distinct beaches (i.e., Foce Verde, Capo Portiere, and Sabaudia), each characterized by a different type of sand. For each location, the adopted approach allowed for the systematic classification of the various types of plastic waste found. Three PLS-DA classification models were developed using a cascade detection strategy. The first model was designed to distinguish plastics from other materials in sand samples, the second to detect plastic particles in the sand, and the third to classify the type of polymer composing each identified plastic particle. Obtained results showed the correctly detection of plastics from sand and other materials (i.e., sensitivity = 0.892–1.000 and specificity

= 0.909–0.996). Furthermore, the recognition of polymer type was satisfactory, according to the performance statistical parameters (i.e., sensitivity = 1.000 and specificity = 0.991–1.000). This research confirms the potential of the NIR-HSI approach as a reliable, non-invasive method for plastic debris monitoring and polymer classification.

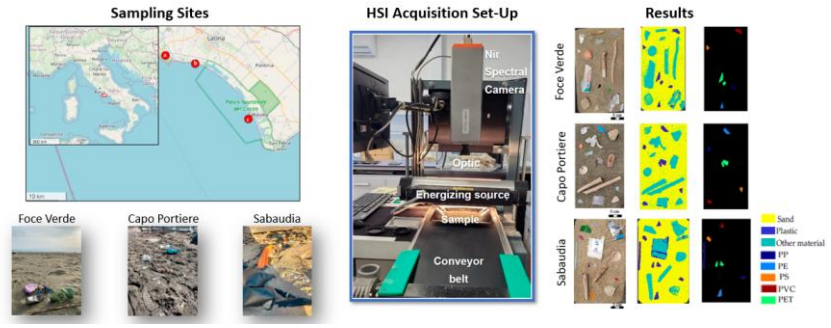

Figure 4.6.3: Schematic representation of Case study 3: Hyperspectral imaging for detecting plastic debris on shoreline sands to support recycling.

Case study 4: Marine microplastic classification by hyperspectral imaging: Case studies from the Mediterranean Sea, the Strait of Gibraltar, the Western Atlantic Ocean and the Bay of Biscay (Palmieri et al., 2024b)

The study aims the characterization of MP samples collected from unique geographical locations, including the Mediterranean Sea, Strait of Gibraltar, Western Atlantic Ocean and Bay of Biscay utilizing advanced HSI techniques working in the SWIR range (Figure 4.6.4). More in detail, an ad hoc hierarchical classification approach was developed and applied to optimize the identification of polymers. Morphological and morphometrical attributes of MP particles were simultaneously measured by digital image processing. Results showed that the collected MPs are mainly composed of PE followed by PP, PS and EPS. The investigated MPs belong to the fragments (86.8%), lines (9.2%) and films (4.0%) categories. Rigid (thick-walled) fragments were found at all sampling sites, while film-type MPs and lines were absent in some samples from the Mediterranean Sea and the Western Atlantic Ocean. Rigid fragments and lines are mainly made of PE, whereas PP is the most common polymer for the film category. Average Feret diameter of MP fragments decreases from EPS (3–4 mm) to PE (2–3 mm) and PP (1–2 mm). In conclusion, the proposed setup strategies based on HSI approach enable the classification of the polymers constituting MP particles and, at the same time, to measure and classify them by shape. Such multiple characterizations of MP samples at the individual level are proposed as a useful tool to explore the environmental selection of MP features (i.e., composition, category, size, shape) and to advance the understanding of the role of weathering, hydrodynamic and other phenomena in their transport and fragmentation.

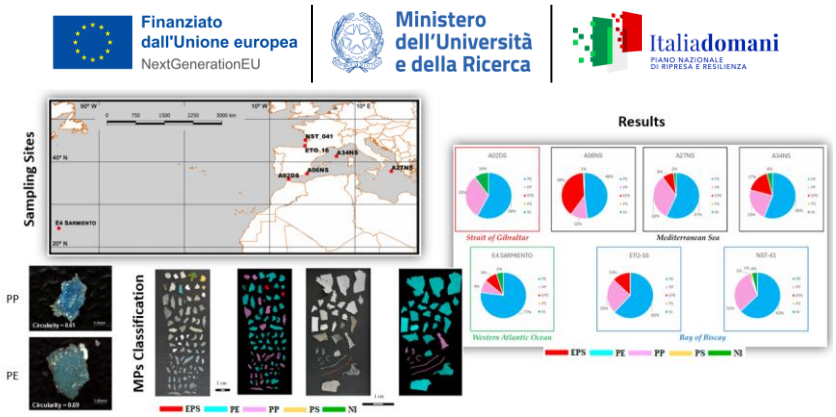

Figure 4.6.4: Schematic representation of Case study 4: Marine microplastic classification by hyperspectral imaging: Case studies from the Mediterranean Sea, the Strait of Gibraltar, the Western Atlantic Ocean and the Bay of Biscay.

Case study 5: Ground-based hyperspectral imaging for the detection of plastic waste on coastal areas

The aim of the work was to explores the application of a ground-based HSI Pan&Tilt system (DV s.r.l., Padua, Italy) for the detection and classification of plastic waste in sandy beach environments (Figure 4.6.5). Plastic waste pollution along coastal environments is a critical contributor to marine litter and a precursor to MP formation. The field trials were carried out at Torre Guaceto beach located in a natural protected area along the Adriatic coast of the Apulia region (Brindisi, Italy). Hyperspectral images were acquired using a system working in the VIS-NIR range, enabling accurate differentiation of polymer types under natural lighting conditions. The proposed approach includes in-field data acquisition, radiometric and spectral correction procedures and data-driven analysis for material discrimination in complex sandy environments. The results demonstrated the system's effectiveness in identifying and classifying plastic debris, including items partially buried in sediment or obscured by vegetation. By capturing detailed spectral fingerprints of macroplastics, this approach provides a robust basis for tracing potential sources of MP formation, enabling early intervention and pollution mitigation.

Figure 4.6.5: Schematic representation of Case study 5: Ground-based hyperspectral imaging for the detection of plastic waste on coastal areas.

Case study 6: Fast characterization of marine plastic litter by portable NIR spectroscopy for monitoring purposes

The aim of the study was to develop and test an in-situ analysis methodology for marine plastic debris based on portable NIR spectroscopy (Figure 4.6.6). This methodology allows for the direct identification of different types of polymers in the field and their distribution in relation to the environmental characteristics

of the sampling site. Compared to traditional laboratory techniques, the use of portable instrumentation offers a significant advantage for field analysis, reducing the need to transport samples to the laboratory and allowing for real-time data collection. For this purpose, a sampling campaign was conducted at the Laguna de La Algaida (Puerto Real, Spain) and 342 plastic samples larger than 5 mm were collected and analyzed using the portable JDSU MicroNIR spectrometer. After spectra were acquired, several preprocessing methods were applied and an exploratory analysis based on PCA was performed. By observing the score plots, it was possible to classify the plastics based on polymer type: PE, PP, and PS. However, some samples, such as transparent, black, or highly degraded plastics, were not identified. These samples were analyzed in the laboratory using ATR-FTIR spectroscopy to determine the polymer type. Based on the results obtained, it was possible to observe that the distribution of plastic waste is significantly influenced by coastal morphology and the type of vegetation present. In particular, areas closer to the coast have higher concentrations of flexible plastic waste, such as plastic films and bags, often trapped in vegetation, while rigid materials are transported further before settling. In conclusion, the portable MicroNIR spectrometer proved to be a fast and efficient tool for in-situ analysis.

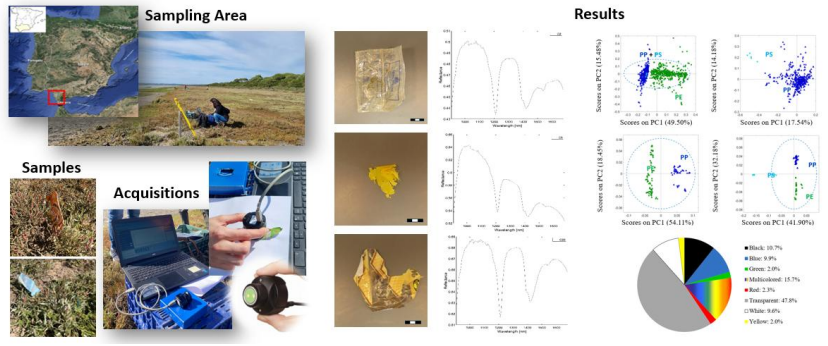

Figure 4.6.6: Schematic representation of Case study 6: Fast characterization of marine plastic litter by portable NIR spectroscopy for monitoring purposes.

Case study 7: Microplastic pollution from pellet spillage: Analysis of the Toconao ship accident along the Spanish and Portuguese coasts (Cocozza et al., 2025)

The aim of the study was to investigate a coastal stretch of 633 km in Asturias and Galicia (Spain) and Northern Portugal to assess pellets' concentration on 31 beaches. Specifically, the study was conducted to monitor the Toconao ship accident that occurred in December 2023, when 25 tons of pellets were lost from the vessel into the northwest Atlantic Ocean in front of the Portuguese coast (Figure 4.6.7). Field surveys were carried out in March 2024 and focused on sampling plastic pellets deposited along the shoreline. In total, 7263 pellets were sampled and characterized by size, degradation level, and color. One subset was characterized by weight (40% of the total) and another subset by polymer type (15% of the total) using ATR-FTIR spectroscopy. The results reveal that 94% of the 31 surveyed beaches contain pellets, with concentration values varying from 0 to 40.3 pellets/kgdw. By combining the accounted variables like size, degradation level, color, weight and polymer type, it emerges that 48.0% of the collected pellets could be linked to the Toconao spill.

Figure 4.6.7: Schematic representation of Case study 7: Microplastic pollution from pellet spillage: Analysis of the Toconao ship accident along the Spanish and Portuguese coasts.

Case study 8: Cost-effective approaches for microplastic pellets characterization using a machine learning tool (Scarrica et al., 2025)

The work aimed to develop a simplified methodology for pellet polymer classification using a Random Forest model that requires a limited set of training variables (Figure 4.6.8). Effective microplastic management requires reliable methods for their identification and classification, but the high cost of required equipment hinders large-scale implementation. However, artificial intelligence offers a promising solution for polymer analysis. The developed approach reduces model complexity while maintaining high classification performance, emphasizing simplicity, speed and efficiency. The method was tested on several pellet samples collected from the coasts of Spain, Portugal and Vulcano Island (Italy). The results highlight the robustness of the proposed model and its suitability for application in different environmental contexts. By balancing accuracy with computational efficiency, the proposed approach represents a practical tool for pellet classification.

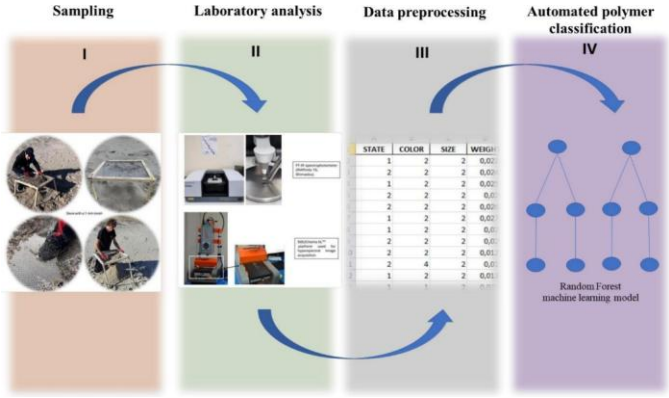

Figure 4.6.8: Schematic representation of Case study 8: Cost-effective approaches for microplastic pellets characterization using a machine learning tool.

Analytical method 1: Definition of the optimal analytical protocol for fast and efficient microplastic classification by HSI (Serranti et al., 2024)

The results obtained show the high efficiency of the proposed models, with very good classification results for the 3 polymers (Figure 4.6.9). The comparison of prediction results obtained by the three models highlights some differences. More in detail, PLS-DA provided the best performances for the MPs acquired with a spatial resolution of 150 µm, whereas the ECOC-SVM model showed the best classification results on the samples acquired at 30 µm. Regarding the two different spectral ranges, the results showed few differences between the NIR (1000-1700 nm) and the SWIR (1000-2500 nm) ranges. In conclusion, based on the results, the following general recommendations are proposed:

- For efficient and cost-effective analysis of MPs larger than 250 µm, a spatial resolution of 150 µm/pixel, a spectral range of 1000-1700 nm and a linear classification model such as PLS-DA are optimal. Instead, a higher spatial resolution of 30 µm/pixel, a broader spectral range of 1000-2500 nm and a non-linear model like ECOC-SVM are recommended for MP particles smaller than 250 µm.
- For a more detailed analysis of MP particles also in terms of morphological and morphometrical parameters, it is better to use the 30 µm/pixel resolution.
- The limit of detection (LOD) is 250 µm for the 150 µm/pixel resolution and ranges from 100 to 200 µm for the 30 µm/pixel resolution.

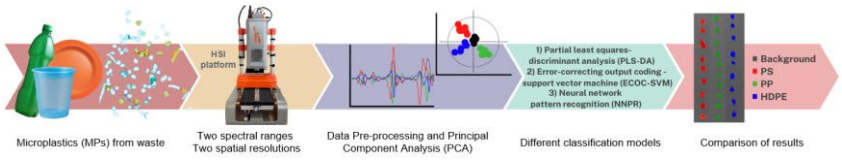

Figure 4.6. 9: Schematic representation of the Analytical method 1: Definition of the optimal analytical protocol for fast and efficient microplastic classification by HSI.

Analytical method 2: Custom micro-HSI scanner for microplastic detection and classification (Serranti et al., 2025)

The results obtained demonstrate that the use of the prototype, in combination with chemometrics, allows for the identification of different polymer types based on their distinct spectral signatures (Figure 4.6.10). However, as the microplastics' size decreases, the spectral contrast reduces, impacting the identification accuracy and highlighting the relationship between spectral quality and microplastic particle size. Furthermore, due to the reduced spectral quality, the detection of MPs smaller than 150 µm remains challenging.

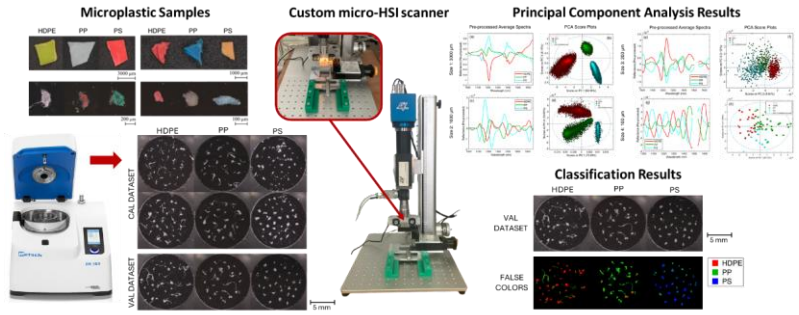

Figure 4.6.10: Schematic representation of Analytical method 2: Custom micro-HSI scanner for microplastic detection and classification.

4.6.5 Scientific products and dissemination

Publications:

Cocozza P., Gorga E., Palmieri R., Villano C., Bonifazi G., Anfuso G., Serranti S. - Fast characterization of marine plastic litter by portable NIR spectroscopy for monitoring purposes (*Manuscript under preparation*).

Serranti S., Capobianco G., Gorga E., Cucuzza P., Bonifazi G., Rizzo A., Lapietra I., Mastronuzzi G., Mele D - Direct identification of microplastics in marine sediments by hyperspectral imaging and machine learning (*Manuscript under review*).

Cocozza, P., Scarrica, V. M., Rizzo, A., Serranti, S., Staiano, A., Bonifazi, G., & Anfuso, G. (2025). Microplastic pollution from pellet spillage: Analysis of the Toconao ship accident along the Spanish and Portuguese coasts. *Marine Pollution Bulletin*, *211*, 117430. https://doi.org/10.1016/j.marpolbul.2024.117430

Cocozza, P., Serranti, S., Setini, A., Cucuzza, P., & Bonifazi, G. (2024). Monitoring of contamination by microplastics on sandy beaches at Vulcano Island (Sicily, Italy) by hyperspectral imaging. *Environmental Science and Pollution Research*, 1-14. https://doi.org/10.1007/s11356-024-34972-6

Palmieri, R., Gasbarrone, R., Bonifazi, G., Piccinini, G., & Serranti, S. (2024). Hyperspectral Imaging for Detecting Plastic Debris on Shoreline Sands to Support Recycling. *Applied Sciences*, *14*(23), 11437. https://doi.org/10.3390/app142311437

Palmieri, R., Serranti, S., Capobianco, G., Cózar Cabañas, A., Martí Morales, E., & Bonifazi, G. (2024). Marine Microplastic Classification by Hyperspectral Imaging: Case Studies from the Mediterranean Sea, the Strait of Gibraltar, the Western Atlantic Ocean and the Bay of Biscay. *Applied Sciences*, *14*(20), 9310. https://doi.org/10.3390/app14209310

Scarrica, V. M., Cocozza, P., Anfuso, G., Staiano, A., Bonifazi, G., Rizzo, A., & Serranti, S. (2025). Cost-effective approaches for microplastic pellets characterization using a machine learning tool. *Ecological Informatics*, 103230. https://doi.org/10.1016/j.ecoinf.2025.103230

Serranti, S., Capobianco, G., Cucuzza, P., & Bonifazi, G. (2024). Efficient microplastic identification by hyperspectral imaging: A comparative study of spatial resolutions, spectral ranges and classification models to define an optimal analytical protocol. *Science of the Total Environment*, *954*, 176630. https://doi.org/10.1016/j.scitotenv.2024.176630

Conference proceedings indexed in Scopus:

Rizzo, A., Serranti, S., Cucuzza, P., Lisco, S., Marsico, A., Bonifazi, G., & Mastronuzzi, G. (2024). Application of hyperspectral imaging and machine learning for the automatic identification of microplastics on sandy beaches. In Algorithms, Technologies, and Applications for Multispectral and Hyperspectral Imaging XXX (Vol. 13031, pp. 181-193). SPIE. https://doi.org/10.1117/12.3013227 SPIE Defense + Commercial Sensing Conference (21-25 April 2024, National Harbor, Maryland, United States).

Serranti, S., Bonifazi, G., Capobianco, G., Gorga, E., D'Agostini, M., & Dall'Ava, A. (2025). Custom hyperspectral imaging scanner for microplastic detection and classification: hardware and data processing specifications. In Algorithms, Technologies, and Applications for Multispectral and Hyperspectral Imaging XXXI (Vol. 13455, pp. 247-257). SPIE. https://doi.org/10.1117/12.3052766 SPIE Defense + Commercial Sensing 2025 (13-17 April 2025, Orlando, Florida, United States).

Presentations at International Conferences:

Bonifazi G., Capobianco G., Cocozza P., Mastronuzzi G., Rizzo A., Serranti S. - Identification of plastic debris on beaches by ground-based hyperspectral imaging - ECDS 2023: Emerging Concepts & Design for Sustainability (8-11 October 2023, Villers-sur-Mer, Calvados, France).

Cocozza P., Serranti S., Setini A., Cucuzza P., Bonifazi G. - Monitoring of contamination by microplastics on sandy beaches at Vulcano island (Italy) by different spectroscopic techniques - 5th International Conference on Pollutant Toxic Ions and Molecules (6-9 November 2023, Caparica, Portugal).

Capobianco, G., Cucuzza, P., Gorga, E., Serranti, S., Rizzo, A., Lapietra, I., Mastronuzzi, G., Mele, D., Bonifazi, G. - Hyperspectral imaging applied to microplastic monitoring in marine sediments from a highly

contaminated coastal site (Taranto, southern Italy) - 11th International Conference on Sustainable Solid Waste Management (19-22 June 2024, Rhodes, Greece).

Rizzo A., Barracane G., Bonifazi G., Capobianco G., Gorga E., Mele D., Scardino G., De Santis V., Lapietra I, La Salandra M., Lisco S., Liso S., Marsico A., Mastronuzzi G., Parise M., Serranti S., Scicchitano G., Sozio A. - Litter distribution in marine and coastal sediments: highlights from ongoing research projects - SGI-SIMP: Geology for a sustainable management of our Planet (3-5 September 2024, Bari, Italy).

Rizzo A., Anfuso G., Barracane G., Bonifazi G., Capobianco G., Cucuzza P., Gorga E., Lapietra I., Lisco S., Liso S., Marsico A., Mastronuzzi G., Mele D., Parise M., Scardino G., Serranti S., Sozio A., Scicchitano G. - Litter distribution in marine and coastal environments: case studies from the Apulia region (Southern Italy) – LITTORAL 2024: European Coastal Challenge Summit (24-27 September 2024, Constanta, Romania).

Gorga E., Serranti S., Capobianco G., Bonifazi G. - Identification and Classification of Microplastics by a Micro-Hyperspectral Imaging Scanner Prototype - NIR2025: 22nd International Conference on Near Infrared Spectroscopy (8-12 June 2025, Rome, Italy).

Capobianco G., Cucuzza P., Rizzo A., Bonifazi G., Mastronuzzi G., Serranti S. - Ground-based hyperspectral imaging for the detection of plastic waste on coastal areas - CSI2025: XLIV. Colloquium Spectroscopicum Internationale (27-31 July 2025, Ulm, Germany).

Cocozza P., Gorga E., Palmieri R., Villano C., Anfuso G., Bonifazi G., Serranti S. - Fast characterization of marine plastic litter by portable NIR spectroscopy for monitoring purposes and sustainable recycling - ISWA 2025: World Congress & Exhibition Re-imagine waste. "Towards a wasteless future or a wasteful planet?" (27-29 October 2025, Buenos Aires, Argentina).

Abstracts accepted for presentations at International Conferences:

S. Serranti, G. Bonifazi, G. Capobianco, P. Cocozza, E. Gorga, A. Polettini, M. Falzarano, R. Pomi, A. Rossi, A. Rizzo, I. Lapietra, S. Lisco, A. Marsico, G. Mastronuzzi, D. Mele - Rapid identification and classification of macro- and microplastics in coastal and marine environments by innovative spectral sensing technologies - SWRMA2026: Sustainable Water Management and Resource Adaptation International Conference (17-18 June 2026, Roma, Italy).

Dissemination:

Rizzo A., Bonifazi G., Capobianco G., Gorga E., Mele D., Scardino G., De Santis V., Lapietra I., La Salandra M., Lisco S., Liso S., Marsico A., Mastronuzzi G., Parise M., Serranti S., Scicchitano G., Sozio A. - Litter distribution in marine and coastal sediments: case studies from Apulia Region - RETURN Dissemination Workshop (1-2 February 2024, Turin, Italy).

Pagliaccia B., Santini G., Lubello C., Maisto G., Gori R., Francalanci S., Polettini A., Falzarano M., Cincinelli A., Sforzi L., Serranti S., Capobianco G., Gorga E., Falsini S., Colzi I., Rizzo A. - Microplastics: from the detection to the characterization of their effects into the environment - RETURN Dissemination Workshop (19-21 June 2024, Bari, Italy).

Rizzo A., Capobianco G., De Santis V., Gorga E., Lapietra I., Lisco S., Liso S., Marsico A., Mastronuzzi G, Mele D., Parise M., Scardino G., Scicchitano G., Serranti S. - Macro and Micro Litter distribution in marine and coastal sediments: highlights from ongoing research activities - RETURN Dissemination Workshop (19-21 June 2024, Bari, Italy).

Serranti S., Capobianco G., Cucuzza P., Gorga E., Bonifazi G. - Definition of the optimal analytical protocol for the rapid and efficient characterization of microplastics by hyperspectral imaging - RETURN Dissemination Workshop (27-29 November 2024, Bologna, Italy).

Gorga E., Bonifazi G., Capobianco G., Cocozza P., Serranti S. - Development of spectral sensing methodologies for monitoring and rapid identification and classification of macro- and microplastics dispersed in terrestrial and marine environments – RETURN Spoke VS4 Plenary Meeting (30-31 October 2025, Rome, Italy).

4.7 Contaminant bioaccumulation in biota and biological responses (OGS)

4.7.1 Introduction

Mercury contamination in the Adriatic Sea has resulted in the accumulation of methylmercury (MeHg) in marine food webs, with implications for ecosystem functioning and human exposure. Assessing MeHg transfer across trophic levels and understanding key biogeochemical processes in coastal sediments are therefore essential.

This section presents two complementary methodological approaches: (i) trophodynamic ecosystem modelling to quantify MeHg bioaccumulation across the Adriatic Sea food web, and (ii) genome-scale metabolic modelling to investigate microbial sulfur cycling and hydrogen sulfide (H_2S) dynamics in the surface sediments of the Venice Lagoon.

the Ecopath with Ecosim–Ecotracer framework. Using extensive empirical data and modelled planktonic MeHg concentrations, the tool quantifies methylmercury transfer across the food web and reproduces trophic magnification patterns. By combining dietary uptake, respiration-driven assimilation and temperature-dependent elimination, the model provides a basin-scale estimates of exposure for ecologically and commercially important species, strengthening the overall framework for ecosystem-based contaminant and risk assessment.

Bioaccumulation model for mercury in lagoonal species of commercial interest has been developed and coupled with high-resolution hydrodynamic–biogeochemical simulations. This framework has been applied to Tapes philippinarum, a species of central socio-economic relevance in the Venice Lagoon, enabling the quantification of temporal variability in Hg and MeHg uptake and the assessment of risks for human consumption relative to the Tolerable Weekly Intake.

The genome-scale metabolic model (GSM) tailored to microbial communities in the Venice Lagoon. This modelling framework exploits genomic information to better characterise metabolic pathways relevant for sulphur cycling and for the microbial production of hydrogen sulphide (H_2S), a process tightly linked to redox dynamics and organic-matter degradation in an ecosystem undergoing both anthropogenic pressures, including organic chemical pollution and climate-driven changes. The GSM approach offers a novel way to integrate metagenomic datasets with biogeochemical models, thus improving the representation of microbially mediated contaminant transformations.

4.7.2 Case study description

The Northern Adriatic is a shallow, semi-enclosed shelf system that is strongly influenced by land-derived inputs (freshwater, nutrients and pollutants). Mercury (Hg) contamination has major historical point sources: (i) the Idrija Hg mine (Slovenia), whose legacy is transferred downstream via the Soča/Isonzo River to the Gulf of Trieste and adjacent northern Adriatic sediments and waters (Širca et al., 1999; Pavoni et al., 2021), and (ii) releases from chlor-alkali plants in the upper Adriatic lagoons—classically the industrial area of Venice Lagoon (Bloom et al., 2004) and the Torviscosa chlor-alkali plant impacting the Marano–Grado Lagoon system (Piani et al., 2005). Beyond total Hg loads, risk is driven by methylmercury (MeHg), the most toxic and bioaccumulative species, whose production is tightly coupled to organic matter dynamics. MeHg is formed predominantly in the oxic water column of deep ocean, but sediment are also an important site for Hg methylation, which is promoted near oxic–anoxic interfaces in organic-rich coastal sediments (Sunderland et al., 2006). In the Northern Adriatic, episodic stratification, high organic-matter delivery from productive waters, and sediment diagenesis can therefore link eutrophication/primary production to the creation of anoxic microniches and enhanced Hg methylation, increasing the potential for MeHg entry into food webs in coastal lagoons and nearshore areas.

4.7.3 Methodological framework

Mercury bioaccumulation and its controlling processes were investigated through an integrated, multi-scale methodological framework designed to capture processes operating from ecosystem to microbial levels. The methodology combines three complementary modelling components addressing (i) trophic transfer of methylmercury in the Adriatic Sea, (ii) site-specific mercury bioaccumulation in the Venice Lagoon, and (iii) benthic microbial processes regulating sediment redox conditions.

At the basin scale, trophodynamic modelling was used to quantify methylmercury (MeHg) transfer across the Adriatic Sea food web, from primary producers to top predators. This component provides an ecosystem-level representation of bioaccumulation and biomagnification patterns based on trophic interactions and empirical contaminant data.

At the lagoon scale, mercury cycling and organism-level exposure were assessed for the Venice Lagoon, a system historically impacted by industrial mercury contamination. A coupled fate and transport–bioaccumulation framework was applied to simulate Hg and MeHg uptake in a key benthic organism, allowing site-specific evaluation of bioaccumulation dynamics under local environmental conditions.

To complement these approaches, microbial-scale modelling was used to resolve benthic biogeochemical processes in lagoon sediments. In particular, a genome-scale metabolic modelling framework was applied to investigate microbial sulfur cycling and hydrogen sulfide (H_2S) dynamics, which strongly influence sediment redox conditions and indirectly affect mercury sequestration and mobility.

Together, these methodological components provide a coherent framework to link food-web bioaccumulation, local organism exposure, and benthic microbial processes, enabling an integrated assessment of mercury dynamics in the Adriatic Sea and the Venice Lagoon.

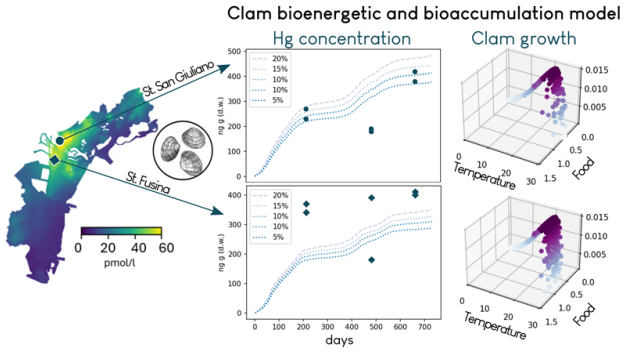

Figure 4.7. 1: Scheme of the off-line coupling between the SHYFEM-Hg model and the bioenergetic-bioaccumulation model for clams. The dotted lines represent the time evolution of total Hg concentration in the clam at the two stations San Giuliano (upper panel) and Fusina (lower panel) modeled by varying the assimilation efficiency. The 3d plots show the growth rate as a function of water temperature and food availability (concentration of organic particles).

4.7.3.1 Analytical methods

n.a

4.7.3.2 Experimental methods

n.a

4.7.3.3 Modelling approaches

Three complementary modelling approaches were applied to investigate mercury bioaccumulation and benthic biogeochemical processes at different ecological scales.

Ecosystem-scale trophodynamic model

Mercury bioaccumulation in the Adriatic Sea food web was simulated using **Ecopath with Ecosim (EwE)** coupled with the **Ecotracer** routine. EwE is a trophodynamic ecosystem modelling framework that represents species or groups of species with similar ecological characteristics as functional groups and

describes trophic interactions based on mass-balance and time-dynamic principles (Christensen and Walters, 2004; Libralato et al., 2020).

The Ecotracer module enables the simulation of contaminant transfer within food webs by tracking contaminant flows associated with biomass exchanges and accounting for dietary uptake, elimination, decay, and physical exchange processes (Christensen et al., 2008; Serpetti et al., 2025). In this study, Ecotracer was used to simulate methylmercury (MeHg) bioaccumulation across trophic levels, from primary producers to top predators, allowing the quantification of trophic magnification patterns at the basin scale.

Lagoon-scale bioaccumulation model

At the lagoon scale, mercury cycling and bioaccumulation were investigated in the Venice Lagoon, a system historically contaminated by industrial discharges from the Porto Marghera area (Rosati et al., 2020). Hg and MeHg bioaccumulation was simulated using a coupled **high-resolution fate and transport model** and a **zero-dimensional, individual-based bioaccumulation model**, applied at multiple lagoon sites.

This modelling framework resolves environmental exposure concentrations of mercury species and simulates uptake, accumulation, and elimination processes at the organism level for the bivalve *Tapes philippinarum*, a key benthic species relevant for ecosystem functioning and human consumption. The approach enables site-specific assessment of bioaccumulation dynamics under local environmental conditions.

Microbial genome-scale metabolic model

Benthic biogeochemical processes in surface sediments of the Venice Lagoon were investigated using a **community genome-scale metabolic model (cGEM)** (Saidi et al. in prep**.)**. The model focuses on microbial sulfur cycling and hydrogen sulfide (H_2S) dynamics, processes that strongly influence sediment redox conditions and play a key role in regulating metal speciation and binding in sediments.

The cGEM was developed by merging 11 individually curated genome-scale metabolic models derived from metagenome-assembled genomes of key sulfur-cycling bacteria (Banchi et al., 2024). Genome-scale metabolic modelling enables the reconstruction of microbial metabolic networks linking genes, reactions, and metabolites and allows simulation of metabolic fluxes under different environmental constraints (Wieder et al., 2015; Lennon et al., 2024).

Microbial sulfate reduction rates in the Venice Lagoon sediments are among the highest reported in coastal environments (Zaggia et al., 2007), leading to substantial hydrogen sulfide production that can accumulate under low-oxygen conditions and pose ecological risks (Brigolin et al., 2021). When oxygen or alternative electron acceptors are available, sulfur-oxidizing and denitrifying bacteria mitigate sulfide accumulation (Heijs and van Gemerden, 2000; Cardoso et al., 2006).

Although mercury transformations are not explicitly simulated within the genome-scale model, the resolved microbial processes provide mechanistic insight into benthic conditions that influence mercury sequestration and potential remobilization. This addresses the need for more explicit biological mechanisms in ecosystem models, as highlighted by recent studies (Wieder et al., 2015; ASM, 2023; Cavicchioli et al., 2019).

Model implementation and runs

For the **ecosystem-scale trophodynamic model**, the Ecopath with Ecosim (EwE) framework coupled with the Ecotracer routine was implemented for the Adriatic Sea using a functional-group representation of the ecosystem. Environmental methylmercury (MeHg) concentrations were imposed as steady-state boundary conditions to allow the system to reach equilibrium contaminant levels across trophic groups. Long-term simulations were performed to ensure convergence of MeHg concentrations and stability of model outputs. For functional groups lacking empirical concentration data, initial MeHg values were estimated based on trophic level relationships derived from the compiled dataset. Model outputs were evaluated by comparison with observed MeHg concentrations, with particular attention to invertebrate groups used for model validation.

The **lagoon-scale fate and transport–bioaccumulation model** was implemented for different sites in the Venice Lagoon under specific environmental conditions (Rosati et al., in prep.). Outputs from the fate and transport model provided site-specific exposure concentrations of Hg and MeHg in water and sediments.

These concentrations were used as inputs for the zero-dimensional, individual-based bioaccumulation model applied to the bivalve *Tapes philippinarum*. Simulations focused on steady-state bioaccumulation patterns, providing baseline estimates of organism-level mercury accumulation under current conditions and allowing comparison among lagoon sites.

The **community genome-scale metabolic model (cGEM)** was implemented using a constraint-based modelling framework. Environmental conditions were applied as boundary constraints on nutrient availability, electron acceptors, and organic substrates. Model runs were designed to explore alternative environmental scenarios affecting microbial metabolism, with particular emphasis on sulfate reduction, hydrogen sulfide (H_2S) production, and pollutant degradation pathways. Flux balance analysis was used to quantify changes in metabolic flux distributions under different conditions, allowing the identification of scenarios associated with elevated H_2S production or enhanced pollutant removal.

Across all modelling approaches, simulations were designed to represent long-term, quasi-equilibrium conditions rather than short-term transient events. Although the three models operate at different biological and spatial scales and are not dynamically coupled, their coordinated implementation provides complementary insights into food-web bioaccumulation, site-specific organism exposure, and benthic microbial processes. Together, these model runs support an integrated interpretation of mercury bioaccumulation patterns and benthic biogeochemical controls in the Adriatic Sea and the Venice Lagoon.

4.7.4 Results

Mercury bioaccumulation in the Adriatic Sea food web

A database of Hg and MeHg concentrations in the biota of the Adriatic Sea was created for model validation and future studies. A first calibrated version of the model was obtained in a 0-dimensional configuration and provided the bioaccumulation in the Adriatic Sea biota.

The compilation of methylmercury (MeHg) data for the Adriatic Sea biota revealed clear and systematic variations across trophic groups.

Model results shown in Table 4.2.1 show overall a strong trophic magnification pattern, with MeHg concentrations increasing from primary producers and small invertebrates to higher predators. Primary producers and microbial groups exhibited extremely low concentrations ($<10^{-3}$ g/t), however, the largest increase in MeHg concentrations occur between the water and primary producers, which bioconcentrate MeHg to values approximately 300,000 times the value of seawater. Intermediate trophic levels -including decapods, cephalopods, and small pelagic fish- displayed mid-range concentrations (0.03–0.7 g/t), reflecting dietary pathways and differences in metabolic rates and feeding strategies. High trophic-level predators, particularly large pelagic fish and demersal piscivores, showed substantially higher concentrations (0.7–1.5 g/t), indicative of cumulative dietary exposure. Marine mammals displayed the highest recorded values in the dataset, with common bottlenose dolphin (13.8 g/t) and mid-large odontocetes (8.1 g/t) representing the upper end of the bioaccumulation spectrum. These findings are consistent with global observations for long-lived predators in semi-enclosed basins.

Between trophic levels (TL), the average concentration increase of secondary trophic levels is 13 times the value of primary producers. TL3 organisms increase MeHg concentration 3 times over TL 2, and TL4 organisms increase in concentration is 8-fold. Mid-large odontocetes, the only TL 5 group have a 5,5 fold increase over TL 4 organisms' concentrations. Thus, for living organisms there is an average increase in MeHg concentration between each trophic level of 7.5, and a 3,500-fold increase between TL 5 and TL 1.

Model validation against invertebrate observations showed a good agreement. This indicates that the EwE–Ecotracer configuration captures the dominant processes governing MeHg accumulation, including dietary assimilation, respiration-based uptake for fish and cephalopods, and elimination through predation, mortality. The calibrated Ecotracer model represents a valuable tool for scenario analysis. This capability is particularly relevant for supporting risk assessment, spatial management, and ecosystem-based fisheries management in the Adriatic Sea.

Group	MeHg (g/t)	Type	Trophic Level (est.)	Habitat	Diet	Commercial relevance
Seabirds	0,192	Vertebrate	4,06	Surface/Div	General consumer	Low/variable
Marine turtles	0,144	Vertebrate	3,41	Benthopela	General consumer	Low/variable
Mid-large odontocetes	8,106	Vertebrate	5,20	Pelagic	Piscivore	Low/variable
Common bottlenose dolphin	13,8	Vertebrate	4,85	Pelagic	Piscivore	Low/variable
Striped dolphin	5,165	Vertebrate	4,86	Pelagic	Piscivore	Low/variable
Fin whale	0,278	Vertebrate	4,28	Pelagic	General consumer	Low/variable
Rays skates (slope)	0,106	Vertebrate	3,70	Slope - mixe	General consumer	Low/variable
Rays skates (shelf)	0,596	Vertebrate	4,04	Shelf - mixe	General consumer	Low/variable
Sharks (slope)	0,415	Vertebrate	4,51	Slope - mixe	Piscivore	Low/variable
Sharks (shelf)	1,01	Vertebrate	4,46	Shelf -mixec	Piscivore	Low/variable
Blackmouth catshark	0,318	Vertebrate	4,36	Demersal	Piscivore	Low/variable
Large pelagic fish	0,627	Vertebrate	4,84	Pelagic	Omnivore / carnivore	Low/variable
Medium pelagic fish	0,992	Vertebrate	4,61	Pelagic	Omnivore / carnivore	Low/variable
Demersal piscivorous fish (slope)	0,705	Vertebrate	4,76	Demersal	Piscivore	Low/variable
Demersal piscivorous fish (shelf)	0,322	Vertebrate	4,46	Demersal	Piscivore	Low/variable
Demersal fish (slope)	1,109	Vertebrate	3,65	Demersal	General consumer	Low/variable
Demersal fish (shelf)	0,254	Vertebrate	3,43	Demersal	General consumer	Low/variable
Epipelagic fish	0,075	Vertebrate	3,99	Epipelagic	Omnivore / carnivore	Low/variable
Mesopelagic crustacean feeding fish	0,067	Invertebrate	3,60	Mesopelagi	General consumer	Moderate
Zooplankton jellyfish feeding fish	0,171	Invertebrate	3,25	Bathypelagi	Zooplanktivore	Moderate
Other flatfishes	0,119	Vertebrate	3,56	Demersal	General consumer	Low/variable
Turbot and brill	0,065	Vertebrate	4,76	Demersal	General consumer	Low/variable
Gurnads	0,217	Vertebrate	3,58	Demersal	Omnivore / carnivore	High commercial relevance
Other gadids	0,458	Vertebrate	4,06	Mixed	Omnivore / carnivore	Low/variable
Other small pelagics	0,03	Vertebrate	3,56	Pelagic	General consumer	Low/variable
Mackerels	0,309	Vertebrate	4,25	Pelagic	Omnivore / carnivore	High commercial relevance
Anglers	0,388	Vertebrate	4,98	Bathydemer	Piscivore	Low/variable
Sardine (age 0)	0,064	Vertebrate	3,41	Pelagic-neri	General consumer	High commercial relevance
Sardine (age 1+)	0,052	Vertebrate	3,40	Pelagic-neri	General consumer	High commercial relevance
Anchovy (age 0)	0,064	Vertebrate	3,41	Pelagic-neri	General consumer	High commercial relevance
Anchovy (age 1+)	0,03	Vertebrate	3,41	Pelagic-neri	General consumer	High commercial relevance
Solea (age 0)	0,036	Vertebrate	3,07	Demersal	General consumer	High commercial relevance
Solea (age 1)	0,043	Vertebrate	3,17	Demersal	General consumer	High commercial relevance
Solea (age 2+)	0,013	Vertebrate	3,18	Demersal	General consumer	High commercial relevance
Red mullet (0,i)	0,076	Vertebrate	3,51	Demersal	Omnivore / carnivore	High commercial relevance
Red mullet (1,m)	0,353	Vertebrate	3,43	Demersal	Omnivore / carnivore	High commercial relevance
Hake (size 0)	0,085	Vertebrate	3,72	Generalist	Omnivore / carnivore	High commercial relevance
Hake (size 1)	0,159	Vertebrate	4,42	Demersal	Omnivore / carnivore	High commercial relevance
Hake (size 2)	0,216	Vertebrate	4,48	Demersal	Omnivore / carnivore	High commercial relevance
Other cephalopods (slope)	0,018	Invertebrate	3,76	Slope - mixe	General consumer	Moderate
Other cephalopods (shelf)	0,01	Invertebrate	4,00	Shelf - mixe	General consumer	Moderate
Squids	0,073	Invertebrate	4,50	Mixed	General consumer	Moderate
Common cuttlefish	0,009	Vertebrate	3,92	Benthic	General consumer	Low/variable
Musky-Horned octopus	0,019	Invertebrate	4,39	Benthic	General consumer / scavenger	Moderate
Mantis shrimp (0,i)	0,116	Invertebrate	3,76	Benthic	General consumer	High commercial relevance
Mantis shrimp (1,m)	0,146	Invertebrate	3,90	Benthic	General consumer	High commercial relevance
Norway lobster (0,i)	0,054	Invertebrate	3,31	Benthic	General consumer / scavenger	High commercial relevance
Norway lobster (1,m)	0,609	Invertebrate	3,31	Benthic	General consumer / scavenger	High commercial relevance
Blue and red shrimp	0,05	Invertebrate	3,26	Benthic	Invertebrate predator / scavenger	High commercial relevance
Red giant shrimp	0,068	Invertebrate	3,44	Benthopela	Invertebrate predator / scavenger	High commercial relevance
Deep-water rose shrimp (0)	0,05	Invertebrate	3,26	Benthopela	Invertebrate predator / scavenger	High commercial relevance
Deep-water rose shrimp (1+)	0,072	Invertebrate	3,47	Benthopela	Invertebrate predator / scavenger	High commercial relevance
Caramote prawn	0,036	Invertebrate	3,07	Benthic	Invertebrate predator	Moderate
Decapods: Reptantia (slope)	0,043	Invertebrate	3,17	Slope benth	Invertebrate predator / scavenger	Moderate
Decapods: Reptantia (shelf)	0,03	Invertebrate	2,96	Shelf benthi	Invertebrate predator / scavenger	Moderate
Decapods: Natantia (slope)	0,045	Invertebrate	3,20	Slope benth	Invertebrate predator / scavenger	Moderate
Decapods: Natantia (shelf)	0,059	Invertebrate	2,96	Shelf benthi	Invertebrate predator / scavenger	Moderate
Suprabenthic macrocrustaceans	0,006	Invertebrate	2,00	Suprabenth	Scavenger	Moderate
Clams	0,035	Invertebrate	2,00	Benthic	Filter feeder	Moderate
Scallops	0,068	Invertebrate	2,00	Benthic	Filter feeder	High commercial relevance
Other benthic invertebrates	0,084	Invertebrate	2,07	Benthic	Invertebrate predator / scavenger	Moderate
Jellyfish	0,0735	Invertebrate	3,49	Mixed	Planktivores	Moderate
Seagrasses	0,004	Plant	1,00	Euphotic zo	Primary producer / microbial	
Seaweed	0,004	Plant	1,00	Euphotic zo	Primary producer / microbial	
Macrozooplankton & Euphasiacea	0,0411	Invertebrate	3,14	Mixed	Zooplanktivore	Moderate
Mesozooplankton	0,000686	Invertebrate	2,41	Mixed	Zooplanktivore	Moderate
Microzooplankton	0,000236	Invertebrate	2,69	Mixed	Zooplanktivore	Moderate
Bacterioplankton	0,00595	Invertebrate	2,00	Mixed	Primary producer / microbial	Moderate
Diatoms	0,000016	Plant	1,00	Euphotic zo	Primary producer / microbial	Moderate
Dinoflagellates	0,001194	Plant	1,00	Euphotic zo	Primary producer / microbial	Moderate

Table 4.7. 1: Model results: Methylmercury concentrations (g/t) in muscle tissues for living groups in the EwE model for the Adriatic Sea and their Ecological traits: Trophic levels are estimated from diet composition in the EwE model. Diet information derives from diet composition in the EwE model. Diet information derives from the FAIRSEA project documentation ('Fisheries in the AdriatIc Region – a Shared Ecosystem Approach') and primary literature sources.

Results Hg in the Venice Lagoon and its clams

Modeled concentrations of mercury species in the Venice Lagoon exhibit pronounced temporal and spatial variability within the lagoon, aligning well with available observations (Bloom et al., 2004). In certain areas, these concentrations exceed those found in the open Mediterranean Sea by up to two orders of magnitude. The presence of inorganic mercury in the water is strongly influenced by sediment resuspension, which is notably mitigated by benthic vegetation, while MeHg is more influenced by other factors (Rosati et al., 2024).

Results of the bioaccumulation model are in good agreement with the experimental data of total Hg (HgT) concentration in clam over two years (Sfriso et al., 2008), although the agreement is higher at Fusina station than at San Giuliano. Sensitivity simulations show that the best results (lowest absolute errors, 0.22) are achieved when adopting slow excretion rates (β in the range 10-7 – 5 10-5) and low availability of Hg species associated to refractory POM (α in the range 5% and 10%).

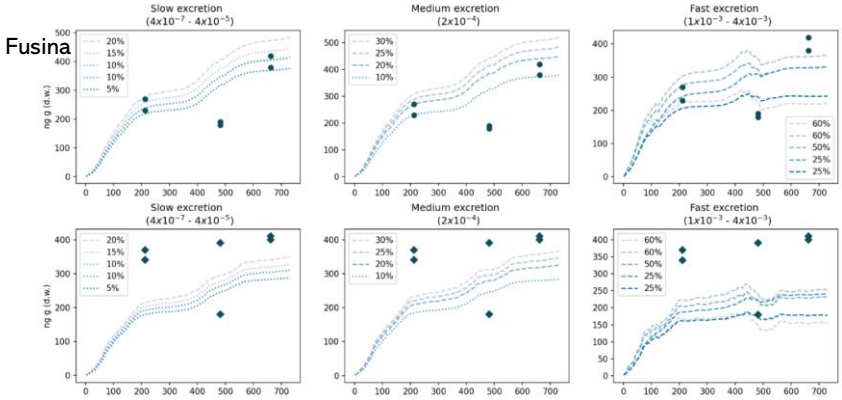

Figure 4.7.2: Modeled bioaccumulation (dotted lines) of total Hg in clams (ng g-1d.w.) over time against experimental field data of farmed clams at Fusina (circles) and San Giuliano (diamonds) stations (Sfriso et al., 2008). The left panels show the output of simulations with slow excretion rates, the intermediate panels show simulations with medium excretion rates, and the right panels show simulations with high excretion rates. The different lines dotted in each pane represent the output from each sensitivity simulation.

Model results projected over 10 years highlighted that in the long run, Hg in clam tissues remain lower at Fusina than at San Giuliano station (Figure 4.7.3a,), although clams reached a larger size at the former station (up to 55 mm) than at the latter (up to 50 mm) (Figure 4.7.3b,d). Based on these projections, we estimated the risk to humans from Hg exposure related to consumption of clamsclam from the Venice Lagoon (Table 4.7.2). This was done by assuming a HgT and MeHg concentration of 90 and 4 ng g^{-1} w.w., respectively, and an amount of clams per serving equal to 100 g for children and 200 g for adults. The resulting intake of HgT (9 and 18 µg) MeHg (0.4 and 0.8 µg) per serving is well below the "Tolerable Weekly Intake" (TWI) adjusted for body mass, estimated to be 80 and 280 µg (TWI_{HgT}) and 26 and 91 µg (TWI_{MeHg}) for children and adults, respectively, so 8.8 and 15.5 servings per week would be needed to exceed the HgT and MeHg threshold for children. This analysis thus suggests that clams from the Venice Lagoon are safe for human consumption as it concerns exposure to Hg species.

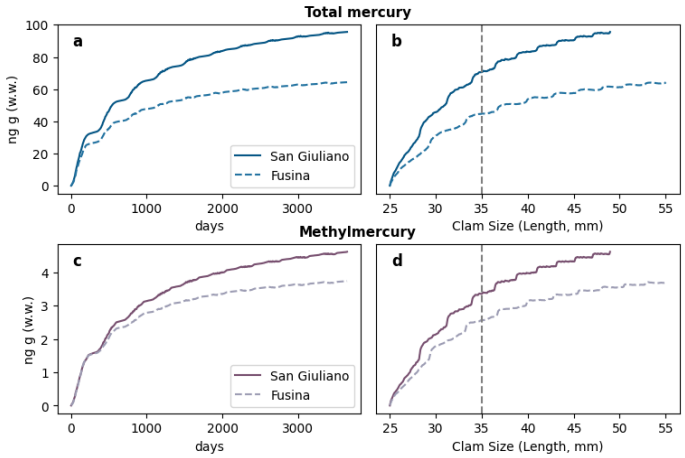

Figure 4.7.3: Modeled1.8.4 – bioaccumulation (ng g-1w.w.) of total Hg (a, b) and MeHg (c, d) in clams from contaminated areas of the Venice Lagoon over 10 years of simulation.

	Hg concentration in clam	Human body weight	TWI (normalized)	TWI (weight based)	Clams serving	Hg content per serving
Children	ng/g w.w.	kg	ug/kg(bw)week	ug/week	g(clams)	ug(Hg)
HgT	90	20	4	80	100	9
MeHg	4	20	1.3	26	100	0.4
Adult	ng/g w.w.	kg	ug / kg(bw) week	ug/week	g(clams)	ug(Hg)
HgT	90	70	4	280	200	18
MeHg	4	70	1.3	91	200	0.8

Table 4.7.2: Parameters used to estimate risk to human from Hg exposure related to consumption of clams from the Venice Lagoon. The concentration of HgT and MeHg in clams are obtained from model simulation (Figure 4.7.4). Body weight is assumed to be representative of different age classes. The normalized TWI (Tolerable Weekly Intake) is from EFSA, 2012, and was used in combination with the body weight to calculate the weight-based TWI. This was compared with the estimated content of Hg and MeHg in one serving of clams.

Results GSM

Metabolic interactions within Venice lagoon microbial community

Model simulations revealed a strong functional trade-off between pollution (represented by toluene degradation) and microbial community growth under anoxic conditions. Across an extensive parameter sweep (2,500 scenarios), 785 feasible steady-state solutions were obtained, showing a consistent and significant negative relationship between toluene uptake and community growth rate (Pearson $r = -0.848$, $p < 0.0001$; Figure 4.7.4).

Each additional unit of toluene uptake resulted in an average 6–7% reduction in relative community growth, indicating that pollutant degradation imposes a substantial metabolic cost at the community level. This pattern reflects functional specialization within the microbial assemblage, where only a subset of sulfur-cycling taxa is capable of degrading toluene. Increased toluene availability therefore promotes these degraders at the expense of non-degrading taxa, reducing overall community growth.

This emergent trade-off highlights how pollutant removal and ecosystem functioning may be constrained by microbial metabolic allocation, and demonstrates the ability of the community genome-scale model to identify process-level limitations relevant for benthic bioremediation strategies.

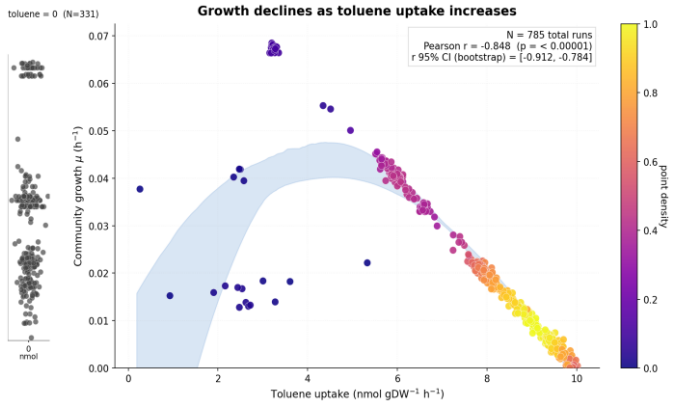

Figure 4.7.4: Toluene uptake trades off with community growth. Scale color: density of runs (N = 785); gray points: zero toluene uptake (N = 331).

Additional model simulations explored the effect of single-electron acceptor amendments on hydrogen sulfide (H_2S) production and toluene degradation under strictly anoxic, sulfate-reducing conditions. The introduction of alternative electron acceptors altered community metabolism by partially suppressing sulfate reduction and redirecting electron flow toward competing respiratory pathways.

Among the tested amendments, nitrate and nitrite (NO_3^-/NO_2^-) showed the strongest dual effect, simultaneously reducing H_2S production and enhancing toluene uptake. Model results indicated reductions of up to 38% in H_2S production and increases of up to 59% in toluene removal relative to the sulfidic baseline, albeit at the cost of reduced community growth. In contrast, ferric iron (Fe^{3+}) produced more limited effects on both sulfide suppression and pollutant degradation.

These results suggest that nitrate- and nitrite-based amendments are the most effective options for achieving dual control of sulfide accumulation and aromatic hydrocarbon degradation in sulfidic lagoon sediments, consistent with experimental and field evidence that nitrate availability suppresses sulfate reduction while supporting denitrifying degradation pathways.

4.7.5 Scientific products and dissemination

C.f. Section 4.1.5

4.8 From hazard to risk: assessing single and cumulative hazards of land-based pollution in the Adriatic Sea (OGS)

4.8.1 Introduction

This Chapter translates the fate-and-transport results presented in the previous sections (4.1 and 4.7) into risk-relevant products for selected contaminants and marine hazards. We combine modelling outputs with vulnerability assessments (oil-spill drift and stranding) and ecotoxicological benchmarks (plastics pharmaceuticals, and mercury bioaccumulation) to derive indicators of potential risk for marine ecosystems.

In addition to single-hazard assessments for oil, mercury, pharmaceuticals and microplastics, we develop a cumulative, multi-hazard representation for the Adriatic Sea. The cumulative assessment integrates the normalised risk layers introduced in the previous chapters into a single decision-support index for marine environments. These layers are harmonised on a common grid and combined through a data-driven multi-criteria decision analysis (MCDA) workflow to provide (i) a strict multi-hazard index where all criteria co-occur and (ii) complementary sub-indices and an extended "union-of-support" index to maximise spatial coverage.

4.8.2 Case study description

-

4.8.3 Methodological framework

4.8.3.1 Analytical methods

n.a.

4.8.3.2 Experimental methods

n.a.

4.8.3.3 Modelling methods

Oil spill risk

The oil-spill assessment follows the established risk framework defined as a function of Hazard (H), Exposure (E), and Vulnerability (V) (UNDRO, 1979; Cardona, 2005; Menoni et al., 2012). In this context, **Hazard** represents the potential presence of oil in the marine environment resulting from accidental releases associated with maritime activities and the physical processes governing oil transport and fate. Hazard therefore integrates incident occurrence with the simulated spatial and temporal distribution of oil derived from AIS-based traffic analysis and Lagrangian modelling.

Exposure describes the interaction between the oil hazard and coastal or marine receptors and is expressed through spatially explicit metrics of time-integrated oil presence and shoreline stranding derived from the fate-and-transport simulations presented in Section 4.1. **Vulnerability** reflects the intrinsic sensitivity and value of receptors once exposed and integrates geomorphological, environmental, and socio-economic dimensions following established coastal risk-assessment approaches.

Overall oil-spill **risk** is obtained by combining hazard, exposure, and vulnerability within a spatially explicit framework, consistently with the methodology developed by Melaku Canu et al. (2015)**.** The specific implementation adopted here for the Adriatic Sea, including the selection of indicators, spatial resolution, and vulnerability layers, follows the analysis presented by Bandelj et al. (2024)**,** to which the reader is referred for methodological and application details.

Screening-level risk for microplastics, pharmaceuticals, and mercury

Microplastics (RQ)

Risk from microplastics is assessed using the standard Risk quotient framework, defined as RQ = PEC/PNEC, where PEC is the predicted environmental concentration derived from the transport simulations described in Section 4.1, and PNEC is the predicted no-effect concentration (ECHA, 2008; ECHA, 2016). At screening level, RQ < 1 indicates acceptable risk, whereas RQ ≥ 1 indicates that adverse effects cannot be excluded and that refined assessment or management actions may be required.

The PNEC for marine microplastics is derived from the probabilistic species sensitivity distribution (pSSD) developed by Adam et al. (2021), Figure 4.8.2, which includes 23 marine taxa. Three alternative hazard concentrations were adopted to reflect different levels of conservatism: 0.2 µg L^{-1} (5th percentile), 0.5 µg L^{-1} (mean), and 0.8 µg L^{-1} (95th percentile), Table 4.10.2. For each grid cell, RQ is computed as the ratio between the simulated concentration and the selected hazard concentration, providing a spatially explicit screening-level indicator of ecological risk.

Pharmaceuticals (RQ based on HC5)

Pharmaceutical risk is expressed as a Risk Quotient (RQ), defined as the ratio between modelled exposure concentrations (EP) and Hazard Concentration 5 (HC5) thresholds for the protection of 95% of species. HC5 values of 116 ng L^{-1} for Diclofenac and 159 ng L^{-1} for Ibuprofen were derived from a literature review conducted within the NBFC framework.

$$RQ = \frac{[EP]_{(x,y,z)}}{HC_5}$$

RQ values are interpreted using standard screening criteria (RQ < 1: low concern; RQ ≥ 1: potential concern). Although pharmaceutical residues generally exhibit limited bioaccumulation, they may induce biological effects at low concentrations; therefore, a concentration-based screening approach is appropriate (Mezzelani et al., 2018; Mezzelani et al., 2020; Mezzelani & Regoli, 2022; Gómez-Regalado et al., 2023).

Mercury (dietary RQ for planktivorous fish)

Mercury risk is assessed from modelled methylmercury (MeHg) concentrations in plankton functional types to estimate dietary exposure for planktivorous fish. Results of the simulations produced by OGSTM-BFM-Hg (Rosati et al. (2022) are presented in Section 4.1.

A screening-level Risk Quotient is computed as the ratio between the modelled MeHg concentration in plankton and an ecotoxicological threshold associated with adverse reproductive effects in fish (0.04 µg g^{-1} wet weight), selected as a sensitive and ecologically relevant benchmark (Depew et al., 2012). The RQ is calculated from the ratio of the modeled concentration of MeHg in different plankton types (diatoms, microzooplankton, and mesozooplankton) and the ecotoxicological threshold.

$$RQ = \frac{[MeHg]_{(plankton)(x,y,z)}}{Threshold_{repr}}$$

This approach provides a conservative estimate of dietary risk for lower trophic levels, directly based on model outputs and without additional assumptions on biomagnification.

Integrated multi-hazard risk index

To synthesise heterogeneous risk indicators into a cumulative perspective, a multi-criteria decision analysis (MCDA) framework is applied (Huang et al., 2011; Esmail and Geneletti, 2018). Seven spatial criteria are considered, representing **screening-level indicators of marine risk**: Diclofenac RQ, Ibuprofen RQ, microplastics HQ, mercury bioaccumulation, and oil-spill risk indices for bunker, crude, and diesel fuels.

All criteria are re-projected and resampled onto a common grid covering the Adriatic Sea, then transformed into dimensionless risk scores in the range [0,1]. Objective criterion weights are derived using the CRITIC method (CRiteria Importance Through Intercriteria Correlation), which quantifies the informational content of each indicator based on spatial variability and inter-criterion correlation (Diakoulaki et al., 1995). Criteria are then aggregated using the TOPSIS method (Technique for Order of Preference by Similarity to Ideal Solution), which ranks grid cells based on their distance from an ideal low-risk and high-risk configuration (Hwang and Yoon, 1981; Lai et al., 1994).

The analysis produces: (i) a **strict multi-hazard index**, computed only where all criteria are available; (ii) hazard-group sub-indices (chemical contamination, oil spill, pharmaceuticals); and (iii) a **union-of-support index**, which extends spatial coverage by renormalising weights over the subset of criteria available at each cell. A Monte Carlo uncertainty analysis based on weight perturbation is used to assess the robustness of the integrated indices (Chen et al., 2022).

4.8.4 Results

Risk evaluation oil

For each oil type (bunker, diesel, crude), separate risk maps were produced and aggregated through a weighted mean reflecting relative occurrence and persistence. The resulting "cumulative oil-spill risk index" mapped in Figure 4.8.1, depicts the relative susceptibility of the Northern Adriatic coastline, classified into four levels: very low (1–2), low (3–5), medium (6–7), and high (8–9). The modelling logic ensures comparability across scales and replicability under varying scenarios, while the square-root transformation applied to composite layers preserves interpretability of ordinal scores.

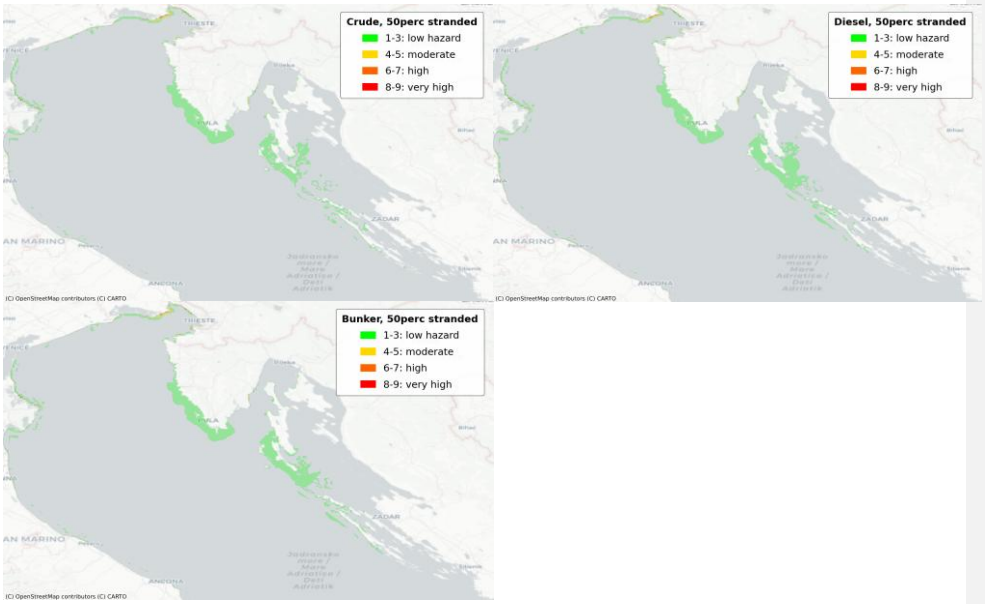

Figure 4.8.1: Oil risk assessment in the Adriatic Sea for Crude, Diesel and Bunker oil types.

Risk evaluation plastics

Risk evaluation shows that simulated microplastic concentrations in the surface waters of the Adriatic Sea are generally well below the toxicity thresholds established by Adam et al. (2021). When the strictest threshold ($HC_{0.2}$ = 0.2 µg L^{-1}, corresponding to the 5th percentile of the PNEC distribution) is applied, most of the basin displays HQ values between 0.1 and 0.5 (Figure 4.8.2, top left). Localised areas with HQ ≥ 1 occur only near major river mouths and within narrow coastal bands along the western and northern Adriatic, reflecting the influence of riverine emissions and coastal retention zones. These hotspots are spatially limited and remain confined to the nearshore region.

Using the central PNEC estimate ($HC_{0.5}$ = 0.5 µg L^{-1}), HQ values decrease proportionally (Figure 4.8.2, top-right). In this scenario almost the entire basin falls below HQ = 1 and the majority of grid cells lie in the HQ < 0.2 class, indicating a large safety margin relative to the best-estimate toxicity threshold. Only a few coastal cells adjacent to the most heavily loaded rivers approach HQ ≈ 1. With the most permissive but still ecologically plausible threshold ($HC_{0.8}$ = 0.8 µg L^{-1}, corresponding to the 95th percentile of the PNEC distribution), almost all modelled HQ values are below unity (Figure 4.8.2, bottom-left).

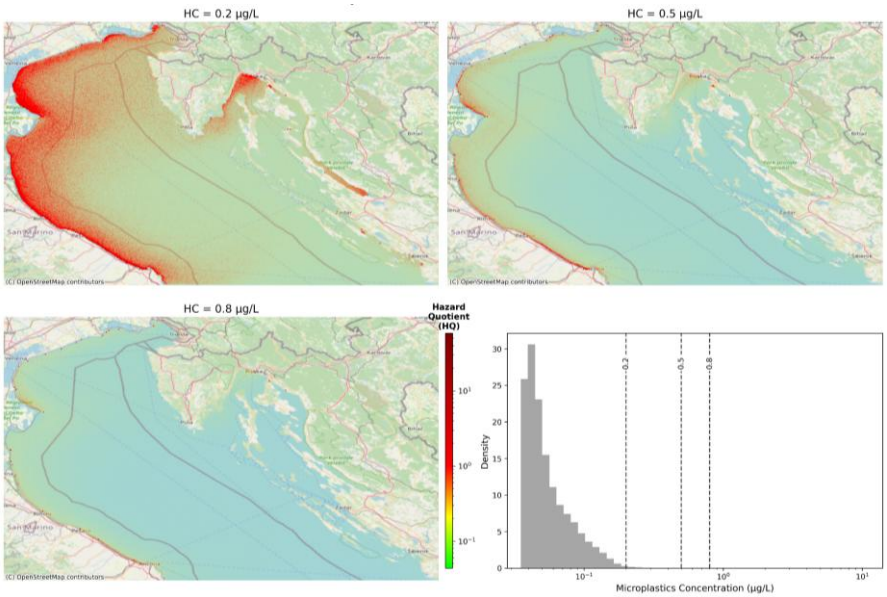

Figure 4.8.2: HQ computed for $HC_{0.2}$ (top-left), $HC_{0.5}$ (top-right), $HC_{0.8}$ (bottom-left), and histogram of the concentrations (log-scale) reporting the three thresholds.

The generally low risk associated with microplastics can be seen in the distribution of HQ values in Figure 4.8.2, bottom-right. This trend is consistent with the global assessment by Adam et al. (2021), who found that ecotoxicological risks for marine waters are currently unlikely, although not strictly zero. Overall, our results suggest that current average concentrations estimated in the Adriatic Sea are unlikely to cause widespread ecotoxicological effects in the water column

Risk evaluation pharmaceuticals

The RQ for Diclofenac in the Adriatic Sea was always below 1, indicating no risk, while for Ibuprofen, the RQ exceeded 1 in large areas of the Italian coast, suggesting a possible concern (Figure 4.8.3). These results can support further prioritization of future research.

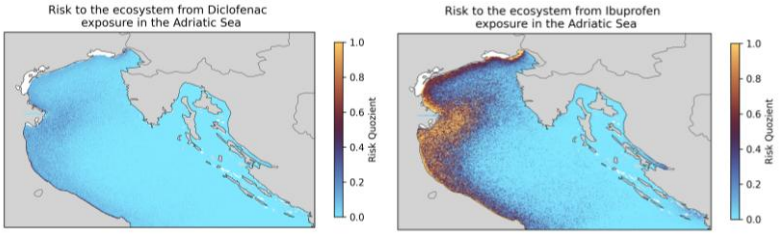

Figure 4.8.3: Spatial distribution of the Risk Quotient for Diclofenac and Ibuprofen in the surface waters of the Adriatic Sea obtained from the ratio between the average concentrations -EP- and the ecotoxicological thresholds HC_5.

Risk evaluation, mercury

Risk from Hg exposure to planktivorous fish was estimated to be overall low (Figure 4.8.4), with the RQ never exceeding 1. However, a noticeable spatial heterogeneity in the RQ highlighted a higher vulnerability for

the ecosystem of the Southern Adriatic Sea (RQ about 0.6) than for the northern area (RQ < 0.2). The risk index presented here is calculated for planktivorous fish to maintain a reasonable degree of uncertainty by directly using the model outputs without further assumptions. However, if an average increase in concentration of 7 times per trophic level is assumed, as suggested by Lavoie et al. (2013) and confirmed here by the food web model in Thematic Chapter 4.2, the diet exposure of higher trophic levels could become significant.

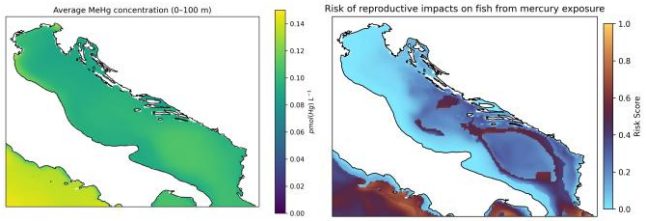

Figure 4.8.4: Modeled distribution of MeHg in water in the upper 100 m of the Adriatic Sea (annual average) and estimated reproductive risk for planktivorous fish estimated from MeHg concentrations in different plankton functional types (Figure 4.1.4) and ecotoxicological thresholds from the literature.

Commentato [AR1]: ?

Integrated multi-risk indices (CRITIC–TOPSIS)

CRITIC weights and dominant contributors

CRITIC weights (Figure 4.8.5) show how different criteria contribute to the integrated signal. Within Chemical Contamination, Hg and IBU receive the highest weights, indicating strong spatial contrast and relatively low redundancy with other chemical indicators; microplastics has intermediate weight, while DCF contributes less distinct information. Within the Oil Spill group, the three fuel layers have comparable weights, with bunker and crude slightly higher than diesel, consistent with their mutually correlated spatial patterns. In the Pharmaceuticals group, IBU dominates the weight structure, and DCF contributes secondarily. In the full seven-criterion ("All Maritime") configuration, IBU and Hg are the most influential criteria, followed by microplastics, while DCF and the three oil-spill layers retain lower but still non-zero and mutually comparable weights. This weighting scheme ensures that the integrated index is driven primarily by criteria carrying robust spatial contrast, while maintaining representation of all hazard domains.

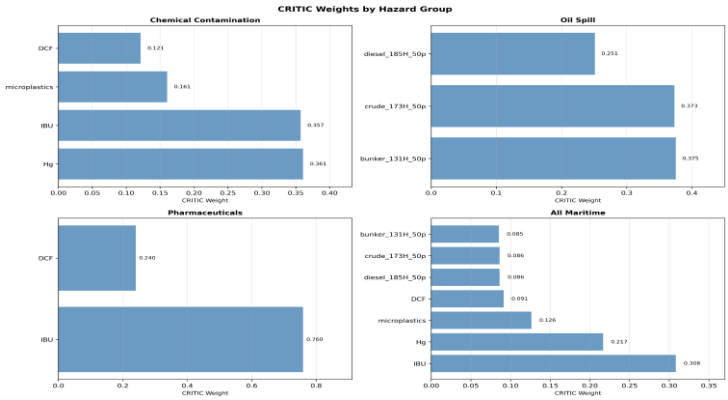

Figure 4.8.5: CRITIC weights for individual hazard groups and overall multi-risk index. Group-specific CRITIC weights are shown for (a) Chemical Contamination (DCF, microplastics, IBU, Hg), (b) Oil Spill (bunker, crude, diesel), and (c) Pharmaceuticals (DCF, IBU), together with (d) the "All Maritime" configuration where all seven criteria are considered simultaneously. Within each group, criteria with higher spatial variability, lower redundancy with the others and better coverage receive larger weights. In the overall "All Maritime" index, IBU and Hg emerge as the most influential criteria, followed by microplastics, while the three oil-spill layers retain relatively low but comparable weights.

TOPSIS index

CRITIC-weighted TOPSIS indices (Figure 4.8.6) show specific spatial patterns and differences in spatial coverage across hazard groups. Chemical contamination and pharmaceuticals cover broad areas and capture basin-scale coastal gradients, whereas the oil-spill sub-index is spatially more restricted and emphasises discrete hotspots.

The strict "All Maritime" index, computed only where all seven criteria co-occur, provides a fully comparable multi-risk ranking but is strongly limited by the spatial footprint of the oil-spill layers. As a result, it highlights truly multi-hazard conditions only within a relatively constrained space where complete overlap exists.

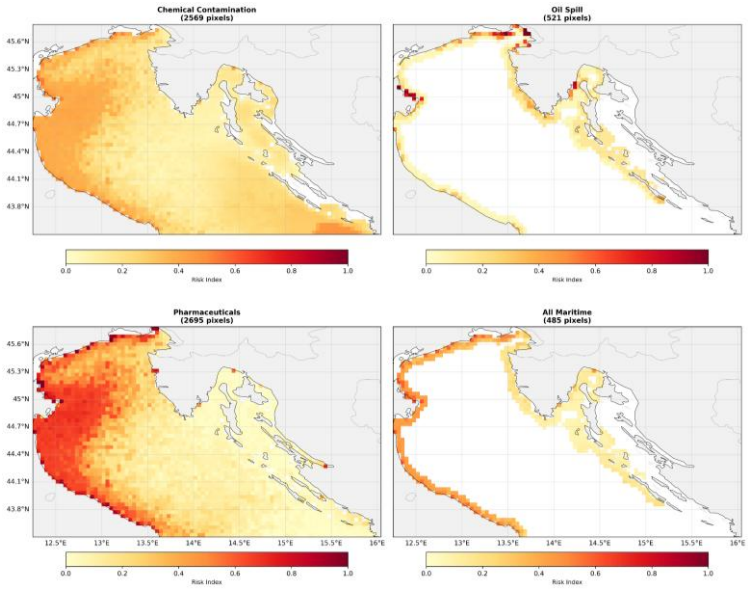

Figure 4.8.6: CRITIC-weighted TOPSIS risk indices for (a) Chemical Contamination, (b) Oil Spill , (c) Pharmaceuticals, and (d) All Maritime ("strict" intersection of supports). Warmer colours indicate higher composite risk. The sub-indices reveal distinct spatial patterns and coverage for each hazard group, while the All Maritime map shows where a fully integrated multi-hazard index can be computed.

Union-of-support multi-hazard index

To address the limited coverage of the strict index, a union-of-support TOPSIS index is introduced (Figure 4.8.7). This index uses the same CRITIC–TOPSIS weight structure but relaxes the requirement for all seven criteria to be present. At each grid cell, the global CRITIC weights are renormalised over the subset of the criteria that are actually present, and the TOPSIS index then calculated as the closeness to the Negative Ideal Solution (NIS). This approach extends the spatial coverage of the index and highlights local hot-spots (maxima) that are visible within the sub-groups but are smoothed in the All Maritime index, while also preserving the general risk patterns identified by the strict methodology.

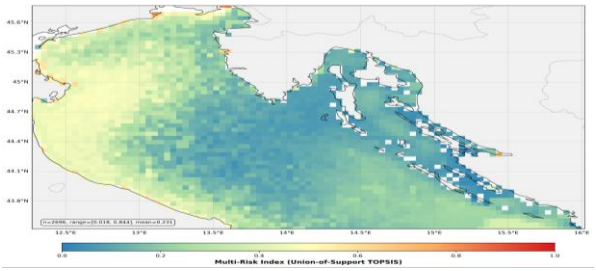

Figure 4.8.7: Map of the union of support TOPSIS.

Uncertainty analysis

Uncertainty is assessed through a Monte Carlo perturbation of the global CRITIC weight vector and propagates these changes through the CRITIC–TOPSIS workflow (Chen et al., 2022). Starting from the baseline weights (α = 0.5), 100,000 alternative weight vectors are drawn from a Dirichlet distribution with concentration κ = 10, allowing substantial deviations while preserving the overall ranking of criteria. For each realisation, both the strict and union-of-support multi-hazard indices are recomputed. For the strict index, the Monte Carlo mean (Figure 4.8.8, top-left) is almost indistinguishable from the baseline strict multi-hazard map, confirming that the main hotspots along the Italian coast and in the northern Adriatic, as well as lower-risk areas along much of the eastern coastline, persist across a wide range of plausible weight configurations. The corresponding standard deviation map (Figure 4.8.8, top-right) shows moderate variability concentrated along the Italian nearshore and in a few transition zones between moderate and high risk, while the rest of the domain exhibits relatively low variability. Overall, the main multi-risk patterns and hotspot locations remain stable under weight perturbations.

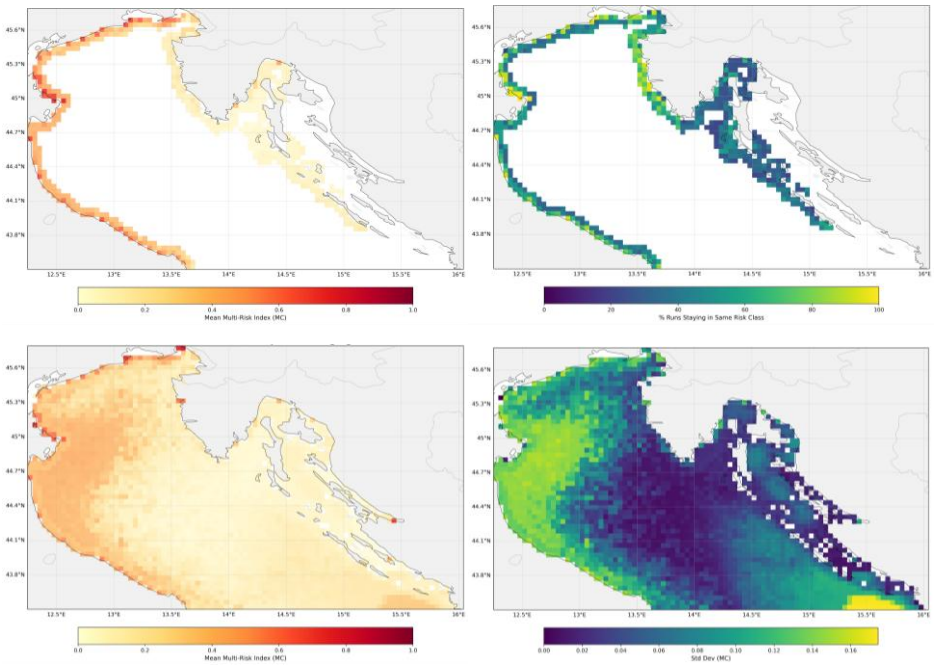

Figure 4.8.8: Monte Carlo mean and standard deviation of the strict (top) and union-of-support (bottom) multi-risk indices under CRITIC weight perturbations (100 000 runs, Dirichlet κ = 10).

For the union-of-support index, the Monte Carlo mean (Figure 4.8.8, bottom-left) closely reproduces the baseline union-of-support pattern, with elevated multi-hazard along the Italian shelf and northern Adriatic and lower values in the central basin and much of the Croatian side. The standard deviation map (Figure 4.8.8, bottom-right) indicates somewhat higher sensitivity along the Italian coastline and at the southern and north-western margins, where multiple criteria overlap and data coverage is more heterogeneous, but comparatively low variability over large parts of the central basin and eastern offshore region.

Overall, these Monte Carlo results show that both the strict and union-of-support indices are robust to substantial perturbations of the CRITIC weights: the main spatial patterns of multi-hazard are preserved, and the locations of high-priority areas remain stable. Additional tests with alternative values of the CRITIC coverage exponent α yielded rank correlations greater than 0.99 relative to the baseline solution (not shown), indicating that the indices are also only weakly sensitive to this structural parameter.

Limitations

The CRITIC–TOPSIS framework offers a consistent method for integrating heterogeneous indicators, but several limitations should be considered when interpreting the results (Steele et al., 2009). The indices depend on the quality, representativeness, and spatial coverage of the input layers, while uncertainties in the underlying datasets and models are not explicitly propagated. Spatial coverage is uneven: the strict index is limited to areas where all criteria co-occur, whereas the union-of-support index extends coverage but may rely on fewer indicators in some locations. Furthermore, the analysis includes only the seven modelled pressures and does not provide a comprehensive assessment of marine risk.

Additional assumptions arise from normalising indicators to a common [0,1] scale and from the choice of aggregation rules, which may influence the relative contribution of criteria, particularly near low-to-moderate risk transitions. The framework provides a static representation and does not explicitly capture seasonal variability or short-term extremes. Finally, CRITIC derives objective, data-driven weights without incorporating stakeholder preferences, and TOPSIS is compensatory, allowing high values in one criterion to offset low values in others. The uncertainty analysis addresses only weight variability; a more comprehensive approach would require formal propagation of uncertainties across data inputs, preprocessing, and modelling steps.

4.8.5. Scientific products and dissemination

C.f. Section 4.1.5

4.9 Physiological effects of microplastics in model water plants and possible applications of phytoremediation in contaminated water (UNIFI-2)

4.9.1 Introduction

Aquatic vegetation has fundamental ecological functions, since it provides habitats for different organisms and is implicated in vital processes, such as nutrient cycling, water cleaning, etc. Considering the great importance of macrophytes (water plants) in maintaining a good ecological balance in freshwater and coastal environments, two different species were used as model water plant to investigate the phytotoxicity of microplastics (MPs) and possible application in phytoremediation.

A growing number of studies has documented the toxic or harmful effects of MPs on living organisms. Most research to date has focused on animals inhabiting marine and coastal environments, with more recent attention shifting toward terrestrial plants and animals. Within this expanding field, aquatic plants remain comparatively understudied, despite being important sinks for plastic particles. Microplastics pose a potential threat water and coastal environments, compromising their key ecological functions, including serving as habitats for diverse organisms and supporting essential processes such as nutrient cycling and water purification.

In recent years, the impact of MPs on a range of submerged macrophytes has increasingly been investigated, with particular emphasis on their effects on growth and physiological traits. A variety of responses has been reported in free-floating macrophytes, depending on polymer type, particle size, and concentration. Several studies report clear alterations in biometric and physiological parameters of *Spirodela polyrhiza*, accompanied by significant changes in both primary and secondary metabolisms. Furthermore, our recent study on the same species (Dainelli et al. 2024) revealed that MPs are able to induce epigenetic effects, by altering DNA methylation patterns, with an unusual hypermethylation at 5′-CCGG sites. Conversely, MPs have been shown to adhere to the roots of *Lemna minor* and *Spirodela polyrhiza* without impairing growth (Dovidat et al., 2020). Among recent findings, the potential of free-floating macrophytes for plastic particle adsorption is increasingly recognized. *L. minor*, for example, has been shown to interact with diverse types of MPs (Rozman et al., 2022) and to contribute to the removal of approximately 0.5–3% of various particles in constructed wetlands (Milošloža et al., 2025). To optimize the application of free-floating macrophytes in such remediation strategies, not only their capacity to retain MPs on plant surfaces requires investigation, but also an additional, largely unexplored aspect may play a key role.

Plants release a wide range of compounds capable of mediating particle aggregation, potentially facilitating MP recovery through retention systems. Since MP-induced alterations in root exudation are well documented in terrestrial plants, similar compounds are likely released by free-floating macrophytes. Given that plant exudates comprise a chemically diverse array of molecules, they may contain components able to interact with particle surfaces, modify their physicochemical properties, and ultimately promote aggregation.

4.9.2 Case study description

The research activity focused on the effects of micro- and nanopollutants (MNPs) on plants:

In a first study, the effects of polyethylene terephthalate micro- and nanoplastics (PET-MNPs) were investigated in the model freshwater species *Spirodela polyrhiz*a (L.) Schleid., with a particular focus on particle-induced epigenetic effects, specifically alterations in DNA methylation patterns.

In a second study *Azolla filiculoides*, an aquatic fern was used as an indicator to evaluate the toxic impacts of PET MNPs. In particular the effects on the symbiotic association between *A. filiculoides* and the nitrogen-fixing cyanobacterium *Trichormus azollae* were investigated.

The third work aimed to investigate the interaction between MPs and the floating freshwater plant *Spirodela polyrhiza*, assessing its potential application in phytoremediation. The work specifically focused on:

i) the plant's capacity to retain MPs;
ii) the plant surface structures involved in particle adhesion and the strength of this sequestration;
iii) the nature of MP-induced plant exudates and their potential role in promoting MP aggregation.

This experimental approach contributes to advancing our understanding of both the effects of MPs on free-floating macrophytes and the fate and transport of MPs in aquatic environments. In particular, it provides insights into the role of macrophytes in retaining MPs and their possible application in phytoremediation strategies.

4.9.3 Methodologies

In the three studies, both plants of *A. filiculoides* and *S. polyrhiza* were grown in hydroponic solutions and maintained under controlled temperature, light, and humidity throughout the experiment.

Fluorescent MPs were used for the treatments to allow precise visualization of their distribution on the plant surface and within the solutions.

4.9.3.1 Analytical methods

Regarding, polyethylene terephthalate (PET) micronanoplastics (MNPs) they were produced in house from commercial water bottles, following the protocol described by Ekvall et al. (2019) with modifications (Figure 4.9.1). Briefly, the bottle surfaces were previously washed with standard laboratory glassware detergent to avoid contaminations (e.g. bacteria, proteins, nucleic acids, etc.), cut with into approximately 0.5 mm^2 pieces using scissors, and then flushed abundantly with deionized water. The plastic fragments were then air-dried and sterilized under UV-C irradiation for 1 h. Subsequently, 4 g of plastic pieces were placed in a beaker containing 150 mL of distilled water and mechanically fragmented using an immersion blender operated at maximum speed for 2 min. After each blending cycle, 50 mL of the suspension were collected using a sterile syringe and filtered through a Miracloth filter (pore size 22–23 µm). This procedure was repeated for a total of 20 cycles, with 2 min pauses between cycles and additional 5 min pauses after the 5th, 10th, and 15th cycles to prevent overheating. Once a total volume of 1 L was collected, the resulting MNP suspension was transferred to a glass bottle and stored at 4 °C until further use.

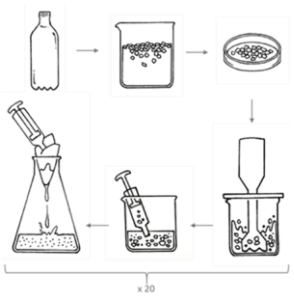

Figure 4.9.1: Scheme of the MNPs in solution starting from a plastic bottle by mixer.

The latter were treated with fluorescent MPs to allow precise visualization of their distribution on the plant surface and within the solutions. The area of fMPs in the medium growth was assessed at the beginning of the experiment and divided by classes size as shown in Figure 4.9.2.

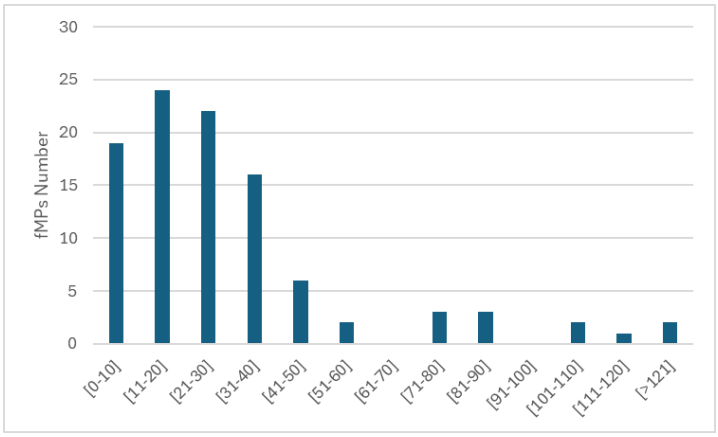

Figure 4.9. 2: Number of fMP particles at T0, divided by size classes.

4.9.3.2 Experimental methods

Spirodela polyrhiza strain 9509 (Figure 4.9.3a), gently provided by the University of Jena (Germany), was acclimated for two weeks before testing in a climate chamber with the following controlled conditions: 24/16 ◦C day/night, light intensity 300 µmol m^{-2} s^{-1}, 16-h (day) photoperiod and relative humidity 60–65 %. After acclimation, one flask was used as inoculum culture (hereafter T0) and one colony (2–4 fronds) was randomly transferred from it to each test vessel. Three different treatment conditions were applied as shown in Figure 4.9.3b: i) control (C), 50 mL N-medium prepared in distilled water; ii) 50 mL N-medium prepared in PET-MNP solution diluted 1:2 (v/v) with distilled water (PET ½, MNP concentration ≈ 0.05 g L− 1); iii) 50 mL N-medium prepared in pure PET-MNP solution (PET, approximative MNP concentration ≈ 0.1 gL− 1). The number of replicates per treatment group was 16, for a total of 48 test vessels.

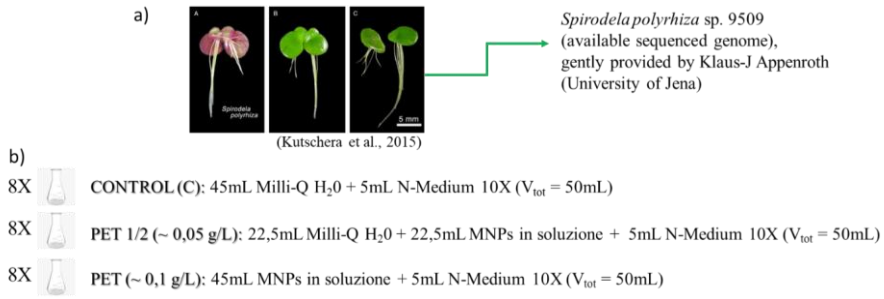

Figure 4.9.3: a) *Spirodela polyrhiza* sp. 9509 morphology. b) Experimental set-up: treatment with PET MNPs on *S. polyrhiza.*

Azolla filiculoides plants were tested under three different treatment conditions (Figure 4.9.4a): i) control (C) with H-40 medium prepared in distilled water; ii) H-40 medium prepared in a PET-MNP solution diluted 1:2 (v/v) with distilled water (PET ½), where the MNP concentration was ~0.05 g L^{-1};iii) H-40 medium prepared in a pure PET-MNP solution (PET) with a MNP concentration of ~ 0.1 g L^{-1}.

For each treatment, six replicates were set up, for a total of 18 test beakers. After 10 days, the impact of PET-MNPs on the water fern's growth, anatomy, photosynthetic efficiency and ionomic profile was investigated, as well as the effects of MNP exposure on *T. azollae* heterocyst frequency and size and on the relative abundance of the symbiotic cyanobacterium (Figure 4.9.4b) based on DNA estimation.

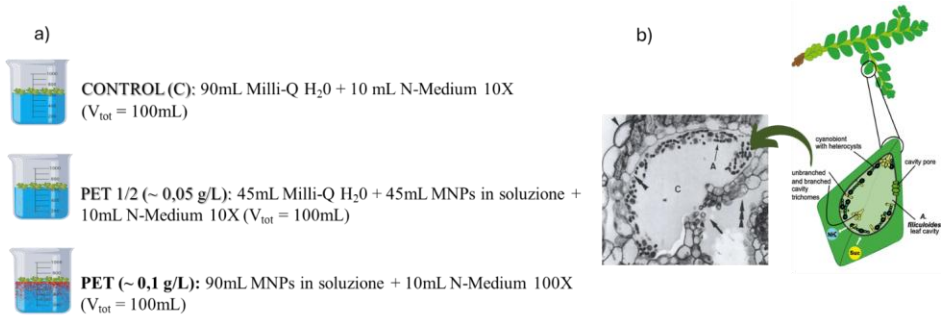

Figure 4.9.4: a) Experimental set-up: treatment with PET MNPs on *Azolla filiculoides* (L.) Schleid; b) *T. azollae* present in the leaves.

Manufactured blue-fluorescent spherical MPs with diameter between 1 and 5 µm were used to prepare N-medium with a particle concentration of 0.05 g L-1, which was then administered to *S. polyrhiza* colonies for one week under controlled conditions (MP+S). The experimental setup also included two control conditions: N-medium without plants but containing MPs at 0.05 g L-1 (MP), and growth medium *with S. polyrhiza* but without MPs (S) (Figure 4.9.5).

After one week of exposure the plant growth was measured (fresh and dry weight) together with other parameters useful assess the possible phytotoxicity of MPs, such as tissue accumulation of macro- and micronutrients. To evaluate aggregation capacity by the plants, the number of items in solution and their area were analyzed at the end of the experiment using optical light microscopy and the Zeta potential of particles was also measured at the start and end of the test.

To investigate the possible effects of root exudates in MP aggregation and removal, the solutions were analyzed using LC-MS/MS untargeted metabolomics.

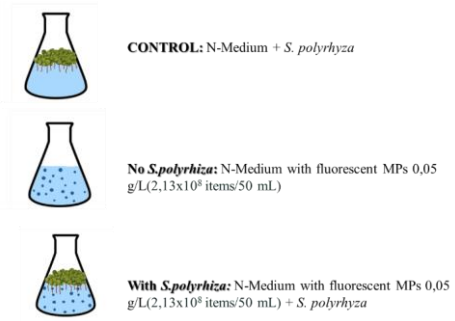

Figure 4.9.5: Experimental set-up: treatment with fluorescent MPs on *Spirodela polyrhyza.*

4.9.3.2 Modelling approaches

n.a.

4.9.4 Results

In the first experiment, plants treated with both MNP concentrations showed significantly reduced fresh and dry weights (Figure 4.9.6a and b). ΨETo (i.e., the probability that a PSII-trapped electron is transferred beyond reduced QA, or an estimate of the oxidized plastoquinone pool size) and PI_abs (i.e., the potential for energy conservation from absorbed photons in PSII to the reduction of electron acceptors) were significantly reduced in samples treated with the highest PET concentration.

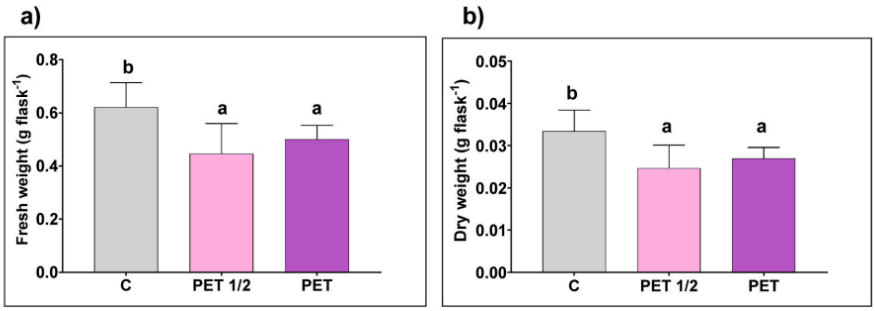

Figure 4.9. 6: a) Fresh and b) dry weight of *S. polyrhiza* plants grown in absence (C) or in presence of MNPs at different concentrations (PET ½ and PET) for ten days.

Starch concentration (% dry weight) was also significantly reduced in MNP-treated plants. Ionomic analysis revealed an alteration in the concentration of several elements (K, Ca, Mg, Fe, Mn, Zn, Cu) in the tissues of treated plants, highlighting that plastic particles are able to interfere with nutrient uptake (Figure 4.9.7).

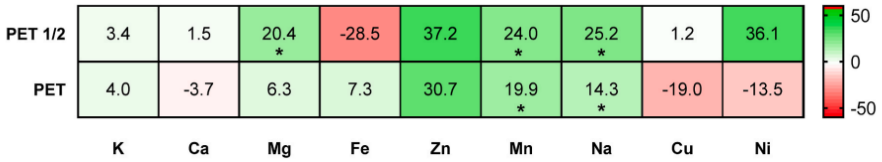

Figure 4.9.7: Heatmap showing ionome variation of *S. polyrhiza* plants grown in presence of MNPs at different concentrations (PET ½ and PET) for ten days. Colour scale indicates decreased (red), unchanged (white) or increased (green) element concentration in respect to the control. The percentage of variation is reported, together with asterisks indicating the significant difference between the element concentrations in treated and control plants (at least $p < 0.05$).

The methylation-sensitive amplification polymorphism (MSAP) technique was used to assess possible changes in DNA methylation levels induced by plastic particles. The analysis showed unusual hypermethylation in 5'-CCGG sites that could be implicated in DNA protection from dangerous agents (i.e. reactive oxygen species) or in the formation of new epialleles.

In *Azolla filiculoides*, PET-MNPs did not cause alterations in the growth of *Azolla filiculoides*; however, ten days of exposure were sufficient to induce a significant decrease in chlorophyll content, in the concentrations of Ca, Mn, and Co, and to alter root anatomy (Figure 4.9.8).

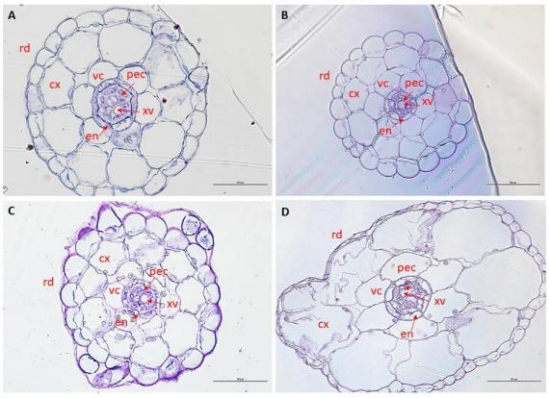

Figure 4.9.8: Root cross section closer to the apex, 40×: A–B) control; C–D) PET½. Rhizodermis (rd), cortex (cx), vascular cylinder (vc), endodermis (en), pericycle (pec), vascular xylem (xv).

These results suggest a possible PET-MNP–induced nitrogen limitation in the fern, likely resulting from the negative impact of the particles on its symbiont *Trichormus azollae*. Consistently, treated plants showed reduced nitrogen levels and impaired uptake of essential elements. Moreover, PET-MNP exposure led to a decrease in the relative abundance of the N_2-fixing cyanobacteria and to marked alterations in the symbiont's phenotype (Figure 4.9.9).

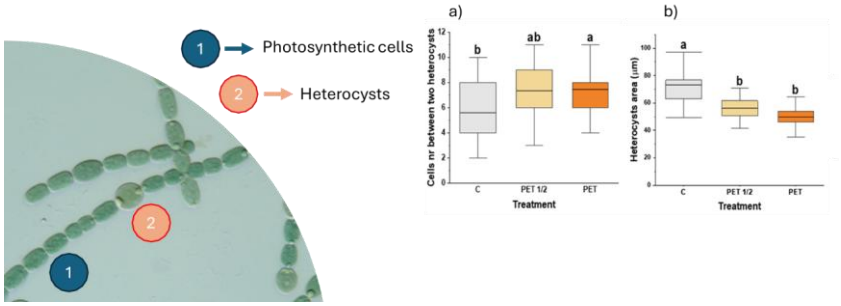

Figure 4.9.9: a) Number of cells between heterocysts and b) heterocysts area of Trichormus azollae collected from A. filiculoides cultivated in water or with MNPs at the two different concentrations. Red arrows indicate the heterocysts.

Regarding *Spyrodela polyrhiza*. the presence of particles did not affect plant growth in terms of frond number and total frond area, and no differences were observed between the treatment and control group in fresh and dry weight at the end of the week of exposure. In addition, tissue accumulation of macro- and micronutrients was not affected by the presence of MPs.

At the end of the experiment, 400 fluorescent particles were observed at the optical light microscopy, and their sizes were categorized into classes. In the control condition (only MPs without the plants), smaller particles predominated, with a significant number in the 0-10 µm² class (Figure 4.9.10). In contrast, particles in the treatment condition (MP in presence of Spirodela plants) were less abundant in the smaller classes and

more prevalent in larger ones, indicating particles aggregation in the presence of *S. polyrhiza* (Figure 4.9.11b). The treatment condition showed a significantly lower number of items (Figure 4.9.11a), suggesting particle adsorption by the roots and underside of the fronds, confirmed by confocal microscopy analysis (Figure 4.9.12). The binding force of the MPs on *S. polyrhiza* was strong, as a large quantity of them remained on the surfaces even after washing and incubation for 4 days in an MP-free medium.

The Zeta potential of control MPs remained stable at -17 mV, while those incubated with plants showed a less negative value of -11 mV. These effects on the behavior of particles in solution in the presence of S. polyrhiza are thought to result from the exudation of specific compounds by the plant-root system. Preliminary data from LC-MS/MS untargeted metabolomics identified specific metabolic features exuded only in the presence of MPs. Therefore, the exudation of specific compounds by the plant-root system seems to be involved in MP aggregation in solution.

The results showed that floating plants can contribute to MP aggregation and surface adsorption. Validating this role could have potential biotechnological applications in the phytoremediation of water systems.

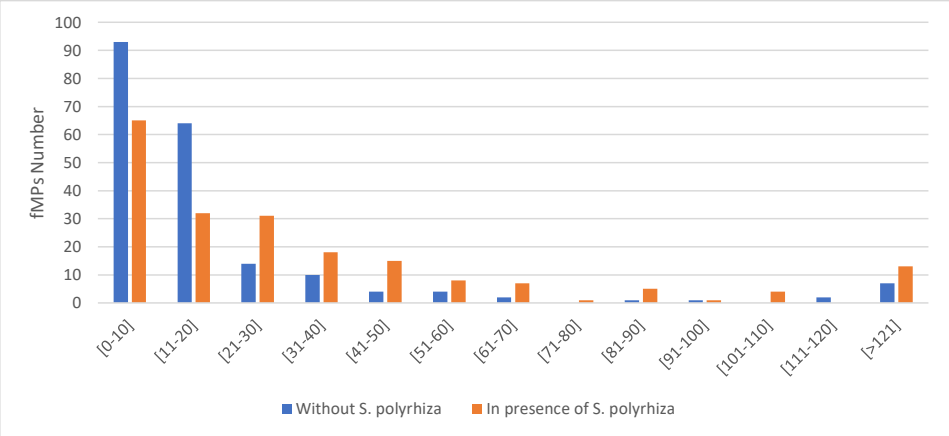

Figure 4.9.10: Number of fMP particles without or in presence of S. polyrhiza at T7, divided by size classes.

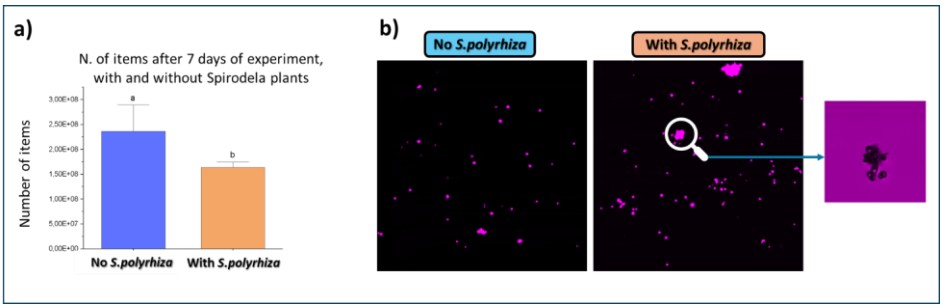

Figure 4.9.11: Results after 7 days of cultivation. a) number of MP items counted in the solution without and with *S. polyrhiza* plants; b) images of MP items in final solutions and their aggregation in presence of plants.

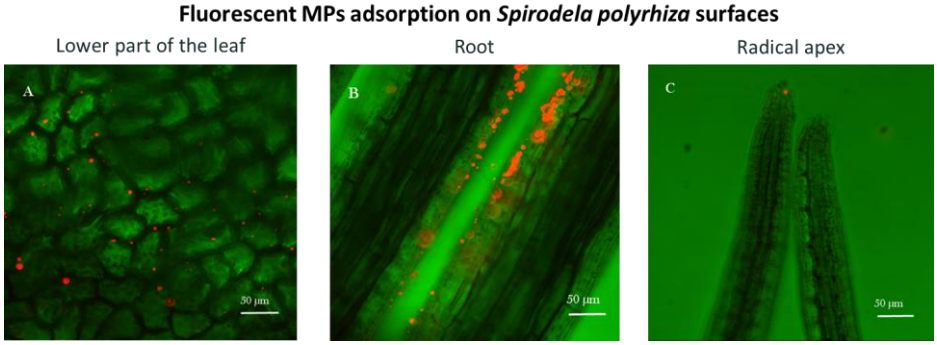

Figure 4.9.12: Confocal microscopy images of *S. polyrhiza* plant tissues with fluorescent MPs adsorbed on the surface.

4.9.5 Scientific products and dissemination

Organization of events

09-30 September 2023. Organization of the exhibition by the artist Annarita Serra: Serra in serra le opere sostenibili di Annarita Serra in mostra all'Orto botanico di Firenze. Link: https://www.unifisostenibile.unifi.it/upload/sub/Locandine/Locandina%20mostra.pdf

08 September 2023. Workshop at the Botanical Garden of Florence on the dispersion of plastics in the environment, held at the opening of the exhibition by the artist Annarita Serra. Link: https://www.unifisostenibile.unifi.it/art-349-serra-in-serra-le-opere-sostenibili-di-annarita-serra-in-mostra-all-orto-botanico-di-firenze.html

Oral presentations and posters

1 - 2 September 2023. Poster presentation at the Symposium CSGI in Naples "Effect of micro-nanoplastics from airborne pollution on *Tillandsia usneoides* as a green biosensor" Falsini S., Colzi I., Chelazzi D., Dainelli M., Schiff S., Papini A., Coppi A., Gonnelli C., Ristori S.

08 September 2023. Oral presentation within the workshop Serra in serra: le opere sostenibili di Annarita Serra in mostra all'Orto botanico di Firenze Gli impatti delle micro e nanoplastiche sulle piante Falsini S., Colzi I., Dainelli M., Coppi A., Papini A., Ristori S., Gonnelli C.

22 May 2024. Oral presentation at the Workshop Environmental degradation: "Micro(bio)plastics 1 in Florence: Effetti di micro e nanoplastiche su specie vegetali in ambiente acquatico e Terrestre". Falsini S., Colzi I., Gonnelli C., Papini A.

5–7 February 2025. Oral presentation at the Conference of Young Botanists (CYBO 2025) in Genoa: "Deciphering plant-microplastic interactions in freshwaters through Spirodela polyrhiza: towards phytoremediation applications" Dainelli M., Falsini S., Boutet S., Colzi I., Coppi A., Corso M., Papini A., Ristori S., Stefano G., Gonnelli C.

3-5 December 2025. Oral presentation at the Return Final in Meeting in Naples: "Effect of micro-nanopollutants on plants" Falsini S., Papini A., Gonnelli C., Colzi I.

List of Publications:

Dainelli M., Chiavacci B., Colzi I., Coppi A., Corti E., Daghio M., Falsini S., Ristori S., Papini A., Toni E., Viti C., Gonnelli C., Impact of PET micro/nanoplastics on the symbiotic system Azolla filiculoides-Trichormus azollae, Chemosphere 2024 368, 143718. https://doi.org/10.1016/j.chemosphere.2024.143718

Dainelli M., Castellani M.B., Pignattelli S., Falsini S., Ristori S., Papini A., Colzi I.*, Coppi A., Gonnelli C. (2024). Growth, physiological parameters and DNA methylation in Spirodela polyrhiza (L.) Schleid exposed to PET micro-nanoplastic contaminated waters. Plant Physiology and Biochemistry 207, 108403. https://doi.org/10.1016/j.plaphy.2024.108403.

Dainelli M., Falsini S., Boutet S, Colzi I., Coppi A., Corso M., Corti E., Martina M., Papini A., Ristori S., Giovanni S., Gonnelli C. Deciphering plant-microplastic interactions in Spirodela polyrhiza towards phytoremediation applications: methylome dynamics and exudate-mediated effects, In progress

5. Conclusions

Deliverable DV4.3.4 provides a comprehensive, integrated, and multiscale assessment of the fate, transport, and impacts of contaminants and microplastics in coastal and marine environments, addressing key scientific challenges associated with emerging pollutants, their bioaccumulation and biomagnification, and the reduction of uncertainty in observations and numerical models. By combining modeling frameworks with advanced monitoring, analytical, and experimental approaches, the activities carried out within Task 4.3.2 significantly contribute to a deeper understanding of contaminant dynamics across interconnected marine environmental compartments, including water, sediments, and biota.

A major outcome of this Deliverable is the development and application of process-based modeling approaches capable of simulating contaminant pathways from different sources to marine ecosystems and organisms. The integration of Lagrangian transport models, biogeochemical cycles, food web models, and genomics-based approaches represents a novel and robust framework for assessing the environmental fate of mercury, microplastics, and pharmaceuticals, as well as their bioaccumulation potential. These tools enable the investigation of contaminant behavior across different spatial and temporal scales, supporting scenario analysis and risk assessment in complex systems.

Significant progress was achieved in quantifying contaminant bioaccumulation and biomagnification, particularly for mercury within Adriatic food webs. The coupling of spatially explicit transport models with food web and multi-risk modeling approaches provided robust evidence of trophic transfer processes and synergistic effects among multiple stressors, supporting the evaluation of risks to ecosystems and human health.

The Deliverable also provides a detailed and comprehensive assessment of microplastics**,** documenting their density, distribution, and composition across onshore, nearshore, offshore, and water-column compartments. Observed abundances in seawater and fish confirm the pervasive bioavailability of microplastics and their relevance for marine food webs and seafood safety.

Extensive field sampling, laboratory analyses, and innovative observation techniques provided critical empirical data to support and validate modeling efforts. In port and lagoon environments, spatially resolved sediment analyses and high-resolution hydrodynamic and bathymetric datasets enabled the development of multiscale dispersion models that successfully reproduced plastic transport pathways and accumulation zones while explicitly accounting for uncertainty, representing a critical step toward more reliable predictive tools for environmental management. Such investigations emphasized the combined influence of hydrodynamics, freshwater inputs, seabed processes, and weather-driven circulation on contaminant accumulation and redistribution.

Detailed analyses of beach litter (BL) highlighted the influence of hydrodynamic forcing and coastal morphology on accumulation patterns. Standard in situ monitoring and high-resolution observational approaches, including drone-based surveys, hyperspectral imaging, portable near-infrared spectroscopy, significantly enhanced the capacity to detect, classify, and quantify plastics in heterogeneous environmental matrices. These approaches contribute to the harmonization of monitoring practices and the reduction of analytical uncertainty, supporting large-scale and long-term assessments.

Significant progress was also achieved in observation and analytical methodologies. Novel hyperspectral imaging (HSI) and portable near-infrared (NIR) spectroscopy protocols enabled rapid, non-destructive, and accurate identification and classification of macro- and microplastics in sandy beaches and marine sediments.

The Deliverable further highlights the importance of linking physical processes, biological responses, and contaminant dynamics. Experimental studies on aquatic plants revealed previously unexplored biological–physical interactions, including microplastic-induced metabolic responses and aggregation processes, suggesting potential roles for vegetation in microplastic dynamics and phytoremediation strategies.

Overall, DV4.3.4 demonstrates the added value of a multidisciplinary and collaborative framework integrating observations, experiments, and advanced modeling across marine and coastal environmental compartments. The developed methodologies, models, and datasets provide a solid scientific basis for future research, improving risk assessment, predictive capabilities, uncertainty reduction, and supporting the definition of

evidence-based environmental polices aimed at mitigating coastal and marine degradation and protecting ecosystems and human health.

Finally, it is worth highlighting that the activities carried out within Task 4.3.2 have fostered a strong and productive collaboration among research groups from multiple institutions. This collaborative effort has been successfully capitalized through the production of several joint scientific publications, coordinated participation in national and international conferences, and the submission of national and international research project proposals. In this context, the NEREIDAS Project “implemeNtation of innovativE educational actions foR thE protectIon of mexico anD colombiA marine environmentS” (Call: ERASMUS-EDU-2024-CBHE), co-funded by the European Union, represents a concrete outcome of this collaboration and involves the active participation of the UNIROMA1 and UNIBA research teams.

6. References

6.1 References of Thematic Chapter 4.1 (OGS)

Berry, A., et al. (2011). OILTRANS: A Lagrangian oil spill transport and fate model.

Bandelj, V., Gianni, F., Canu, D., Laurent, C., Querin, S., Zunino, S., Suban, V., Pegan, U., Perkovič, M., Luin, B., Martinić, V., Pilepić, A. (2024). NAMIRS D2.1 – Report on Environmental Risk Assessment. Central European Initiative, OGS, UL-FPP, ATRAC.

Bruschi, A., Lisi, I., De Angelis, R., Querin, S., Cossarini, G., Di Biagio, V., Salon, S., Solidoro, C., Fassina, D., Ancona, S., Silvestri, C. (2021). Indexes for the assessment of bacterial pollution in bathing waters from point sources: The northern Adriatic Sea CADEAU service. *Journal of Environmental Management*, 293, 112878. https://doi.org/10.1016/j.jenvman.2021.112878

Escudier, R., et al. (2022). Mediterranean Sea Physics Reanalysis. Copernicus Marine Service (CMS).

Giordano, P., et al. (2025a). High-resolution MITgcm hindcast of the Northern Adriatic Sea (2017–2021).

Giordano, P., et al. (2025b). Description of the hydrodynamic setup of the Northern Adriatic MITgcm configuration.

Jokuty, P., et al. (2022). *A Catalogue of Crude Oil and Oil Product Properties (1999) – Revised 2022*. Environment and Climate Change Canada, Report EE-165.

Laurent, C., Querin, S., Solidoro, C., Melaku Canu, D. (2020). Modelling marine particle dynamics with LTRANS-Zlev: Implementation and validation. *Environmental Modelling & Software*, 125, 104621. https://doi.org/10.1016/j.envsoft.2020.104621

Marshall, J., Adcroft, A., Hill, C., Perelman, L., Heisey, C. (1997). A finite-volume, incompressible Navier–Stokes model for studies of the ocean on parallel computers. *Journal of Geophysical Research*, 102, 5753–5766.

Melaku Canu, D., Solidoro, C., Bandelj, V., Quattrocchi, G., Sorgente, R., Olita, A., Fazioli, L., Cucco, A. (2015). Assessment of oil slick hazard and risk at vulnerable coastal sites. *Marine Pollution Bulletin*, 94(1–2), 84–95.

Melaku Canu, D., Querin, S., Laurent, C., Bandelj, V., Solidoro, C. (2019). Oil spill dispersion and extension of mixing zone maps. HarmoNIA Project, Deliverable T3.1.3.

Menoni, S., Molinari, D., Parker, D., Ballio, F., Tapsell, S. (2012). Assessing multifaceted vulnerability and resilience in order to design risk mitigation strategies. *Natural Hazards*, 64, 1–26.

Meijer, L. J. J., et al. (2021). More than 1000 rivers account for 80% of global riverine plastic emissions into the ocean. *Science Advances*, 7(18), eaaz5803.

Querin, S., Bensi, M., Cardin, V., Solidoro, C., Bacer, S., Mariotti, L., Stel, F., Malačič, V. (2016). Saw-tooth modulation of the deep-water thermohaline properties in the southern Adriatic Sea. *Journal of Geophysical Research: Oceans*, 121, 4585–4600. https://doi.org/10.1002/2015JC011522

Rosati, G., Canu, D., Lazzari, P., Solidoro, C. (2022). Assessing the spatial and temporal variability of methylmercury biogeochemistry and bioaccumulation in the Mediterranean Sea with a coupled 3D model. *Biogeosciences*, 19, 3663–3682. https://doi.org/10.5194/bg-19-3663-2022

Rosati, G., Solidoro, C., Laurent, C., Aveytua Alcázar, L., Umgiesser, G., Canu, D. (2024). Mercury cycling in contaminated coastal environments: modeling the benthic–pelagic coupling and microbial resistance in the Venice Lagoon. *Water Research*, 261, 121965. https://doi.org/10.1016/j.watres.2024.121965

Umgiesser, G., Canu, D., Cucco, A., Solidoro, C. (2003). A finite element model for the Venice Lagoon: SHYFEM. *Coastal Engineering*, 47, 409–437.

UNDRO (1979). *Natural Disasters and Vulnerability Analysis*. Report of the Expert Group Meeting, United Nations Disaster Relief Organization.

UNISDR (2005). *Hyogo Framework for Action 2005–2015: Building the resilience of nations and communities to disasters*. United Nations International Strategy for Disaster Reduction.

Vichi, M., Lovato, T., Lazzari, P., Cossarini, G., Gutierrez Mlot, E., Mattia, G., Masina, S., McKiver, W., Pinardi, N., Solidoro, C., Tedesco, L., Zavatelli, M. (2015). The Biogeochemical Flux Model (BFM): Equation description and user manual. BFM Report Series, Version 5.2.

WWF (2018). *Out of the plastic trap: Saving the Mediterranean from plastic pollution*. World Wide Fund for Nature.

6.2 References for Thematic Chapter 4.2 (UNIBA)

Abelouah, M.R., Ben-Haddad, M., Rangel-Buitrago, N., Hajji, S., El Alem, N., Ait, Alla A. (2022). Microplastics pollution along the Central Atlantic coastline of Morocco. Mar. Pollut. Bull. 174, 113190. https://doi.org/10.1016/j.marpolbul.2021.113190.

Akarsu, C., Sonmez, V.Z., Altay, M.C., Pehlivan, T., Sivri, N. (2022). The spatial and temporal changes of beach litter on Istanbul (Turkey) beaches as measured by the clean-coast index. Mar. Pollut. Bull. 176, 113407. https://doi.org/10.1016/j. marpolbul.2022.113407

Alkalay, R., Pasternak, G., Zask, A. (2007). Clean-coast index - A new approach for beach cleanliness assessment. Ocean & Coastal Management, volume 50, issues 5–6, 2007, pages 352-362, (ISSN 0964-5691).

Andriolo, U., Gonçalves, G., Sobral, P., Font´an-Bouzas, ´A., Bessa, F. (2020a). Beach-dune morphodynamics and marine macro-litter abundance: an integrated approach with unmanned aerial system. Sci. Total Environ. 749, 141474.

Andriolo, U., Goncalves, G., Bessa, F., Sobral, P. (2020b). Mapping marine litter on coastal dunes with unmanned aerial systems: A showcase on the Atlantic Coast. Sci. Total Environ. 736, 139632.

Anfuso, G., ´Alvarez, O., Dilauro, G., Sabato, G., Scardino, G., Sozio, A., Rizzo, A., (2024). A first attempt to describe the real-time behavior and fate of marine litter items in the nearshore and foreshore under low energetic marine conditions. Water 16 (3), 409.

Araújo, M.C.B., Costa, M.F. (2019). A critical review of the issue of cigarette butt pollution in coastal environments. Environ. Res. 172, 137–149.

Asensio-Montesinos, F., Oliva, Ramírez M., Aguilar-Torrelo, M.T., Anfuso, G. (2021b). Abundance and distribution of cigarette butts on coastal environments: examples from southern Spain. J. Mar. Sci. Eng. 9 (2), 129.

Battaglini, E., Miralles, P., Lotti, N., Soccio, M., Fiorini, M., Coscoll`a, C. (2024). Analysis of microplastics in commercial vegetable edible oils from Italy and Spain. Food Chem. 443, 138567. https://doi.org/10.1016/j.foodchem.2024.138567.

Blott, S.J., Pye, K. (2001). GRADISTAT: a grain size distribution and statistics package for the analysis of unconsolidated sediments. Earth Surf. Process. Landf. 26 (11), 1237–1248. https://doi.org/10.1002/esp.261.

Crichton, E.M., No¨el, M., Gies, E.A., Ross, P.S. (2017). A novel, density-independent and FTIR-compatible approach for the rapid extraction of microplastics from aquatic sediments. Anal. Methods 9 (9), 1419–1428. https://doi.org/10.1039/C6AY02733D.

Dalle Mura, I., Barbone, E., Battista, D., Giannuzzi, C. G., Ranieri, S., Strippoli, G., ... & Ungaro, N. (2022). Chapter A first assessment of microplastics in the sea waters off the Puglia region.

Dosovitskiy, A. (2021) An Image Is Worth 16 × 16 Words: Transformers for Image Recognition at Scale. Proceedings of the IEEE/CVF Conference on Computer Vision and Pattern Recognition, New York City, 23-26 June 2021, 45-67.

Everingham, M., van Gool, L., Williams, C. K. I., Winn, J., & Zisserman, A. (2010). The PASCAL Visual Object Classes (VOC) Challenge. *International Journal of Computer Vision*, *88*(2), 303-338. https://doi.org/10.1007/s11263-009-0275-4

Fleet, D., Vlachogianni, T., Hanke, G. (2021). A joint list of litter categories for marine macrolitter monitoring. Joint Research Centre: Luxembourg 52. https://doi.org/10.2760/127473

Galgani, F., Ruiz-Orej´on, L.F., Ronchi, F., Tallec, K., Fischer, E.K., Matiddi, M., Anastasopoulou, A., Andresmaa, E., Angiolillo, M., Bakker, Paiva M., Booth, A.M., Buhhalko, N., Cadiou, B., Clar`o, F., Consoli, P., Darmon, G., Deudero, S., Fleet, D., Fortibuoni, T., Fossi, M.C., Gago, J., G´erigny, O., Giorgetti, A., Gonz´alez- Fern´andez, D., Guse, N., Haseler, M., Ioakeimidis, C., Kammann, U., Kühn, S., Lacroix, C., Lips, I., Loza, A.L., Molina, Jack M.E., Nor´en, K., Papadoyannakis, M., Pragnel-Raasch, H., Rindorf, A., Ruiz, M., Set¨al¨a, O., Schulz, M., Schultze, M., Silvestri, C., Soederberg, L., Stoica, E., Storr-Paulsen, M., Strand, J., Valente, T., van Franeker, J., van Loon, W.M.G.M., Vighi, M., Vinci, M., Vlachogianni, T., Volckaert, A., Weiel, S., Wenneker, B., Werner, S., Zeri, C., Zorzo, P., Hanke, G. (2023). European Commission. Joint Research Centre & MSFD Technical Group on Marine Litter. https://doi.org/10.2760/59137. - Guidance on the monitoring of marine litter in European seas: an update to improve the harmonised monitoring of marine litter under the Marine Strategy Framework Directive. Publications Office

Hanke, G., Galgani, F., Werner, S., Oosterbaa, n L., Nilsson, P., Fleet, D., Kinsey, S., Thompson, R.C., franeker van J., Vlachogianni, T., Scoullos, M., Veiga, J.M., Palatinus, A., Matiddi, M., Maes, T., Korpinen, S., Budziak, A., Leslie, H., Gago, J. & Liebezeit, G. (2013). Guidance on Monitoring of Marine Litter in European Seas: a guidance document within the Common Implementation Strategy for the Marine Strategy Framework Directive. JRC Scientific & Policy Reports, MSFD Technical Subgroup on Marine Litter. Publications Office of the European Union, Luxembourg. doi: 10.2788/99475.

Hanke, G., Walvoort, D., Ruiz-Orej´on, L.F., Van, L., Giorgetti, A., Molina-Jack, M.E., Vinci, M. (2025). European Coastline Macro Litter Trends 2015-2021. Publications Office of the European Union, Luxembourg, p. 2024. https://data.europa. eu/doi/10.2760/0752301. JRC138907.

Kirillov, A., Mintun, E., Ravi, N., Mao, H., Rolland, C., Gustafson, L., ... & Girshick, R. (2023). Segment anything. In *Proceedings of the IEEE/CVF international conference on computer vision* (pp. 4015-4026).

Lin, TY. et al. (2014). Microsoft COCO: Common Objects in Context. In: Fleet, D., Pajdla, T., Schiele, B., Tuytelaars, T. (eds) Computer Vision – ECCV 2014. ECCV 2014. Lecture Notes in Computer Science, vol 8693. Springer, Cham. https://doi.org/10.1007/978-3-319-10602-1_48

Loizidou, X.I., Loizides, M.I., Orthodoxou, D.L. (2018). Persistent marine litter: small plastics and cigarette butts remain on beaches after organized beach cleanups. Environ. Monit. Assess. 190 (7), 414.

Mani, T., Frehland, S., Kalberer, A., Burkhardt-Holm, P. (2019). Using castor oil to separate microplastics from four different environmental matrices. Anal. Methods 11 (13), 1788–1794. https://doi.org/10.1039/C8AY02559B.

Rangel-Buitrago, N., Velez-Mendoza, A., Gracia, C.A., Neal, W.J. (2020). The impact of anthropogenic litter on Colombia's Central Caribbean beaches. Mar. Pollut. Bull. 152, 110909. https://doi.org/10.1016/j.marpolbul.2020.110909.

Rangel-Buitrago, N., Mendoza, A. V., Mantilla-Barbosa, E., Arroyo-Olarte, H., Arana, V. A., Trilleras, J., Gracia, C A., Neal, W. J., & Williams, A. T. (2021). Plastic pollution on the Colombian central Caribbean beaches Marine Pollution Bulletin, 162, 111837. https://doi.org/10.1016/j.marpolbul.2020.111837

Rizzo, A., Sozio, A., Anfusio, G., La Salandra, M., & Sasso, C. (2023). The use of UAV images to assess preliminary relationships between spatial litter distribution and beach morphodynamic trends: the case study of Torre Guaceto beach (Apulia Region, southern Italy). Geografia Fisica E Dinamica Quaternaria, 45(2), 237-250. https://doi.org/10.4461/GFDQ.2022.45.12

Rizzo, A., Scicchitano, G., Mastronuzzi, G. (2024b). A set of guidelines as support for the integrated geo-environmental characterization of highly contaminated coastal sites. Sci. Rep. 14 (1), 8198.

Scarrica, V.M., Aucelli, P.P.C., Cagnazzo, C., Casolaro, A., Fiore, P., La Salandra, M., Rizzo, A., Scardino, G., Scicchitano, G., Staiano, A. (2022). A novel beach litter analysis system based on UAV images and convolutional neural networks. Eco. Inform. 72, 101875. https://doi.org/10.1016/j.ecoinf.2022.101875.

Scopetani, C., Chelazzi, D., Mikola, J., Leini¨o, V., Heikkinen, R., Cincinelli, A., Pellinen, J. (2020). *Olive oil*-based method for the extraction, quantification and identification of microplastics in soil and compost samples. Sci. Total Environ. 733. https://doi.org/10.1016/j.scitotenv.2020.139338.

Sasso, C., Rizzo, A., Mastronuzzi, G., Anfuso, G., Lapietra, I., Liso, I. S., Marsico, A., Sozio, A., & Scicchitano, G. (2025). Unveiling coastal pollution: A multi-technology approach to micro and macro litter assessment for the environmental characterization of beaches Marine Pollution Bulletin, 220, 118423. https://doi.org/10.1016/j.marpolbul.2025.118423

Sozio, A., Scarrica, V. M., Aucelli, P. P., Scicchitano, G., Staiano, A., & Rizzo, A. (2023). Comparing Meanshift/SVM and Mask-RCNN algorithms for beach litter detection on UAVs images. In *2023 IEEE International Workshop on Metrology for the Sea; Learning to Measure Sea Health Parameters (MetroSea)* (pp. 483-487). IEEE.

Sozio, A., Scarrica, V.M., Rizzo, A., Aucelli, P.P.C., Barracane, G., Dimuccio, L.A., Ferreira, R., La Salandra, M., Staiano, A., Tarantino, M.P., Scicchitano, G. (2024). Application of direct and indirect methodologies for beach litter detection in coastal environments. Remote Sens. 16 (19), 3617. https://doi.org/10.3390/rs1619361.

Trani, A., Mezzapesa, G., Piscitelli, L., Mondelli, D., Nardelli, L., Belmonte, G., ... & Zuccaro, M. (2023). Microplastics in water surface and in the gastrointestinal tract of target marine organisms in Salento coastal seas (Italy, Southern Puglia). *Environmental Pollution*, *316*, 120702.

UNEP, 2009. Marine Litter: A Global Challenge. United Nations Environment Program. Nairobi

UNEP/MAP,(2015). Marine Litter Assessment in the Mediterranean. Athens.

United Nations Environment Programme, (2021). From Pollution to Solution: A Global Assessment of Marine Litter and Plastic Pollution. Nairobi.

Vlachogianni, T. (2017). Methodology for Monitoring Marine Litter on Beaches. Macro-Debris (> 2.5 cm). DeFishGear, 1-16.

6.3 References for Thematic Chapter 4.3 (UNIFI)

Cocci, P., Gabrielli, S., Pastore, G., Minicucci, M., Mosconi, G., & Palermo, F. A. (2022). Microplastics accumulation in gastrointestinal tracts of Mullus barbatus and Merluccius merluccius is associated with increased cytokine production and signaling. Chemosphere, 307. https://doi.org/10.1016/j.chemosphere.2022.135813

Mancuso, M., Porcino, N., Blasco, J., Romeo, T., Savoca, S., Spanò, N., & Bottari, T. (2023). Microplastics in the Mediterranean Sea Impacts on Marine Environment. SpringerBriefs in Environmental Science. https://doi.org/https://doi.org/10.1007/978-3-031-30481-1

Santonicola, S., Volgare, M., Cocca, M., & Colavita, G. (2023). Abundance and Characteristics of Fibrous Microplastics and Microfibers Isolated in Mullus barbatus from the Adriatic Sea—Preliminary Investigation. Microplastics, 2(4), 411–421. https://doi.org/10.3390/microplastics2040030

Sharma, S., Sharma, V., & Chatterjee, S. (2021). Microplastics in the Mediterranean Sea: Sources, Pollution Intensity, Sea Health, and Regulatory Policies. Frontiers in Marine Science, 8, 634934. https://doi.org/10.3389/FMARS.2021.634934

6.4 References for Thematic Chapter 4.4 (UNIGE)

Cai, C., Zhu, L., Hong, B. (2023). A review of methods for modeling microplastic transport in the marine environments. Marine Pollution Bulletin, 193, 115136. https://doi.org/10.1016/j.marpolbul.2023.115136

Cutroneo, L., Reboa, A., Geneselli, I., & Capello, M. (2021). Considerations on salts used for density separation in the extraction of microplastics from sediments. Marine Pollution Bulletin, 166, 112216. https://doi.org/10.1016/j.marpolbul.2021.112216

Ji, X., Ma, Y., Zeng, G., Xu, X., Mei, K., Wang, Z., Chen, Z., Dahlgren, R., Zhang, M., Shang, X. (2021). Transport and fate of microplastics from riverine sediment dredge piles: Implications for disposal. Journal of Hazardous Materials, 404(A), 124132. https://doi.org/10.1016/j.jhazmat.2020.124132

Simantiris, N., Avlonitis, M., Theocharis, A. (2022). Simulation of the transport of marine microplastic particles in the Ionian Archipelago (NE Ionian Sea) using a Lagrangian model and the control mechanisms affecting their transport. Journal of Hazardous Materials, 437, 129349. https://doi.org/10.1016/j.jhazmat.2022.129349

Waldschläger, K., Brückner, M.Z.M., Carney Almroth, B., Hackney, C.R., Mehedi Adyel, T., Alimi, O.S., Lynn Belontz, S. (2022). Learning from natural sediments to tackle microplastics challenges: A multidisciplinary perspective. Earth-Science Reviews 228, 104021. https://doi.org/10.1016/j.earscirev.2022.104021

6.5 References for Thematic Chapter 4.5 (UNIPA)

Joseph TM, Unni AB, Joshy KS, Kar Mahapatra D, Haponiuk J, Thomas S (2023) Emerging Bio-Based Polymers from Lab to Market: Current Strategies, Market Dynamics and Research Trends. C 9:30. https://doi.org/10.3390/c9010030

Strain, E.M.A., Lai, R.W.S., White, C.A., Piarulli, S., Leung, K.M.Y., Airoldi, L., O'Brien, A., 2022. Editorial: marine pollution - emerging issues and challenges. Front. Mar. Sci. 9.

6.6 References for Thematic Chapter 4.6 (UNIROMA1)

Cocozza, P., Scarrica, V. M., Rizzo, A., Serranti, S., Staiano, A., Bonifazi, G., & Anfuso, G. (2025). Microplastic pollution from pellet spillage: Analysis of the Toconao ship accident along the Spanish and Portuguese coasts. Marine Pollution Bulletin, 211, 117430. https://doi.org/10.1016/j.marpolbul.2024.117430

Palmieri, R., Gasbarrone, R., Bonifazi, G., Piccinini, G., & Serranti, S. (2024a). Hyperspectral Imaging for Detecting Plastic Debris on Shoreline Sands to Support Recycling. Applied Sciences, 14(23), 11437. https://doi.org/10.3390/app142311437

Palmieri, R., Serranti, S., Capobianco, G., Cózar Cabañas, A., Martí Morales, E., & Bonifazi, G. (2024b). Marine Microplastic Classification by Hyperspectral Imaging: Case Studies from the Mediterranean Sea, the Strait of Gibraltar, the Western Atlantic Ocean and the Bay of Biscay. Applied Sciences, 14(20), 9310. https://doi.org/10.3390/app14209310

Rizzo, A., Serranti, S., Cucuzza, P., Lisco, S., Marsico, A., Bonifazi, G., & Mastronuzzi, G. (2024). Application of hyperspectral imaging and machine learning for the automatic identification of microplastics on sandy beaches. In Algorithms, Technologies, and Applications for Multispectral and Hyperspectral Imaging XXX (Vol. 13031, pp. 181-193). SPIE. https://doi.org/10.1117/12.3013227

Scarrica, V. M., Cocozza, P., Anfuso, G., Staiano, A., Bonifazi, G., Rizzo, A., & Serranti, S. (2025). Cost-effective approaches for microplastic pellets characterization using a machine learning tool. Ecological Informatics, 103230. https://doi.org/10.1016/j.ecoinf.2025.103230

Serranti, S., Bonifazi, G., Capobianco, G., Gorga, E., D'Agostini, M., & Dall'Ava, A. (2025). Custom hyperspectral imaging scanner for microplastic detection and classification: hardware and data processing specifications. In Algorithms, Technologies, and Applications for Multispectral and Hyperspectral Imaging XXXI (Vol. 13455, pp. 247-257). SPIE. https://doi.org/10.1117/12.3052766

Serranti, S., Capobianco, G., Cucuzza, P., & Bonifazi, G. (2024). Efficient microplastic identification by hyperspectral imaging: A comparative study of spatial resolutions, spectral ranges and classification models to define an optimal analytical protocol. Science of the Total Environment, 954, 176630. https://doi.org/10.1016/j.scitotenv.2024.176630

6.7 References for Thematic Chapter 4.7 (OGS)

American Academy of Microbiology (ASM), 2023. Microbes in Models: Integrating Microbes into Earth System Models for Understanding Climate Change. https://asm.org/getmedia/98591c13-2c31-4926-94a4-664e75ebadd3/microbes-in-models-report

Bloom, N.S., Moretto, L.M., Scopece, P., Ugo, P., Tositti, L., 2004. Speciation and cycling of mercury in the Venice Lagoon (Italy). Marine Chemistry 91, 85–99.

Banchi, E., Corre, E., Del Negro, P., Celussi, M., Malfatti, F., 2023. Genome-resolved metagenomics of Venice Lagoon surface sediment bacteria reveals high biosynthetic potential and metabolic plasticity as successful strategies in an impacted environment. Marine Life Science & Technology 6(1), 126–142. https://doi.org/10.1007/s42995-023-00192-z

Brigolin, D., et al., 2021. Early diagenesis in sediments of the Venice Lagoon (Italy) and its relationship to hypoxia. Frontiers in Marine Science 7, 575547. https://doi.org/10.3389/fmars.2020.575547

Cardoso, R.B., Sierra-Alvarez, R., Rowlette, P., Flores, E.R., Gómez, J., Field, J.A., 2006. Sulfide oxidation under chemolithoautotrophic denitrifying conditions. Biotechnology and Bioengineering 95(6), 1148–1157. https://doi.org/10.1002/bit.21084

Cavicchioli, R., Ripple, W.J., Timmis, K.N., et al., 2019. Scientists' warning to humanity: microorganisms and climate change. Nature Reviews Microbiology 17, 569–586. https://doi.org/10.1038/s41579-019-0222-5

Christensen, V., Walters, C.J., 2004. Ecopath with Ecosim: methods, capabilities and limitations. Ecological Modelling 172(2–4), 109–139.

Christensen, V., Walters, C.J., Pauly, D., 2008. Ecotracer: a routine for tracking contaminants and nutrients in Ecopath with Ecosim. Ecological Modelling 210(4), 450–462.

Heijs, S.K., van Gemerden, H., 2000. Microbiological and environmental variables involved in the sulfide buffering capacity along a eutrophication gradient in a coastal lagoon (Bassin d'Arcachon, France). Hydrobiologia 437, 121–131. https://doi.org/10.1023/A:1026590520603

Lennon, J.T., et al., 2024. Priorities, opportunities, and challenges for integrating microorganisms into Earth system models for climate change prediction. mBio 15(5), e00455-24. https://doi.org/10.1128/mbio.00455-24

Libralato, S., et al., 2020. Calibrated Ecopath with Ecosim model for the Adriatic and Ionian region. FAIRSEA project deliverable ('Fisheries in the AdriatIc Region – a Shared Ecosystem Approach'), 147 pp.

Pavoni, E.; Petranich, E.; Signore, S.; Fontolan, G.; Covelli, S. The Legacy of the Idrija Mine Twenty-Five Years after Closing: Is Mercury in the Water Column of the Gulf of Trieste Still an Environmental Issue? Int. J. Environ. Res. Public Health 2021, 18, 10192. https:// doi.org/10.3390/ijerph181910192

Rosati, G., Solidoro, C., Laurent, C., Aveytua Alcázar, L., Umgiesser, G., Canu, D., 2024. Mercury cycling in contaminated coastal environments: modeling the benthic-pelagic coupling and microbial resistance in the Venice Lagoon. Water Research 261, 121965. https://doi.org/10.1016/j.watres.2024.121965

Rosati, G., et al., 2020. Mercury contamination in the Venice Lagoon sediments linked to historical industrial discharges from Porto Marghera. [complete reference as in your bibliography]

Serpetti, N., Piroddi, C., Walters, W.J., Garcia-Gorriz, E., Miladinova, S., Macias, D., 2025. Ecotracer set up to trace microplastics up the Black Sea marine food web. Ecological Modelling 509, 111271. https://doi.org/10.1016/j.ecolmodel.2024.111271

Sfriso, A., Argese, E., Bettiol, C., Facca, C., 2008. Tapes philippinarum seed exposure to metals in polluted areas of the Venice Lagoon. Estuarine, Coastal and Shelf Science 79(4), 581–590. https://doi.org/10.1016/j.ecss.2008.05.012

Širca, A., Rajar, R., Horvat, M., Žagar, D., 1999. Transport of mercury in the Soča/Isonzo River system. Science of the Total Environment 237–238, 287–296. https://doi.org/10.1016/S0048-9697(99)00150-0

Sunderland, E.M., Gobas, F.A.P.C., Heyes, A., et al., 2006. Speciation and bioavailability of mercury in well-mixed estuarine sediments. Marine Chemistry 102, 111–123. https://doi.org/10.1016/j.marchem.2005.09.006

Wieder, W.R., Allison, S.D., Davidson, E.A., et al., 2015. Explicitly representing soil microbial processes in Earth system models. Global Biogeochemical Cycles 29, 1782–1800. https://doi.org/10.1002/2015GB005188

Zaggia, L., et al., 2007. Sulphate reduction in the sediment of the Venice canals (Italy). Marine Pollution Bulletin 54(7). https://doi.org/10.1016/j.marpolbul.2007.09.004

6.8 References for Thematic Chapter 4.8 (OGS)

Adam V, von Wyl A, Nowack B (2021) Probabilistic environmental risk assessment of microplastics in marine habitats Aquatic Toxicology 230 105689 https://doi.org/10.1016/j.aquatox.2020.105689

Bandelj V, Gianni F, Canu D, Laurent C, Querin S, Zunino S, Suban V, Pegan U, Perkovič M, Luin B, Martinić V, Pilepić A (2024) NAMIRS D2.1 – Report on Environmental Risk Assessment Central European Initiative OGS UL-FPP ATRAC

Burmeister H C, Hesse R, Heege T (2014) Assessing the frequency and material consequences of collisions with vessels lying at an anchorage in line with IALA iWrap MkII TransNav 8(1) 61–68

Canu D, Ivankovic D, Vucic I, Lipizer M, Molina Jack M E, Giorgi G (2020) Methodological proposal for assessing risk index of contaminant dispersion and results in case study areas HarmoNIA Project Deliverable T3.2.3 https://doi.org/10.6092/973e19cb-1ab3-43ca-b11a-9be7c900aae2

Cardona O D (2005) Indicators for disaster risk and risk management Program for Latin America and the Caribbean Instituto de Estudios Ambientales Universidad Nacional de Colombia

Chen Y, Shen S, Zhou A (2022) Assessment of red tide risk by integrating CRITIC weight method TOPSIS-ASSETS method and Monte Carlo simulation Environmental Pollution 314 120254 https://doi.org/10.1016/j.envpol.2022.120254

Ciffroy P (2007) Methods for calculating PNECs using species sensitivity distribution SSD with various hypotheses on the way to handle ecotoxicity data WIT Transactions on Biomedicine and Health 11 https://doi.org/10.2495/EHR070251

Depew D C, Basu N, Burgess N M, Campbell L M, Devlin E W, Drevnick P E, Hammerschmidt C R, Murphy C A, Sandheinrich M B, Wiener J G (2012) Toxicity of dietary methylmercury to fish derivation of ecologically meaningful threshold concentrations Environmental Toxicology and Chemistry 31(7) 1536–1547 https://doi.org/10.1002/etc.1859

Diakoulaki D, Mavrotas G, Papayannakis L (1995) Determining objective weights in multiple criteria problems the CRITIC method Computers and Operations Research 22(7) 763–770 https://doi.org/10.1016/0305-0548(94)00059-H

Esmail B A, Geneletti D (2018) Multi-criteria decision analysis for nature conservation a review of 20 years of applications Methods in Ecology and Evolution 9(1) 42–53 https://doi.org/10.1111/2041-210X.12899

European Chemicals Agency (2008) Guidance on information requirements and chemical safety assessment Chapter R10 Characterisation of dose concentration–response for environment

European Chemicals Agency (2016) Guidance on information requirements and chemical safety assessment Chapter R16 Environmental exposure assessment Version 3.0

Gucma L, Montewka J, Podgórski J (2021) Reconstructing maritime incidents and accidents using causal models for safety improvement Journal of Marine Science and Engineering 9 1414

Huang I B, Keisler J, Linkov I (2011) Multi-criteria decision analysis in environmental sciences ten years of applications and trends Science of the Total Environment 409 3578–3594 https://doi.org/10.1016/j.scitotenv.2011.06.022

Hwang C L, Yoon K (1981) Multiple Attribute Decision Making Methods and Applications Springer-Verlag

Lai Y J, Liu T Y, Hwang C L (1994) TOPSIS for MODM European Journal of Operational Research 76 486–500 https://doi.org/10.1016/0377-2217(94)90282-8

Laurent C, Querin S, Solidoro C, Melaku Canu D (2020) Modelling marine particle dynamics with LTRANS-Zlev implementation and validation Environmental Modelling and Software 125 104621 https://doi.org/10.1016/j.envsoft.2020.104621

Lavoie R A, Jardine T D, Chumchal M M, Kidd K A, Campbell L M (2013) Biomagnification of mercury in aquatic food webs a worldwide meta-analysis Environmental Science and Technology 47(23) 13385–13394 https://doi.org/10.1021/es403103t

Melaku Canu D, Solidoro C, Bandelj V, Quattrocchi G, Sorgente R, Olita A, Fazioli L, Cucco A (2015) Assessment of oil slick hazard and risk at vulnerable coastal sites Marine Pollution Bulletin 94(1–2) 84–95

Menoni S, Molinari D, Parker D, Ballio F, Tapsell S (2012) Assessing multifaceted vulnerability and resilience in order to design risk mitigation strategies Natural Hazards https://doi.org/10.1007/s11069-012-0134-4

Petersen J, Michel J, Zengel S, White M, Lord C, Plank C (2019) Environmental Sensitivity Index Guidelines Version 4.0 NOAA Technical Memorandum NOS OR&R 52

Rosati G, Canu D, Lazzari P, Solidoro C (2022) Assessing the spatial and temporal variability of MeHg biogeochemistry and bioaccumulation in the Mediterranean Sea with a coupled 3D model Biogeosciences 19 3663–3682 https://doi.org/10.5194/bg-19-3663-2022

Steele K, Carmel Y, Cross J, Wilcox C (2009) Uses and misuses of multicriteria decision analysis in environmental decision making Risk Analysis 29(1) 26–33 https://doi.org/10.1111/j.1539-6924.2008.01130.x

UNDRO (1979) Natural Disasters and Vulnerability Analysis Report of Expert Group Meeting United Nations

UNISDR (2005) Hyogo Framework for Action 2005–2015 Building the resilience of nations and communities to disasters United Nations

6.9 References for Thematic Chapter 4.9 (UNIFI)

Ekvall, M. T., Lundqvist, M., Kelpsiene, E., Šileikis, E., Gunnarsson, S. B., Cedervall, T., 2019. 642 Nanoplastics formed during the mechanical breakdown of daily-use polystyrene products. 643 Nanoscale Adv. 1 (3), 1055-1061. https://doi.org/10.1039/C8NA00210J

Dainelli M., Chiavacci B., Colzi I., Coppi A., Corti E., Daghio M., Falsini S., Ristori S., Papini A., Toni E., Viti C., Gonnelli C., Impact of PET micro/nanoplastics on the symbiotic system *Azolla filiculoides-Trichormus azollae*, Chemosphere 2024 368, 143718. https://doi.org/10.1016/j.chemosphere.2024.143718

Dainelli M., Castellani M.B., Pignattelli S., Falsini S., Ristori S., Papini A., Colzi I.*, Coppi A., Gonnelli C. (2024). Growth, physiological parameters and DNA methylation in Spirodela polyrhiza (L.) Schleid exposed to PET micro-nanoplastic contaminated waters. Plant Physiology and Biochemistry 207, 108403. https://doi.org/10.1016/j.plaphy.2024.108403

Dovidat, L.C., Brinkmann, B.W., Vijver, M.G., Bosker, T., 2020. Plastic particles adsorb to the roots of freshwater vascular plant Spirodela polyrhiza but do not impair growth. Limnol Oceanogr Lett 5, 37–45. https://doi.org/10.1002/lol2.10118

Martina Miloloža, Ula Putar, Mark Starin, Janja Novak, Gabriela Kalčíková (2025). Understanding microplastic retention in surface flow constructed wetlands: The impact of aquatic macrophytes. Journal of Environmental Chemical Engineering 13, 116097. https://doi.org/10.1016/j.jece.2025.116097.

Rozman U., Kalčíková G. (2022). The Response of Duckweed *Lemna minor* to Microplastics and Its Potential Use as a Bioindicator of Microplastic Pollution. Plants.